International Journal of Thermofluids 20 (2023) 100511

Contents lists available at ScienceDirect

International Journal of Thermofluids

journal homepage: www.sciencedirect.com/journal/international-journal-of-thermofluids

Heat transfer enhancement of tubes in various shapes potentially applied to CO2 heat exchangers in refrigeration systems: Review and assessment

Wenguang Li, Sambhaji Kadam, Zhibin Yu *

School of Engineering, University of Glasgow, G12 8QQ Glasgow, UK

ARTICLE INFO

Keywords:
Carbon dioxide
Heat transfer enhancement
Heat exchanger
Refrigeration system

ABSTRACT

To make carbon dioxide (CO2) heat exchangers in refrigeration systems more efficient and compact, passive methods for heat transfer enhancement produced by tubes in various shapes were surveyed and assessed. The tubes were classified into eight types by proposed classification method based on their geometrical features. The overall thermal-hydraulic performance of each type and the thermal-hydraulic performance of individual tubes in each type were elucidated using friction factor ratio, Nusselt number ratio, performance evaluation criteria (PEC) and enhancement efficiency in laminar and turbulent flow regimes. A critical friction factor ratio of 5, i.e. the friction factor of the tube with heat transfer enhancement is five times the factor of the plain tube, was introduced to assess these methods. The mechanism of heat transfer enhancement, entropy generation rate analysis, second law analysis and field synergy analysis were discussed. The twisted polygon tube, periodical convergent-divergent tube, helically corrugated tube and wavy tube suffer from high pressure drop and poor PEC. The twisted elliptical tube and eccentrical helical tube are the most suitable passive methods for enhancing heat transfer in CO2 heat exchangers due to lower pressure drop and better PEC. Vortex formation, development and thermal boundary layer disruption are associated with the mechanism of heat transfer enhancement in the twisted oval tube, twisted polygon tube, periodical convergent-divergent tube, helically corrugated tube, wavy tube and eccentrical helical tube. Entropy production rate analysis and field synergy analysis are applied in the periodical convergent-divergent tube and twisted oval tube. Heat transfer enhancement inside and outside the twisted oval tube and eccentrical helical tube under CO2 flow conditions is worth being studied in the future.

Introduction

Heat transfer enhancement is the process of improving the effectiveness of heat exchangers either to reduce their size or increase heat transfer rate or decrease pumping power for a fixed heat transfer duty. Heat transfer enhancement can be achieved by using active method, passive method or compound method to generate secondary flows or vortices or intensify turbulence in boundary layers [1,2,3]. The active method applied additional energy to the flow field to accomplish heat transfer enhancement. In the passive method, however, heat transfer enhancement does not rely on the additional energy. In the compound method, two or more active or passive methods are integrated to generate even better heat transfer enhancement than the individual method [1]. Passive methods do not require any external power input, but also have simple construction, high reliability and no moving parts, thus have found extensive applications.

Heat exchangers are important in carbon dioxide (CO2) refrigeration systems, and the effectiveness of the exchangers in gas side needs to be enhanced [4]. To select a potential passive method of heat transfer enhancement for heat exchangers in CO2 refrigeration systems, a survey and assessment was conducted on existing passive methods used in heat transfer enhancement. These basically include dimples, protrusions, rough elements, twisted tape inserts and nanocoating for pipes/tubes [5]. A later literature search indicates that heat transfer enhancement can be realised by using pipes/tubes in various shapes such as twisted oval tube, periodically convergent-divergent tube, twisted polygon tube, twisted multi-lobe tube, helically corrugated tube, conical tube, wavy tube, and eccentrically helical tube. A classification of this kind of methods for heat transfer enhancement is illustrated in Fig. 1.

Currently, there exist a large number of elegant review articles on the passive methods of heat transfer enhancement, as shown Table 1, especially the up-to-date contributions made by [6–13]. Further, the thermal-hydraulic performance of triangular cross-sectional duct was reviewed [14]. The heat transfer in coil heat exchangers with semi-circular, triangular, square, rectangular, trapezoidal cross-sections

* Corresponding author.
E-mail address: Zhibin.Yu@glasgow.ac.uk (Z. Yu).

https://doi.org/10.1016/j.ijft.2023.100511

Available online 4 November 2023

Nomenclature

a, b	semi-major and semi-minor axis lengths of an ellipse, respectively, mm
a	amplitude of the wavy wall as shown in Fig. 17, cm
A	heat transfer area of tube, m^2
Be	Bejan number
c_p	specific heat capacity of fluid at constant pressure, J/kg K
d	inner diameter of a tube, mm
d_0	inner diameter of a plain or reference tube, mm
d_1, d_2	diameter of base and envelope circles of a twisted multi-lobe tube, mm
d_h	hydraulic diameter of a tube or inner diameter of a coil tube, mm
d_{h0}	hydraulic diameter of a plain or reference tube, mm
d_n	nominal diameter of a twisted multi-lobe tube, d_n=0.5(d_1 + d_2), mm
D	coil diameter, mm
De	Dean number
e	lobe height (maximum radial distance of lobe profile to base circle) or profile height of corrugation, mm
f	Darcy friction factor of a tube with heat transfer enhancement
f_0	Darcy friction factor of a plain tube or a reference tube
h	convective heat transfer coefficient outside the tube bundle or in a tube with heat transfer enhancement, W/m^2 K
h_0	convective heat transfer coefficient in a plain or reference tube, W/m^2 K
i, j	coordinate index, i, j=1, 2, 3
ℓ	wavelength of a wavy wall in Fig. 17 or half wavelength of periodical serpentine channel in Fig. 30, cm
L	length of twisted elliptical tube
L_1, L_2	length of contraction and expansion segments in the channel shown in Fig. 18, mm
$\dot{m}$	mass flow rate of fluid in tube, kg/s
n	number of twists, $n = L/s$
n	shape factor of an ellipse
Nu	Nusselt number of a tube with heat transfer enhancement, $Nu = hd/\lambda$ or $Nu = hd_h/\lambda$
Nu_x	local Nusselt number at location x
Nu_0	Nusselt number of a plain tube or a reference tube, $Nu_0 = h_0d_0/\lambda$ or $Nu_0 = h_0d_{h0}/\lambda$
p_1	fluid pressure at inlet of tube, Pa
p_2	fluid pressure at outlet of tube, Pa
Pr	Prandtl number of fluid, $Pr = \nu/\alpha$
Pr_t	turbulent Prandtl number, $Pr_t = \nu_t/\alpha_t$=0.85
$\boldsymbol{q}$	heat flux vector, $\boldsymbol{q} = -\lambda\nabla T$, W/m^2
q_w	wall heat flux of tube, W/m^2
$\mathscr{R}$	equivalent diameter of the circle whose area is equal to the area of an ellipse, mm
$\mathscr{R}_c$	radius of curvature of bends, mm
R_{tube}	inner diameter of eccentrical helical tube, mm
R_{helix}	eccentricity of the helix of eccentrical helical tube, mm
Re	Reynolds number of a tube
Re_x	local Reynolds number at location x
s	twist pitch, m
$\dot{S}_D$	entropy generation rate by dissipations in fluid domain, W/K
$\dot{S}_H$	entropy generation rate by heat conduction and heat transfer in fluid domain, W/K
$\dddot{s}_{DD}$	specific entropy generation by direct viscous dissipation, W/m^3 K
$\dddot{s}_{ID}$	specific entropy generation rate by indirect (turbulent) dissipation, W/m^3 K
$\dddot{s}_{HC}$	specific entropy generation rate by heat conduction with mean temperature gradients, W/m^3 K
$\dddot{s}_{HT}$	specific entropy generation rate by heat transfer with fluctuating temperature gradients, W/m^3 K
T	temperature of fluid, K
T_e	temperature of fluid at edge of boundary layer, K
T_w	wall temperature of tube, K
T_0	environment temperature, K
T_1	fluid temperature at inlet of tube, K
T_2	fluid temperature at outlet of tube, K
u, v, w	fluid velocity in the primary flow direction x, normal direction y to the wall and spanwise direction z, respectively, m/s
U	overall heat transfer coefficient, W/m^2K
u^*, v^*	dimensionless values of u and v, respectively
$\boldsymbol{u}^*$, $\boldsymbol{v}^*$	vectors of u^* and v^*, respectively
u_e	velocity of fluid at edge of boundary layer, m/s
u_i, u_j	time-averaged velocities of fluid in coordinate directions i and j, where i, j=1, 2, 3, m/s
$\boldsymbol{V}^*$	vector of velocity with the components $\boldsymbol{u}^*$ and $\boldsymbol{v}^*$, $\boldsymbol{V}^*=\boldsymbol{u}^*+\boldsymbol{v}^*$, m/s
w	tape width of twisted tape insert or profile width of corrugation, mm
W_1, W_2	width of contraction and expansion segments in the channel shown in Fig. 18, mm
x, y, z	Cartesion coordinates of the twisted elliptical tube axis and tube inner wall, m
x_i, x_j	Cartesian coordinates in directions i and j, m
X_a	exergy (available energy), J
X_d	exergy destruction (loss), J

Greek

α	thermal diffusivity of fluid, m^2/s
α_t	thermal diffusivity caused by fluid temperature fluctuations in turbulent flows, m^2/s
β	angle between velocity victor and temperature gradient of fluid, °
Δp	pressure drop across the tube bundle, Pa
ε	dissipation rate of turbulent kinetic energy, m^2/s^3
η	heat transfer enhancement efficiency
η_X	second law performance
λ	thermal conductivity of fluid, W/m K
μ	dynamic viscosity of fluid, Pa.s
μ_t	dynamic viscosity of turbulent eddy, Pa.s
ν	kinematic viscosity of fluid, m^2/s
ν_t	turbulent eddy viscosity, m^2/s
θ	circumferential angle, rad
ρ	density of fluid, kg/m^3
$\boldsymbol{\tau}$	shear stress tensor due to velocity deformation of fluid, τ_{ij} = $0.5\mu(\partial u_i/\partial x_j + \partial u_j/\partial x_i)$, Pa
φ	nanoparticle volume concentration/fraction in a nanofluid, %
ψ	performance evaluation criteria of heat exchanger
ψ_{nano}	performance evaluation criteria of heat exchanger with nanoparticles in a fluid

Abbreviation

1D	one-dimensional
2D	two-dimensional
3D	three-dimensional
CFD	computational fluid dynamics
EHT	eccentrical helical tube
Exp	experimental
GNP–SDBS	graphene nanoplatelet–sodium dodecylbenzene sulfonate

LES	large eddy simulation	STEH	shell and tube heat exchanger
PCHE	printed circuit heat exchanger	TET	twisted elliptical tube
PEC	performance evaluation criteria	THT	twisted hexagonal tube
RANS	Reynolds-averaged Navier-Stokes	TMT	twisted multi-lobe tube
RNG	renormalisation group	TOT	twisted oval tube
SST	shear stress transport	TPT	twisted polygon tube
SWCNT	single-walled carbon nanotube	TST	twisted square tube

was reviewed [15]. A comprehensive review of Nusselt number correlations for channels with noncircular cross-section was documented [16]. However, a systematic review and comprehensive assessment of heat transfer enhancement approaches based on tubes in various shapes has not been reported. In this article, such a comprehensive review and assessment is conducted to find the most suitable heat transfer enhancement methods that can be applied to heat exchangers in CO2 refrigeration systems. First, the various methods based on tubes in various shapes in single-phase flow conditions are described, and the results achieved by them are explained by using friction factor ratio, Nusselt number ratio, performance evaluation criteria (PEC) and enhancement efficiency. Second, the best methods for heat transfer enhancement in CO2 heat exchangers in refrigeration systems are spotted and evaluated. Third, mechanisms of heat transfer enhancement and various thermodynamics analyses such as entropy generation rate, field synergy and second law analyses for those tubes are summarised and discussed. Finally, further work on those best methods is prospected.

The novelty of the article is as follows: (1) provide an approach for classifying the tubes in various shapes in heat transfer enhancement; (2) assesse the thermal-hydraulic performance of those tubes by using friction factor ratio, Nusselt number ratio, PEC and enhancement efficiency rather than listing empirical correlations of friction factor and Nusselt number collected from the literature; (3) select efficient heat transfer enhancement methods based on the proposed critical friction factor ratio of 5 and PEC value.

Various shapes of cross-sections

Besides tubes with circular cross-section, the other tubes/ducts/channels with various noncircular cross-sections in macro- or micro-level have also found applications in convective heat transfer. These cross-sections include semi-circular, elliptical, triangular, square, rectangular, trapezoidal, hexagonal, octagonal, tri-lobe and five-lobe cross-sections, as shown in Fig. 2.

Because of limitations in fabricating methods in micro-scale, the cross-section of microchannels often is noncircular. For example, the microchannels with noncircular cross-sections are mainly found in heat sinks cooled by water [48–52] or the mini-channels for heat transfer of supercritical carbon dioxide (SCO2) [53,54]. Additionally, the channels with noncircular cross-sections can make heat exchangers more compact [55,56]. For instance, the channels with hexagonal cross-section are employed in so called honeycomb heat exchanger for ordinary fluids [57,58,59] and SCO2 [60,61].

To evaluate advantages of the thermal-hydraulic performance of noncircular tubes over the circular tube, the friction factor ratio (f/f_0), Nusselt number ratio (Nu/Nu_0), enhancement efficiency (η) and PEC of the noncircular tubes (ψ) should be employed. The parameters η and ψ are defined as [62]:

$$\eta = \frac{Nu/Nu_0}{f/f_0}, \psi = \frac{Nu/Nu_0}{\sqrt[3]{f/f_0}} \tag{1}$$

where f and Nu are the friction factor and Nusselt number of a noncircular tube, respectively; f_0 and Nu_0 are the friction factor and Nusselt number of the circular tube, respectively. The ratios f/f_0 and Nu/Nu_0 account for the change in the friction factor and Nusselt number after heat transfer enhancement occurs. η specifies the gain in heat transfer over the penalty in friction factor after heat transfer enhancement. ψ is the ratio of heat transfer rate between the noncircular tube and the circular tube under identical pumping power. ψ must be higher than 1 for effective heat transfer enhancement.

The plots f/f_0-Re, Nu/Nu_0-Re, η-Re, ψ-Re represent the performance of a noncircular tube in heat transfer enhancement compared with the

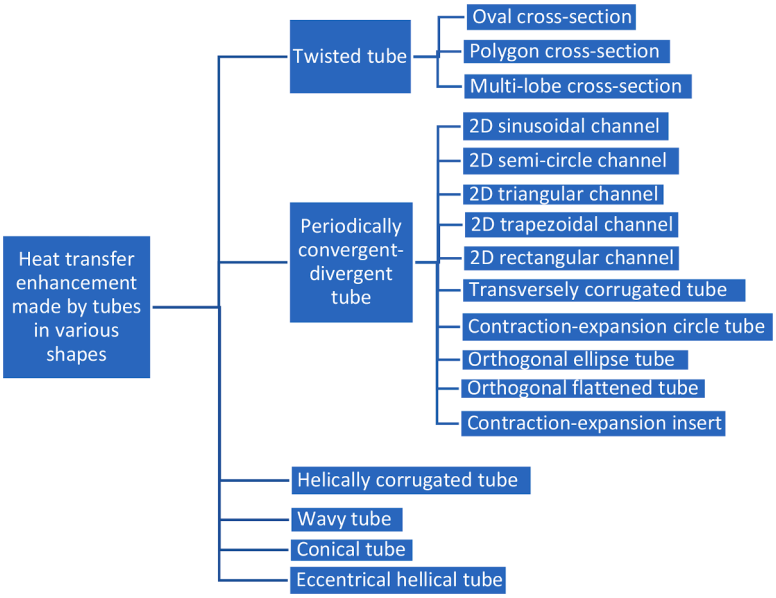

Fig. 1. Classification of passive heat transfer enhancement methods based on tubes in various shapes.

Table 1
Summary of existing review papers on passive methods of heat transfer enhancement.

Contributor	Ref	Passive method (device)
Gupta, Uniyal (2012)	[17]	Porous pin fin, perforated fin array, vortex generator, perforated fin, dimple, grooved fin
Gulia, Punia, Kamboj, Dahiya (2014)	[18]	Twisted tape insert
Kamel (2014)	[19]	Tube bank heat exchanger with vortex generator (delta winglet)
More, Shelke (2014)	[20]	Bump on divergent channel
Wang, Li, Zhang, Xu, Wu (2014)	[21]	Self-rotating insert
Patil, Tandale (2015)	[22]	Twisted tape insert, wire coil insert, conical insert, and conical strip insert
Prajapati, Mane, Mane, Gaikwad (2015)	[23]	Treated surface, rough surface, extended surface, displaced enhancement device, swirl flow device and additive for liquid
Sheikholeslami, Gorji-Bandpy, Ganji (2015)	[24]	Swirl flow device (rough element, corrugated tube, protrusion, diverging-converging tube, twisted tape insert, rib, conical nozzle insert, circular-ring turbulator, twisted ring and coil wire insert)
Thakare, Hole (2015)	[25]	Plate heat exchanger with circular and segmented ribs, rectangular and triangular ribs, and V-ribs
Kumar, Varun, Kumar (2016)	[14]	Triangular cross-sectional duct
Kurnia, Sasmito (2016)	[15]	Non-circular coiled tube
Sonawane, Patil, Chavhan, Dusane (2016)	[26]	Twisted tape insert and wire coil turbulator
Agrawal, Saha, Sharma (2017)	[27]	Shell and tube heat exchanger with elliptical twisted geometry
Gulave, Desale (2017)	[28]	W-shaped rib
Gugulothu, Reddy, Somanchi, Adithya (2017)	[29]	Twisted tape insert, and conical ring
Joshi, Bisht (2017)	[30]	Twisted tape insert
Mokashi, Mohite, Manthale, Lad, Mane (2017)	[31]	Rotating twisted tape insert
Omidi, Farhadi, Jafari (2017)	[32]	Double pipe heat exchanger (longitudinal fin, snail entry, swirl element, propeller-type turbulator, screw tape insert, spined pipe, pin fin, louvered strip, triangular fin, twisted wire brush, helical fin with vortex generator, helical fin with pin fin, coil wire insert, curved fined insert, agitator, two-side grooved tube, variable fin-tip thickness insert, triangular finned insert, out and inside ribs, perforated circular-ring, discontinuous helical turbulator, helical fin, perforated baffle, coil wire insert, circular-ring-wire net insert, grooved tube, various vortex generators)
Parmar, Desai (2017)	[33]	Twisted tape insert, and wire coil turbulator
Ghogare, Gore, Shaikh (2018)	[34]	Twisted tape insert, wire coil
Shriwas, D; Saini (2018)	[35]	Helical oil tube, dimpled tubes, tube with extended surface, twisted tape inserts, swirl vane, phase change material, and nanofluid
Thejaraju, Girish (2019)	[36]	Double pipe heat exchanger (twisted tape insert, coil wire insert, swirl element, louvered strip, helical fin and vortex generator, perforated circular-ring, agitator, discontinuous helical turbulator, plain and longitudinal tube, corrugated tube, twisted square tube, twisted oval tube and twisted tri-lobe tube)
Yousif, Khudhair (2019)	[37]	Twisted tape insert
Datt, Kumar, Bhist, Kothiyal, Maithani (2019)	[38]	Twisted tape insert
Kaggwa, Carson (2019)	[39]	Nanofluid in solar application and nano refrigerant
Ahmed, Abedi (2020)	[40]	Twisted tape insert, delta wing tape insert, wire coil insert, helical coil insert with rib, air foil-shaped insert, v-winglet, nanofluid with twisted tape insert, baffle, wire coil insert, and vortex generator
Sarmiento, Soares, Milanez, Mantelli (2020)	[16]	Circular and non-circular ducts in transition regime
Vora, Oza, Bhatt (2020)	[41]	Twisted tape insert, coil wire, rib, baffle, fin and corrugated surface
Akeedy, Alias, Salman (2021)	[42]	Nanofluid in helical coil and microchannel heat exchangers
Kulkarni, Rathnakumar, Dhanasekaran, Akthar (2021)	[43]	Nanofluid in helical coil heat exchanger
Sharma, Jilte (2021)	[44]	Circular/porous insert, insert with fin, twisted tape insert and other inserts for parabolic trough solar collector
Kumar, Birl (2022)	[45]	Effects of baffle orientation and shape in tube heat exchanger
Kumar, Jaurke (2022)	[46]	Helical tube heat exchanger (twisted square tube, corrugate tube, multi-inner tube)
Ajarostaghi, Zaboli, Javadi, Badenes, Urchueguia (2022)	[6]	Twisted tape insert, conical strip, baffle, winglet, fin, metal foam, helical coil, rough surface, wavy tube, nanofluid
Bhattacharyya, Vishwakarma, Srinivasan, Soni, Goel, Sharifpur, Ahmadi, Issakhov, Meyer (2022)	[7]	Swirl device (twisted tape insert, wire coil insert, ring shaped insert, vortex generator), artificial roughness, modified duct (duct with helical corrugation, dimpled duct, modified duct with insert, twisted tube, wavy channel)
Habibishandiz, Saghir (2022)	[8]	porous media, nanofluid, and microorganism
Li, Wang, Han, Li, Yang, Guo, Liu, Zhang, Zhang, Jiang (2022)	[9]	Concentric (double or triple) pipe heat exchanger
Li, Tan, Yuan, Wang, Wang (2022)	[10]	Twisted elliptical tube
Rukruang, Chimres, Kaew-On, Mesgarpour, Mahian, Wongwises (2022)	[11]	Alternating cross-section tube
Tavousi, Perera, Flynn, Hasan (2023)	[12]	Double pipe heat exchanger (twisted tape insert, coil wire insert, helical screw-tape, wavy strip, helical fin and vortex generator, split longitudinal fin, helical fin, perforated circular-ring, helical surface disk, diverging-converging tube, twisted square tube, corrugate tube, twisted oval tube, conical tube, inner rib, helically coiled tube, wavy tube)
Razzaq, Mushatet (2023)	[13]	Twisted tube heat exchanger (twisted elliptical tube, twisted square tube, twisted tape, ribs, twisted triangular tube, twisted circular tube, and conical ring)

circular tube, where *Re* is the Reynolds number of the noncircular tube. Based on the friction factor and Nusselt number data of the circular, semi-circular, square, triangular, rectangular, elliptical tubes in [53], the ratios f/f_0, Nu/Nu_0, and parameters η, ψ are calculated and illustrated Fig. 3. Since the ratio $f/f_0<1$ is observed, the hydraulic performance of the semi-circular, square, triangular, rectangular, elliptical tubes is better than the circular tube. This is because there are corners in a cross-section of noncircular tubes and secondary flows can emerge in the corners [63]. The secondary flow can enhance convective heat transfer over the tube wall and reduce the streamwise shear stress [64] and eventually decrease the friction factor in some degree. The situation of $Nu/Nu_0>1$, $\eta>1$ and $\psi>1$ occurs in a narrow range of Reynolds

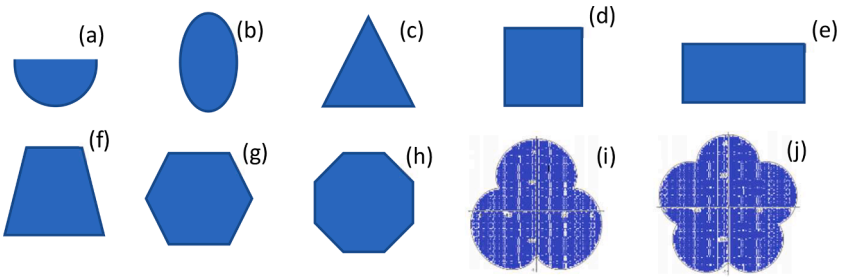

Fig. 2. Various cross-sections of tube used in forced convective heat transfer, (a) semi-circular, (b) elliptical, (c) triangular, (d) square, (e) rectangular, (f) trapezoidal, (g) hexagonal, (h) octagon, (i) tri-lobe, (j) five-lobe, (i) and (j) are adapted from [47].

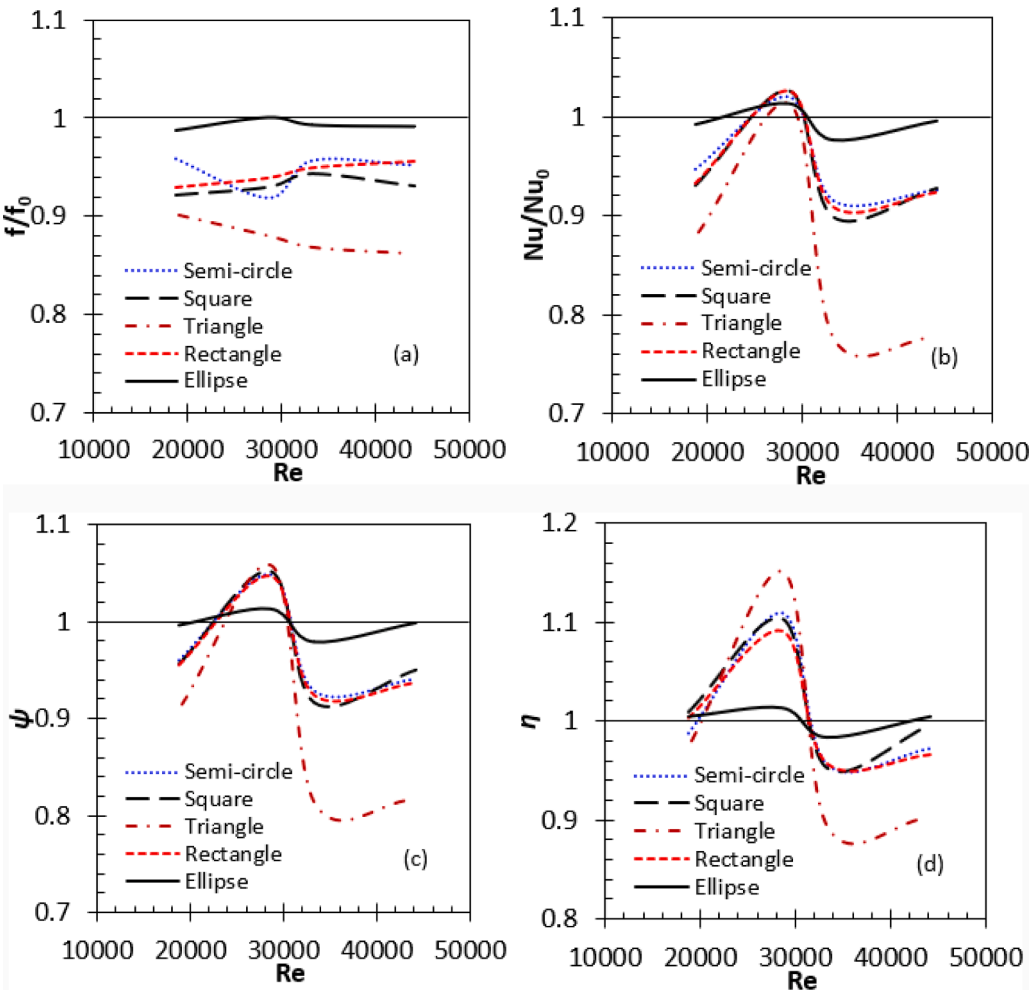

Fig. 3. Friction factor ratio f/f_0, Nusselt number ratio Nu/Nu_0, efficiency η and performance evaluation coefficient ψ of the noncircular tubes to the circular tube, the data after [53].

number only, so that the heat transfer enhancement caused by these noncircular tubes is quite limited.

To improve the heat transfer enhancement of noncircular tubes further, a variety of methods have been proposed by manipulating the noncircular cross-section along the tube axis. The aim of the manipulating is to intensify secondary flow or vortex near solid wall and enhance the convective heat transfer in the noncircular tubes. These methods have been illustrated in Fig. 1 and will be reviewed in the next section.

Tubes in various shapes

The passive heat transfer enhancement methods reviewed in this section include twisted oval tube(TOT), periodically convergent-divergent tube, twisted polygon tube(TPT), twisted multi-lobe tube (TMP), helically corrugated tube, conical tube, wavy tube and eccentrical helical tube(EHT). Except the twisted oval tube and conical tube, the rest methods are named in the paper based on their features in geometry. To evaluate the heat transfer enhancement of these methods, the plots f/f_0-*Re*, Nu/Nu_0-*Re*, η-*Re* and ψ-*Re* as well as Nu/Nu_0-f/f_0, η-f/f_0 and ψ-f/f_0 are presented. The plots f/f_0-*Re*, Nu/Nu_0-*Re*, η-*Re* and ψ-*Re* specify the influence of operational condition on the hydraulic-thermal

performance of an enhancing method, while the plots Nu/Nu_0-f/f_0, η-f/f_0 and ψ-f/f_0 reflect the economic-technical features of the method.

To obtain an overall situation, a summary of the eight passive methods based on tubes in various shapes found in the literature is presented in Table A1 along with their achievements in heat transfer enhancement in the supplemental material. Since the table is quite lengthy, it has to be put into the Appendix. The principal contributions made by the contributors are credited in the table. 67.6 % of results are obtained by using computational fluid dynamics (CFD), 20.5 % of results are achieved by experiment (Exp) and 11.3 % of results are gained by both. 83.5 % studies deal with the heat transfer enhancement inside the tubes, while 16.5 % studies pay attention to the heat transfer enhancement outside the tubes, i.e., in the annulus between the outer tube/shell and the inner tubes.

Twisted oval tube

Twisted oval/elliptical tube (TOT/TET) was proposed in the 1980′s [65–69] and the heat exchangers based on TOT have found extensive applications in chemical, petroleum, power, and steel industrial sectors [70]. An oval tube is the tube with a flattened cross-section by the forces on both sides in the opposite directions as shown in Fig. 4 in industry to reduce manufacturing cost. In research, however, the oval tube means the tube with an elliptical cross-section. TOT is the tube with twisted oval cross-sections along the tube axis. There are two parameters to describe the tube geometrical feature. The first parameter is the pitch s, which is the axial length after one cross-section is turned circumferentially by 360° against the reference cross-section. The second parameter is the aspect ratio a/b, which is the ratio of the major axis a to the minor axis b in length.

Six kinds of studies on heat transfer enhancement have been performed on TOTs, e.g., (1) inside TOT; (2) in the annulus between the outer tube and inner TOT; (3) in shell and tube heat exchanger with TOT; (4) cross TOTs; (5) inside helical coil with TOT; (6) inside U-shaped heat exchanger with TOT. The plots f/f_0-Re, Nu/Nu_0-Re, η-Re and ψ-Re extracted from these studies are shown in Fig. 5, while the plots Nu/Nu_0-f/f_0, η-f/f_0 and ψ-f/f_0 are exhibited in Fig. 6.

Generally, f/f_0=0.90–2.55, Nu/Nu_0=0.88–4.77, ψ=0.91–3.68, and η=0.97–2.52 at Re=1000–2000 and f/f_0=1.13–4.03, Nu/Nu_0=1.16–4.03, ψ=0.82–1.97, and η=0.50–1.40 at Re=2000–65,000 are observed. The heat transfer enhancement outside TOT is better than the enhancement inside TOT. Based on the f/f_0, Nu/Nu_0, ψ and η values, the regime for the best heat transfer enhancement by TOT is spotted at Re≤2000. The effect of TOT on heat transfer enhancement gets weak with increasing Re and becomes much poorer than that at Re≤2000.

Heat transfer inside TOT

In this kind of heat transfer enhancement, the straight TET with constant pitch usually was employed. Experimental and CFD methods were adopted to investigate and understand convective heat transfer inside a TET at constant wall heat flux or temperature. Water, air, propane and epoxy resin have been used as heat transfer fluid in the tube. Effects of aspect ratio and pitch on heat transfer enhancement were identified and optimal geometrical parameters were determined at different Reynolds numbers.

Effects of pitch ratio and aspect ratio. The effect of pitch ratio, aspect ratio and Prandtl number on heat transfer enhancement of TET was simulated by using an in-house CFD computer program in the laminar flow regime (Re=100–500) [71]. The pitch ratio and aspect ratio are defined as s/b and a/b, respectively. The results indicated that PEC rose with increasing Prandtl number, Reynolds number and a/b but declined with increasing s/b.

Five TETs were designed with the pitch ratios: 104/19.02, 152/19.02, 192/19.02 and aspect ratios: 1.60, 1.90, 2.15, 1.76, 1.49, respectively. Each TET was installed in an outer tube with a larger diameter than the TET. The TET was tested with hot water flowing inside the TET and cold water passing the annulus between the TET and the outer tube under counter-flow conditions. It was revealed that the TET with the pitch ratio of 104/19.02r and the aspect ratio of 1.60 had the best thermal-hydraulic performance such as f/f_0=2.0–3.5, Nu/Nu_0=1.5–4.9, ψ=1.3–3.7 at Re=600–55,000 [72]. Here the dimensionless pitch is defined as the ratio of the pitch to the tube inner diameter.

Five TETs with the pitch ratios: 250/20, 200/20, 150/20, 100/20 and aspect ratios: 24/14.5, 26/12.5, 27/11, 28/9, were designed. When

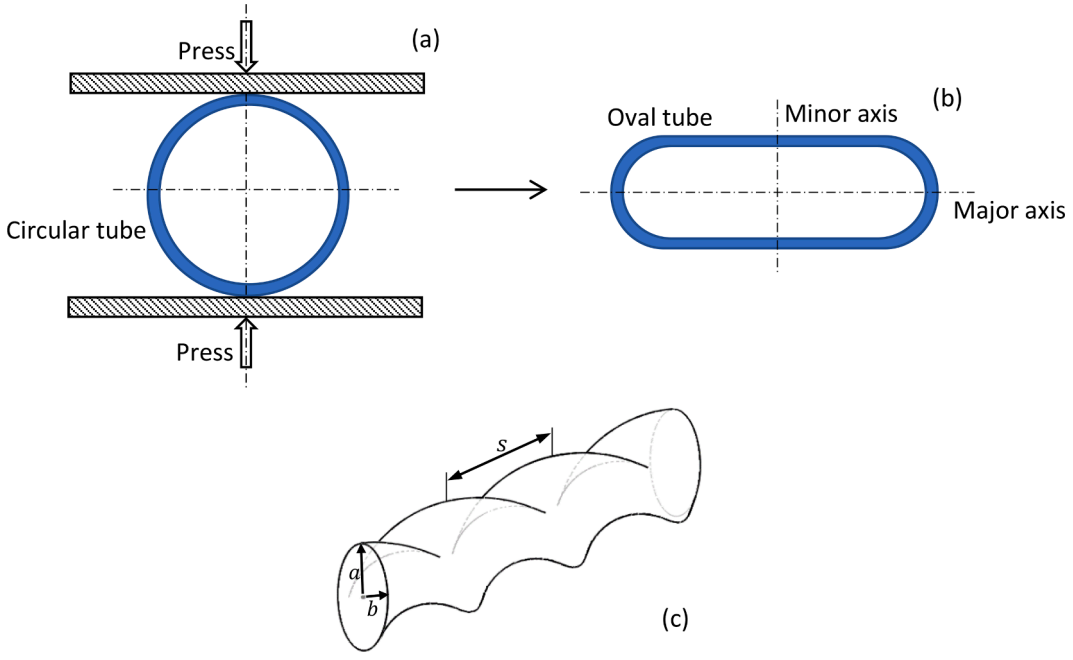

Fig. 4. A circular tube is pressed on both sides in the opposite directions to form an oval tube, and two parameters such as pitch $s$and aspect ratio a/b describing geometry of a twisted oval tube, (a) circular tube, (b) oval tube, and (c) two parameters.

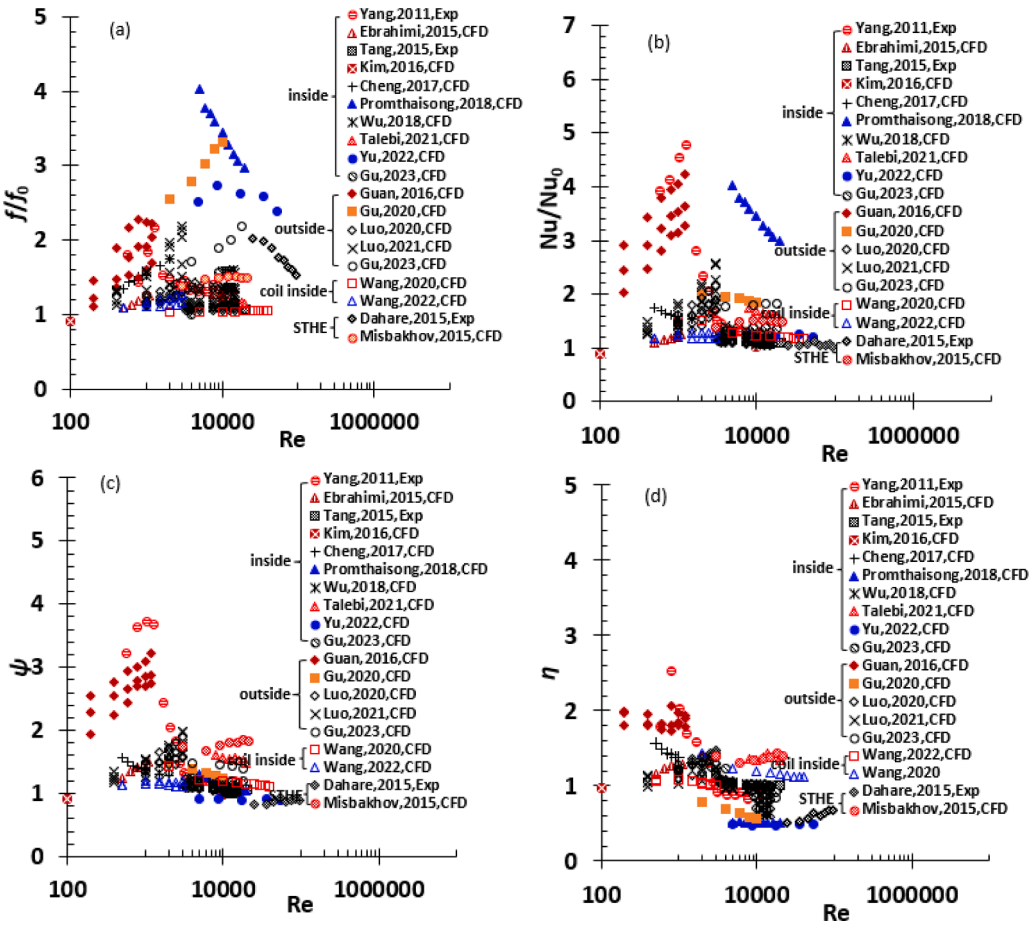

Fig. 5. Thermal-hydraulic Parameters f/f_0, Nu/Nu_0, ψ and η are plotted as a function of Reynolds number *Re* for twisted oval tubes, (a) f/f_0, (b) Nu/Nu_0, (c) ψ and (d) η, inside-heat transfer in side tubes, outside-heat transfer outside tubes, coil inside-heat transfer in coils with twisted oval tube, STHE-shell and tube heat exchanger.

the TET wall temperature was at 350 K, and the water entered the tubes at 300 K temperature, the convective heat transfer of water turbulent flow in these TETs was simulated by using the three-dimensional (3D), steady, incompressible Reynolds-averaged Navier-Stokes (RANS) equations, realisable *k*-ε turbulence model and energy equation in Fluent 6.3. The numerical results showed that the heat transfer coefficient and friction factor rose with increasing aspect ratio but declined with increasing pitch. The pitch ratio of 150/20 and aspect ratio of 28/9 resulted in the best heat transfer enhancement of ψ=1.65–1.73 at *Re*=8000–45,000 [73].

A TET with a pitch ratio of 200/20 and aspect ratio of 24.4/15 was tested under convective heat transfer conditions when the cold water flowed in the TET and the hot water passed through the tube outside in a counter-flow direction. Unfortunately, the heat transfer enhancement with ψ=1.02–1.09 was achieved only [74].

The convective heat transfer of water flowing in the TETs with the pitch ratio of 30 and the aspect ratios of 1.5, 2.0 and 2.5 was simulated at *Re*=500–1100 based on laminar flow model in Fluent 14.0 when the wall temperature was 348.15 K and the water inlet temperature was 298.15 K. The heat transfer enhancement was ranged in f/f_0=1.09–1.26, Nu/Nu_0=1.27–1.62, ψ=1.23–1.50, η=1.16–1.29, and the secondary flow generated by the twisted tube wall played a critical role in the augmentation of convective heat transfer [75].

The TETs with the numbers of twists of 1, 2, 3 and the aspect ratios of 2.5, 1.67, 1.25 were established mathematically. The convective heat transfer of air in those tubes was simulated based on the laminar flow model or the 3D, steady, incompressible RANS equations, realisable *k*-ε turbulence model and energy equation in Fluent 14.0 at *Re*=100, 1000, 10,000, when the tube wall was subject to 300 K temperature and the air temperature at the tube inlet was 400 K. The coordinates of the TET inner wall are described by [76]:

$$\begin{cases} y(\theta,x) = a\cos\theta\cos(2\pi nx/L) + b\sin\theta\sin(2\pi nx/L) \\ z(\theta,x) = b\sin\theta\cos(2\pi nx/L) - a\cos\theta\sin(2\pi nx/L) \end{cases} \quad (2)$$

where *a* and *b* are the semi-major and semi-minor axes, *x* is the coordinate of the TET axis, *y* and *z* are coordinates of the TET inner wall, *n* is the number of twists and is defined as the ratio of the tube length to the pitch, i.e. $n = L/s$, *s* is the twist pitch, *L* is the axis length of TET, θ is the circumferential angle. The best heat transfer enhancement was obtained as high as f/f_0=1.25, Nu/Nu_0=1.5, ψ=1.39, η=1.2 at *Re*=1000 and the number of twists of 1.25 [76]. These parameters were close to or below unit at the other Reynolds numbers.

Five TETs with a fixed number of twists of 3 and aspect ratios of 1.2, 1.4, 1.63, 1.8, 2, four TETs with a fixed aspect ratio of 1.63 and numbers of twists of 6, 4, 3, 2 were employed to investigate the effect of number of twists and aspect ratio on heat transfer enhancement numerically when water flowed in these TETs with a 300 K inlet temperature and a 350 K wall temperature at *Re*=500–2000. The 3D, steady, incompressible RANS equations, well-known low Reynolds number *k*-ε turbulence proposed by Jones and Launder and energy equation were used to simulate the convective heat transfer in these TETs in Fluent 6.3. The results demonstrated that the aspect ratio had little influence on heat transfer enhancement in laminar flow at *Re*=100 but affected largely on heat transfer enhancement in turbulent flow. PEC rose with increasing aspect ratio but reduced with decreasing number of twists. The maximum PEC of 1.7 was predicted at the aspect ratio of 2 and the number of twists of 3 and *Re*=350 [77].

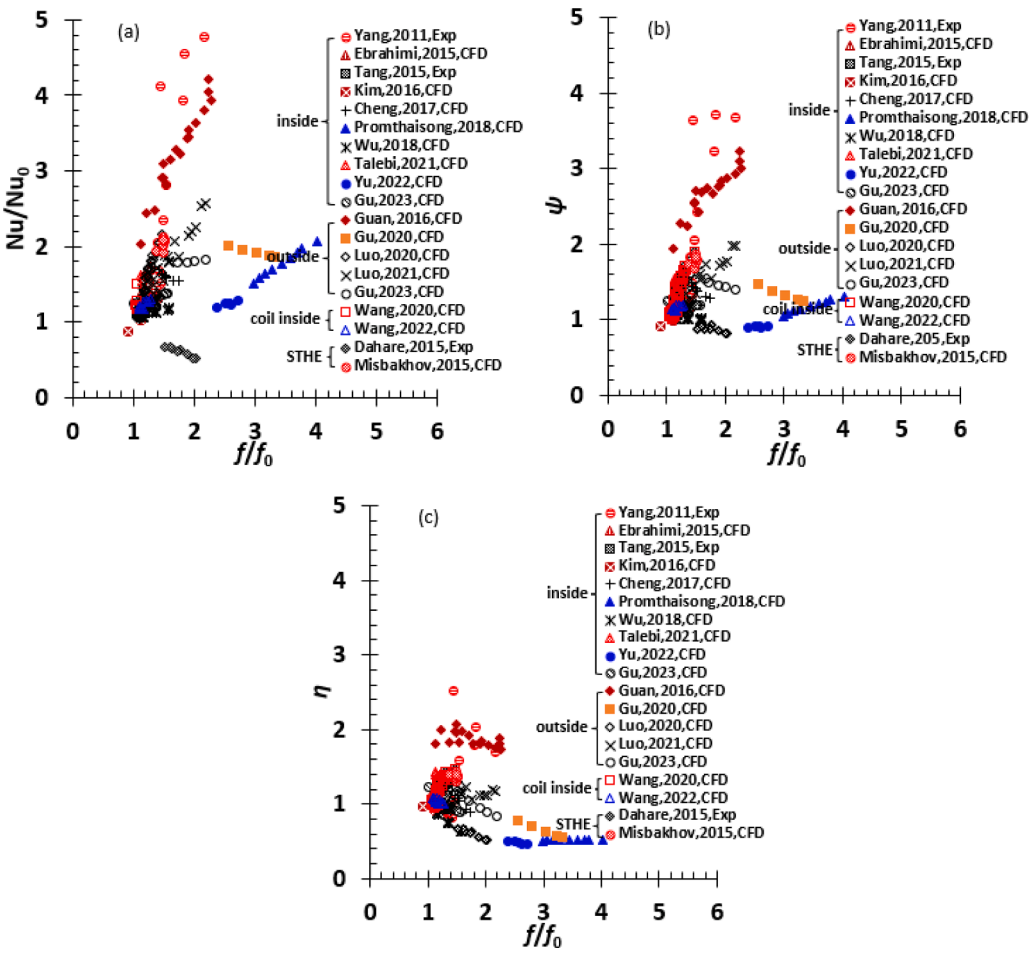

Fig. 6. Parameters Nu/Nu_0, ψ and η are plotted as a function of f/f_0 for twisted oval tubes, (a) Nu/Nu_0, (b) ψ and (c) η, inside-heat transfer in side tubes, outside-heat transfer outside tubes, coil inside-heat transfer in coils with twisted oval tube, STHE-shell and tube heat exchanger.

Three TETs with a fixed aspect ratio of 11.18/5.2 and numbers of twists of 8, 6, 4 were designed, and the convective heat transfer of water in turbulent flow inside them was simulated using the 3D, steady, incompressible RANS equations, Wilcox *k*-ω turbulence model and energy equation in Fluent 15.0 at *Re*=10,000–15,000, when the water temperature was 330 K at the TET inlet and the TET wall temperature was at 300 K. The number of twists had a critical influence on the thermal-hydraulic performance of TET and the best performance was achieved at the number of twists of 6. The TET could suppress the entransy- (heat transport potential capacity, which is a product of heat and temperature [78]) dissipation-based thermal resistance to benefit heat transfer greatly [79].

The experiment of forced convective heat transfer enhancement on titanium alloy TET with a pitch ratio of 10.5 and aspect ratio of 23.5/13.5 (1.74) was performed when water flowed in the TET with a 30 °C inlet temperature at *Re*=19,000–55,000 and the tube was heated uniformly outside by using an electrical coil heater. The empirical correlations for friction factor and Nusselt number were obtained based on the experimental data, and ψ=1.34–1.32 was held at *Re*=19,000–55,000 [80].

The TETs with aspect ratios: 1.06, 1.09, 1.11, 1.14, 1.16, 1.25, 1.42, 1.67 and pitch ratios: 0.6, 0.8, 1, 1.5, 2, 2.5, 3, 3.5, 4 were generated, respectively, and the forced convective heat transfer of air flowing in them at *Re*=5000–20,000 was simulated based on a periodic module-computational domain under a constant inwards wall heat flux of 600 W/m^2. The 3D, steady, incompressible RANS equations, realisable *k*-ε turbulence model and energy equation in Fluent were employed in heat transfer simulations. The results showed that a small aspect ratio and large pitch ratio could reduce the pressure drop. The maximum PEC of 1.30 was estimated at the aspect ratio of 1.11, pitch ratio of 0.6 and *Re*=50000 [81].

A TET with the pitch ratio of 150/20 and aspect ratio of 24/14.5 was generated, and the forced convective heat transfer of water turbulent flow in it was calculated numerically by making use of the 3D, steady, incompressible RANS equations, shear stress transport (SST) *k*-ω turbulence model and energy equation in Fluent when the TET wall temperature was 350 K and the water inlet temperature was 300 K at *Re*=8000–20,000. It was demonstrated that the heat transfer coefficient and pressure drop of the TET were increased by 18 % and 65 %, respectively, compared with the untwisted straight elliptical tube in the same size [82].

The TETs with pitch ratios of 50/17(2.94), 100/17(5.88), 200/17 (11.76) and aspect ratios of 1.5, 2 were designed and the forced convective heat transfer of water flowing in the TETs at *Re*=4062–26,998 was predicted numerically under a constant inwards wall heat flux of 50 kW/m^2. The 3D, steady, incompressible RANS equations, *k*-ω turbulence model and energy equation in Fluent were selected in the simulations. The numerical results showed that the heat transfer was positively affected as the aspect ratio increased and the pitch ratio decreased. The best PEC value of 1.39 was observed at the aspect ratio 2 and pitch ratio of 50/17 and Reynolds number of 4524 [83]. The ratio of the entropy generation rate in the TET and plain circular tube was calculated after CFD simulations were finished, and second law efficiency was estimated. The minimum entropy generation rate and maximum second law efficiency were found at the aspect ratio of 2 and pitch ratio of 50/17 [84].

Nine TETs were designed and manufactured at pitch ratios of 25, 18.75, 12.5 and aspect ratios of 2.13, 3.03, 3.70. The forced convective heat transfer in these TETs was tested in a counter-flow tube-in-tube heat exchanger by using epoxy resin at *Re*=25–110. The liquid of epoxy resin is non-Newtonian fluid, and the thermo-physical properties of the liquid are dependent on temperature. The empirical correlations of *Nu* and *f* as a function of Reynolds number, pitch ratio and aspect ratio for the TETs were cast based on the corresponding experimental data. Compared with pitch ratio, aspect ratio is a chief factor affecting pressure drop and heat transfer performance of TETs for the liquid of epoxy resin [85].

Effect of twist direction. Two cases: the first is tube twisted in one direction only; the second is the tube twisted in two alternative directions were investigated numerically. Under the same flow and thermal conditions, the TET in the first case was subject to the better heat transfer enhancement than that in the second case due to the stronger helical flow [81].

Effect of wall temperature and wall heat flux. The TETs with the pitch ratios: 1.67, 1.43, 1.25 and aspect ratios: 3, 4, 5 were used to investigate the effect of uniform wall temperature and uniform wall heat flux on heat transfer enhancement in laminar flow regime. The force convective heat transfer of air passing through these tubes was calculated numerically at *Re*=600, 700, 800, and 70 °C wall temperature or 30 W/m^2 wall heat flux. The mechanism for the phenomenon, where a larger local Nusselt number in the uniform wall temperature boundary condition than that in the uniform wall heat flux boundary condition in some regions was observed in the TETs, was clarified. The velocity and its gradient contributions to the transport of the heat flux were numerically examined by using the transport equations of heat flux [86]:

$$\frac{D\boldsymbol{q}}{Dt} + \boldsymbol{\tau}\cdot\boldsymbol{q} = \alpha\nabla^2\boldsymbol{q} \tag{3}$$

where α is thermal diffusivity of air, m^2/s, $\boldsymbol{q}$ is heat flux vector, $\boldsymbol{q} = -\lambda\nabla T$, λ is thermal conductivity of air, $\boldsymbol{\tau}$ is shear stress tensor because of the velocity deformation of air, $\tau_{ij} = 0.5\mu(\partial u_i/\partial x_j + \partial u_j/\partial x_i)$, μ is dynamic viscosity of air, x_i and x_j are the Cartesian coordinates in i and j directions, respectively; i and j are coordinate index, i, j=1, 2, 3. It was shown that the velocity and its gradient made a greater contribution to the transport of the heat flux nearly normal to the wall in the uniform wall heat flux boundary condition than in the uniform wall temperature boundary condition in most regions to produce a larger local Nusselt number in a TET in the uniform wall heat flux boundary condition. In some regions, however, the velocity and its gradient contributions to the transport of the heat flux nearly normal to the wall were larger in the latter boundary condition than in the former boundary condition to generate a higher local Nusselt number.

Effect of twisted tape insert. A TET with a pitch ratio of 200/23.1 and an aspect ratio of 29/19.5 was designed. Seven twisted tape inserts, such as solid one-tape, triple-tape, four-tape, five-tape, perforated one-tape, centrally hollow one-tape and ribbed solid one-tape inserts, were installed in the TET, respectively. The forced convective heat transfer of water in turbulent flow through the TET was numerically calculated based on the 3D, steady, incompressible RANS equations, *k*-ω turbulence model and energy equation in Fluent as the tube wall temperature at 373.15 K and the water inlet temperature at 300 K and *Re*=5000–53,000. The Nusselt number and friction factor of the tube with twisted tape insert were increased by 23.4–35.6 % and 149.5–432.6 % compared with the TET without twisted tape insert, respectively. The largest PEC value was found in the TET with the centrally hollow one-tape insert. The PEC declined with increasing number of tapes in an insert, the twist direction of tape against the TET influenced heat transfer rate in minor except for the centrally hollow tape insert [87].

Heat transfer enhancement outside TETs

The heat transfer enhancement outside TETs is related to the forced convective heat transfer in the annulus between the outer tube and the inner TET in a tube-in-tube heat exchanger or the annulus between the shell tube and the bundle of TETs in a shell and tube heat exchanger. Two types of study on this issue can be found in the literature: one is the study on the heat transfer in the annulus alone at a fixed twisted elliptical tube wall temperature; the other one is the study on the heat transfer in a whole heat exchange but the results in the annulus are extracted and analysed only. The studied topics include the effects of pitch and aspect ratios and twist direction of individual tube in a TET bundle on the heat transfer enhancement in the annulus.

Effect of pitch and aspect ratios outside single TET. The TETs with pitch ratios: 200/18.65, 200/16.36, 200/14.97, 150/14.97, 250/14.97 and aspect ratios: 1.54, 2.02, 2.47 were created, and assembled into an outer tube with a diameter of 30 mm, respectively, to form a counter-flow tube-in-tube heat exchanger. The forced convective heat transfer of water flowing in the annulus between the TET and the outer circular tube was simulated based on the 3D, steady, incompressible Navier-Stokes equations and energy equation in laminar regime (*Re*=200–1200) when the TET wall temperature was 373 K and the water temperature was 300 K at the TET inlet. The PEC rose with increasing aspect ratio and decreasing pitch ratio. The best PEC occurred at the pitch ratio of 150/14.97 and aspect ratio of 2.47 [88].

A TET was accommodated in a straight untwisted smooth elliptical tube to form a tube-in-tube heat exchanger. The pitch ratios were 10, 15, 20 and the aspect ratios were 2.5, 2, 1.67 for the TET, respectively. The forced convective heat transfer of water in turbulent flow through the tube was predicted numerically based on the 3D, steady, incompressible RANS equations, renormalisation group (RNG) *k*-ε turbulence model and energy equation in Fluent when the TET wall temperature was fixed at 363 K and the air inlet temperature was given at 293 K and *Re*=4000–15,000. The heat transfer in laminar regime was simulated without the turbulence model at *Re*=1000–3000, too. It was indicated that there was a symmetrical secondary flow in the annulus to improve the heat transfer greatly. The Nusselt number rose with increasing aspect ratio and decreasing pitch ratio. The largest Nusselt number was improved by 116 % but the friction factor was increased by 46 % to raise the PEC up to 1.9 in the case where the pitch and aspect ratios were 10 and 2.5 at *Re*=3000 in comparison with the case where the inner tube is another straight untwisted smooth elliptical tube [89]. The empirical correlations for Nusselt number and friction factor were established as a function of pitch and aspect ratios and Reynolds number in both laminar and turbulent flow regimes.

The straight untwisted outer elliptical tube in [89] was replaced with a TET, thus a double twisted elliptical tube heat exchanger was generated. The twist directions of both the TETs were opposite. The forced convective heat transfer of air in the annulus between the two twisted elliptical tubes was simulated at *Re*=1000–3000 and 4000–15,000 when the pitch and aspect ratios of the inner TET varied. A strong secondary flow was identified in the twisted annulus to enhance the heat transfer significantly. The maximum Nusselt number and friction factor were enhanced by 157 % and 118 % compared with those in the annulus between the straight untwisted outer elliptical tube and an inner TET. As a result, the best PEC value was achieved at 1.98 [90].

Heat transfer enhancement outside TET bundle.

1) Effects of pitch and aspect ratios

The forced convective heat transfer in the annulus of the shell tube and the TET bundle was simulated by employing the 3D, steady,

incompressible RANS equations, realisable k-ε turbulence model and energy equation in Fluent 6.3 when the TET wall temperature of 350 K and the water inlet temperature of 300 K were imposed at Re=5000–25,000. The aspect ratios of the TETs were 1.51, 2, 2.45, 2.8, and the pitch ratios were 80/19.4, 80/16.86, 80/14.94, 50/13.92, 80/13.92, 110/13.92/140/13.92, respectively. The numerical results supported that the Nusselt number and friction factor rose with increasing pitch and aspect ratios. Spiral secondary flow was found in the shell side and its intensity was intensified with increasing aspect and pitch ratios, especially in the cases with the aspect ratio of 2.8 [91].

The forced convective heat transfer in the gap of a TET bundle was simulated by using an explicit filtering large eddy simulation (LES) method in the spectral element CFD code Nek5000 based on periodic domains of triangular and square unit cells surrounding a single TET. The 3D, unsteady, incompressible Navier-Stokes equations and energy equation were adopted in the simulations. The heat transfer in the flow inside the TETs was excluded from the simulations. For the square unit cell, increasing gap between the TETs could reduce friction factor by 11 % and increase Nusselt number over the TETs by more than 20 % in laminar flow regime; in turbulent flow regime, however, the increasing gap reduced friction factor by less than 5 %. For the triangular unit cell, increasing gap could reduce friction factor by 13 % and increase the Nusselt number by about 30 % in laminar flow regime. In turbulent flow regime, the increasing gap could reduce friction factor by less than 5 %. These facts suggest that the gap size exhibits a minor effect on convective heat transfer enhancement outside a TET bundle in turbulent flow regime but a significant influence in laminar flow regime [92].

The forced convective heat transfer of water in a shell and TET heat exchanger in counter-flow mode was numerically predicted by employing the 3D, steady, incompressible RANS equations, SST k-ω turbulence model and energy equation in ANSYS CFX at Re=3000–20,000. The water temperatures at the inlet of the shell and the inlet of the bundle of four TETs were 95 °C and 8 °C, respectively. The twist ratio of the TETs was 2.5. The parameters of f/f_0=1.38–1.52, Nu/Nu_0=1.92–2.12, ψ=1.69–1.86 and η=1.30–1.43 were predicted in the annulus between the shell tube and the bundle of four TETs at Re=3000–20,000 in comparison with the case of plain tube bundle [93].

A counter-flow square channel and TET heat exchanger was proposed and manufactured. The exchanger was composed of a square channel and a bundle of nine TETs. There is a slot on top of the channel near outlet of the TET for warm air at a temperature of 308.15 K to flow into the shell. The opening areas of the slot such as 56.7, 49.14, 41.85 cm^2 were set to alter the inflow flow rate. The cold air with a temperature of 300.15 K was enforced to flow into the TETs in the bundle. The TETs have an aspect ratio of 12/7.77(≈1.54) and the twist ratios of 700/120, 700/100, 700/80. The forced convective heat transfer in the space between the square shell and the bundle was simulated using the 3D, steady, incompressible RANS equations, standard k-ε turbulence model and energy equation in Fluent 18.0. The numerical results showed that the heat transfer coefficient outside the bundle h and the pressure drop across the bundle Δp were decreased with increasing opening area, but the parameter $h/\sqrt[3]{\Delta p}$ varied a little at a fixed air flow rate through the TETs. The heat transfer coefficient h was increased, but the pressure drop Δp and the parameter $h/\sqrt[3]{\Delta p}$ were increased with decreasing pitch. There was a notable spiral flow along the outside wall of the TETs to mix the inflow air and enhance the external heat transfer effect [94].

The effect of twist direction of TETs in a TET bundle on heat transfer in the annulus between the shell and the bundle in a shell and TET heat exchanger was investigated numerically. Two cases were specified: the first is that the central TET is surrounded by the other TETs with the opposite twist direction to the central TET, and the second is that all the TETs in the bundle are in the identical twist direction. The forced convective heat transfer of water in the annulus was predicted numerically using the 3D, steady, incompressible RANS equations, RNG k-ε turbulence model and energy equation in Fluent at Re=2000–10,000 when the TET wall temperature was 350 K and the water inlet temperature was 300 K. The aspect ratios of TETs were 1.5, 2, 3, the pitches were 50, 100, 200 mm, the shell inner diameters were 94, 104, 110 mm, respectively. Basically, the Nusselt number, friction factor and PEC were increased, and the secondary flow became more intense with increasing aspect ratio and decreasing pitch. Compared with the second case, a more uniform temperature field was obtained in the first case, especially the Nusselt number, friction factor and PEC were improved by 12.8 %, 15.2 % and 7.6 %, respectively. The smaller the pitch or the closer to 1 the aspect ratio, the more advantage the first case [95].

A shell and TET heat exchanger with a spiral baffle around the bundle of TETs was designed and the forced convective heat transfer of water flowing in the space between the shell and the TET bundle was analysed numerically when the mass flow rate of water varied in 5.15–15.45 kg/s at a given inlet temperature of 293.15 K and the TET wall temperature was fixed at 393.15 K. The 3D, steady, incompressible RANS equations, realisable k-ε turbulence model and energy equation were employed based on Fluent. The aspect ratio of the TETs was 2, the centre-to-centre gap between the TETs was 25 mm, and the helix angle of the spiral baffle was 15° and 20°, respectively. It turned out that the flow velocity distribution in the shell side of the heat exchanger with a spiral baffle and the bundle of TETs was more uniform and the velocity was increased more near the tube wall than the exchanger with a spiral baffle and a bundle of circular plain tubes. Moreover, the baffle with helix angle of 15° resulted in the shell and TET heat exchanger to have the best thermal-hydraulic performance, i.e. the heat transfer coefficient was improved by 3.3 % and the pressure drop was reduced by 17.1–19.1 %, and the PEC was enhanced by 21.5–22.5 % in comparison with the heat exchanger with the bundle of circular plain tubes [96].

2) Optimisation of pitch and aspect ratios

The forced convective heat transfer of water in the space between the shell and the bundle of TETs in a shell and TET-rod-baffle heat exchanger was simulated based on the 3D, steady, incompressible RANS equations, standard k-ε turbulence model and energy equation in Fluent, when the water velocity varied in 0.1–0.5 m/s at a fixed inlet temperature of 300 K and the TET wall temperature was at 350 K. The pitch and aspect ratios were also altered in the simulations. Heat transfer coefficient and pressure drop were used as the objective functions to optimise the inlet velocity, pitch and aspect ratios by using the genetic aggregation response surface models obtained from the simulations. The sensitivity analysis indicated that the inlet velocity has the most, but the pitch ratio has the least influence on the heat transfer coefficient and pressure drop, the aspect ratio is in between. Compared with the reference heat exchanger, the heat transfer coefficient was increased by 19.17 % and the pressure drop was decreased by 5.74 % after the optimisation [97,98].

Heat transfer enhancement in various heat exchangers

TETs have found applications in counter-flow shell and tube heat exchanger, cross-flow serpentine tube heat exchanger, cross-flow shell and U-shaped tube heat exchanger, cross-flow tube heat exchanger and coil tube heat exchanger. The studies on those heat exchangers were mainly focused on the effects of geometrical parameters of TET on the thermal-hydraulic performance of those exchangers. However, most of the studies tried to provide the heat transfer coefficients in either the tube side or shell side or tube outside rather than the overall heat transfer coefficient. A guideline for the design of those heat exchangers with TET is unlikely established currently.

Counter-flow shell and TET heat exchanger. The forced convective heat transfer inside the TET of a TET-in-TET heat exchanger was measured at Re=1000–17,000 when the diesel and steam flowed in the TET and the annulus between the TET and the outer tube, respectively. The TETs

were subject to three pitch ratios: 11.9, 9.14 and 8.86. The convective heat transfer in the annulus between the shell tube and the bundle of seven TETs with pitches of 0.2 m and 0.3 m was tested when cold water flowed in the bundle but hot water in the annulus at Re=1000–9000. The reference heat exchanger is shell and tube heat exchanger with a spiral groove inner tube bundle. The experimental Nusselt number and friction factor were best fitted to generate empirical correlations. It was confirmed that the thermal-hydraulic performance of the bundle was better at Re<5000, but the performance of the annulus was higher at Re<8000 [99].

A shell and TOT heat exchanger was designed and manufactured, its performance was tested at water velocity of 3 m/s in the TOT and 1.5 m/s in the shell side. The TOT was made of aluminium and consists of the cross-section as shown in Fig. 4(b). The estimated heat transfer coefficient was ranged in 1.74–10.86 kW/m^{2}K [100].

Two types of experiment on forced convective heat transfer were conducted in [101], one was the heat transfer of water in a single TET, and one is the heat transfer in the annulus between the shell tube and the TET bundle. As usual, the heat transfer coefficient and pressure drop inside the TET were greater than inside a smooth circular tube. The heat transfer coefficient outside the TET bundle was higher and the pressure drop was smaller than outside the circular tube bundle in a reference rod-baffle heat exchanger. It was suggested that TET heat exchangers had a more effective thermal-hydraulic performance at a low tube side flow rate but a high shell side flow rate [101]. The corresponding correlations predicting the thermal-hydraulic performance of a shell and TET heat exchanger were proposed based on the experimental data.

A counter-flow shell and TET heat exchanger was designed and fabricated. The exchanger included a circular shell tube and a bundle of seven TETs which have an aspect ratio of 2.8 and twist ratio of 6.9. The forced convective heat transfer inside the shell (hot thermal oil, Re=300–2050) and TET (cold water, Re=12,000–45,000) was tested. The reference heat exchangers were an ordinary shell and tube heat exchanger and a spiral groove shell and tube heat exchanger. The experimental results indicated that the shell and TET heat exchanger exhibited a better heat transfer enhancement effect than the two reference heat exchangers in laminar and turbulent flow regimes. The correlations of Nusselt number and friction factor were established according to the corresponding experimental data [102].

A counter-flow shell and TET heat exchanger was investigated when the TET was subject to the aspect ratios of 1.4, 1.7, and 2, respectively. The forced convective heat transfer of water flowing inside and outside the TETs was simulated separately by using a bulk temperature of 293.15 K and a TET wall temperature of 393.15 K and a periodic computational domain based on the 3D, steady, incompressible RANS equations, RNG k-ε turbulence model and energy equation in Fluent at Re=4000–18,000. It was demonstrated that the pressure drop, heat transfer coefficient and PEC of the TET and shell sides rose with increasing aspect ratio. The heat transfer coefficient and PEC of the TET were improved by 25.17–38.28 % and 18.56–24.21 %, but those of the shell side were increased by 117.99–126.53 % and 40.82–48.28 % at the aspect ratio of 2 [103].

Cross-flow serpentine TET heat exchanger. A cross-flow serpentine TET heat exchanger was proposed for radiators and air conditioners in vehicles. The forced convective heat transfer of the heat exchanger was tested and predicted when hot water flowed in the TET and air flow was crossed the exchanger. The 3D, steady, incompressible RANS equations, standard k-ε turbulence model and energy equation were employed in the prediction in Fluent 14.5 at Re=50,000–350,000. Because the experimental and predicted overall heat transfer coefficients were as large as 500 to 2500 [104], they seemed unrealistic, further confirmation on them is needed.

Cross-flow shell and U-shaped TET heat exchanger. A cross-flow shell and U-shaped TET heat exchanger was designed and constructed and tested when hot air passed through the bundle of ten U-shaped TETs in the shell tube and cold water flowed inside the TETs at Re=25,000–126,000. The Nusselt number, friction factor, pressure drop, and overall heat transfer coefficient were calculated and analysed based on the experimental data of heat transfer. The overall heat transfer coefficient U of the heat exchanger with U-shaped TET bundle was better by 2.23–8.48 % than the exchanger with plain tube bundle [105], see Fig. 7, depending on Reynolds number.

Cross-flow TOT heat exchanger. A cross-flow TOT heat exchanger was proposed and manufactured. The heat exchanger consisted of a bundle of TOTs. Hot water flowed in the TOTs in the bundle and the cold air flowed over the bundle in the cross-flow direction to take heat away. An experiment on forced convective heat transfer in the heat exchanger was performed when the TOTs were staggered in the bundle and the Reynolds number of the air flow varied in 7500–18,000. The air side heat transfer and pressure drop were obtained and correlated to Reynolds number. However, the PEC of the air side was as low as 1.01–1.06 only [106]. The overall heat transfer coefficient is shown in Fig. 7.

The forced convective heat transfer of air flow around the cross-flow TOT heat exchanger in [106] was simulated based on the 3D, steady, incompressible RANS equations, realisable k-ε turbulence model and energy equation in Fluent at Re=600–17,000 by using a periodic fluid domain. The effects of aspect ratio, twist pitch, transverse tube gap, longitudinal tube gap, pitch, diagonal tube gap, and number of TOTs in a bundle on the thermal-hydraulic performance of the heat exchanger were analysed based on CFD results. The air side overall heat transfer coefficient, Nusselt number and pressure drop were correlated to Reynolds number [107]. The corresponding overall heat transfer coefficient is illustrated in Fig. 7.

Coil TET heat exchanger. A TET (aspect ratio=6/4.37) was applied to a coil (helix angle=21.4°, coil diameter D=102 mm, tube diameter d_h=10 mm) heat exchanger and the forced convective heat transfer of water in the coil was tested and simulated at Re=2000–4000. The 3D, steady, incompressible RANS equations, realisable k-ε turbulence model and energy equation in Fluent were adopted in the simulations when the water inlet temperature was 293.15 K and the TET wall temperature was 353.15 K. The PEC=1.24–1.2 was observed for the coil TET heat exchanger in comparison with a plain coil heat exchanger [108].

The forced convective heat transfer of propane flowing in a TET coil

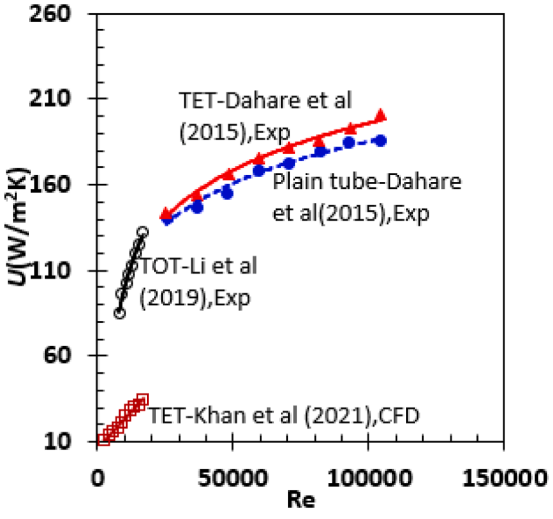

Fig. 7. Overall heat transfer coefficient of the cross-flow heat exchanger with U-shaped twisted ova tube bundle or with plain tube bundle, the data after [105,106,107].

was calculated numerically using the 3D, steady, incompressible RANS equations, RNG k-ε turbulence model and energy equation in Fluent at Re=4000–16,000. The TET twist pitch and aspect ratio varied in 20–100 mm and 1.2–2, while helix angle and radius were changed in 8–12° and 1000–1400 mm, respectively. The results showed that the friction factor and Nusselt number rose with increasing aspect ratio and decreasing twist pitch. The PEC varied in 0.76–1.13 for the TET coils with the geometrical and flow parameters considered [109].

A TET coil was designed with four pitch ratios and four aspect ratios, respectively. The forced convective heat transfer of water or Al_2O_3 nanofluids was predicted in Fluent using the 3D, steady, incompressible Navier-Stokes equations and energy equation in laminar regime at Re=500–3000, inlet temperature of 293.15 K and TET wall temperature of 353.15 K. Compared with the smooth coil, the PEC was ranged in 1.04–1.21 and 1.02–1.23 when the aspect ratio and pitch ratio varied. The effect of Prandtl number on heat transfer enhancement was investigated by using ethylene-glycol and engine-oil as well. It was found that the Nusselt number of engine-oil was 6–6.8 times higher than water. The Nusselt number of nanofluids was higher by 2–18 % than water with increasing Reynolds number and nanoparticle concentration [110].

A TET coil heat exchanger was designed by changing the coil diameter D to study the effect of curvature ratio d_h/D on the thermal-hydraulic performance of water flowing in the exchanger at Re=250–2000. The performance of the exchanger was estimated by using Star-CCM+ based on the 3D, steady, incompressible Navier-Stokes equations and energy equation in laminar regime. The TET had a fixed aspect ratio of 2 and was subject to an isothermal wall temperature of 350 K and a water inlet temperature of 300 K. The TET resulted in an increased Nusselt number, and a slightly increased friction factor compared with the plain coil heat exchanger. The best heat transfer enhancement occurred at d_h/D=0.17 and the corresponding enhancement efficiency was 1.45–1.55 [111]. The correlations of Nusselt number and friction factor were best fitted.

Twisted polygon tube

Twisted polygon tube (TPT) is the twisted tube with a polygon cross-section such as triangular, square, rectangular, trapezoidal and hexagonal section etc., as shown in Fig. 2. It has been a quite new passive technique for heat transfer enhancement since 2015. There are a few experimental and numerical studies on this technique covering the effect of polygon shape and twist ratio on heat transfer enhancement inside and outside TPT. The plots f/f_0-Re, Nu/Nu_0-Re, η-Re and ψ-Re extracted from the literature are illustrated in Fig. 8, and the plots Nu/Nu_0-f/f_0, η-f/f_0 and ψ-f/f_0 are shown in Fig. 9. It is seen that f/f_0=0.39–9.81, Nu/Nu_0=0.83–13.44, ψ=0.73–6.00, η=0.40–1.76 at Re=90–2300 and f/f_0=0.51–14.53, Nu/Nu_0=1.17–14.36, ψ=0.86–6.45, η=0.22–3.78 at Re=2400–12,000 are held. The heat transfer enhancement outside TPT in [112,113] is much better compared with the enhancement inside TPT. The results in [112,113] need to be verified in the future.

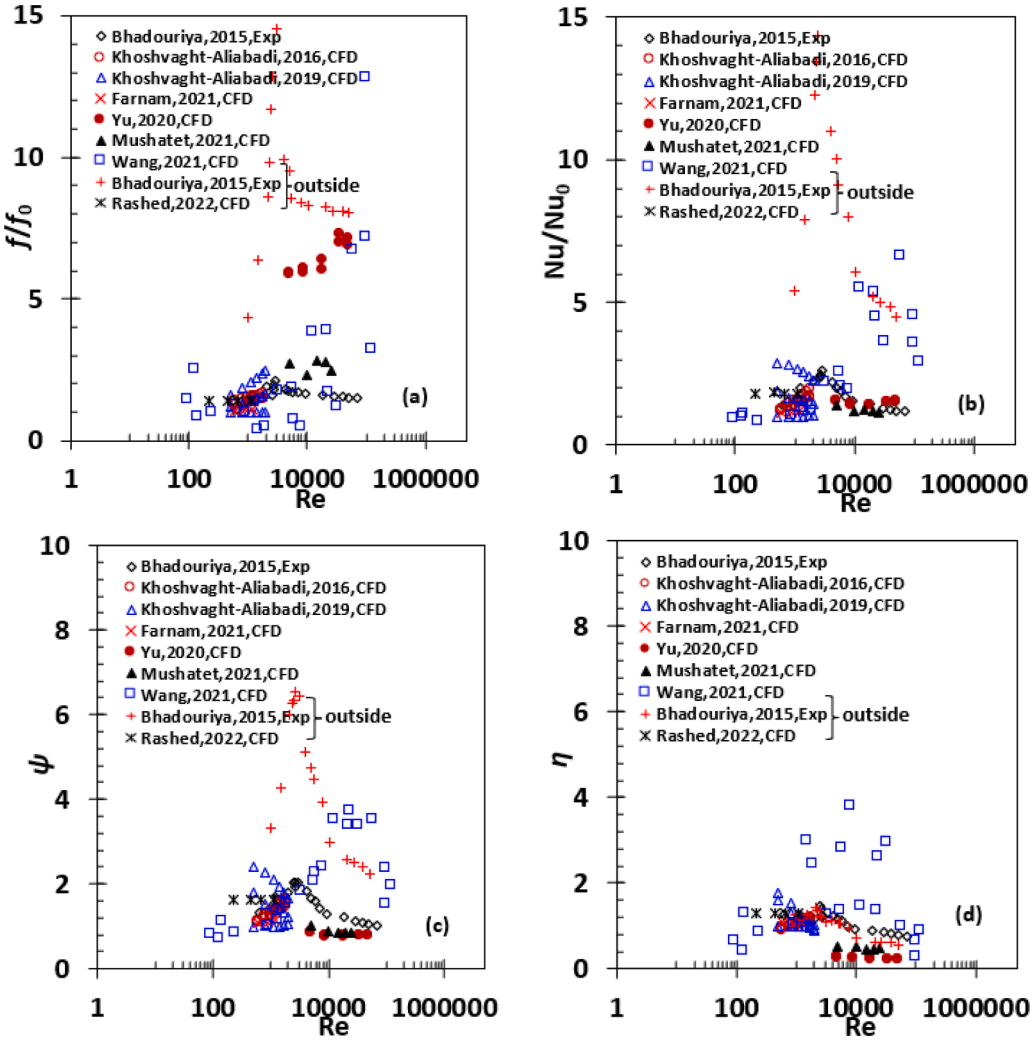

Fig. 8. Thermal-hydraulic parameters f/f_0, Nu/Nu_0, ψ and η are shown as a function of Reynolds number Re for twisted polygon tubes, (a) f/f_0, (b) Nu/Nu_0, (c) ψ and (d) η, outside-heat transfer outside the tubes, the rest data are for heat transfer inside the tubes.

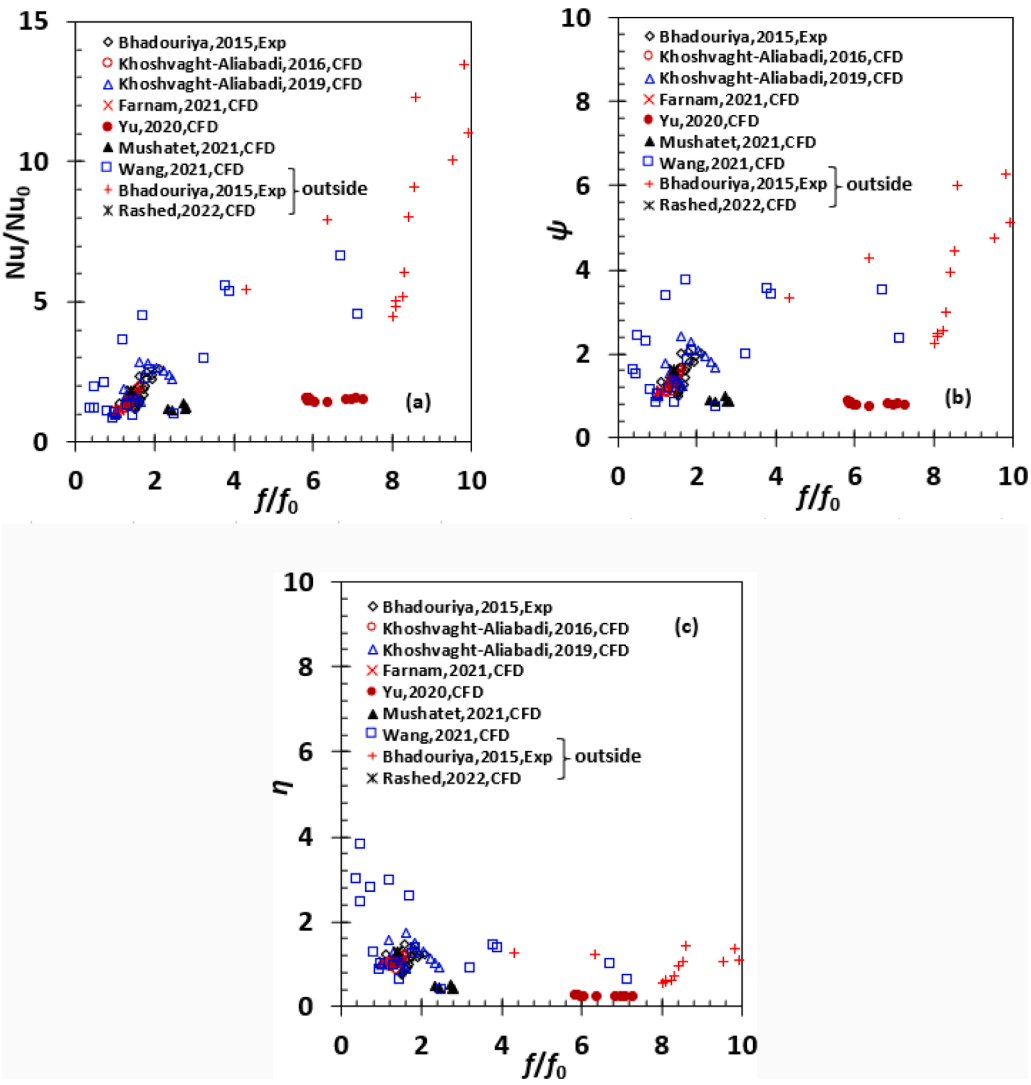

Fig. 9. Parameters Nu/Nu_0, ψ and η are demonstrated as a function of f/f_0 for twisted polygon tubes, (a) Nu/Nu_0, (b) ψ and (c) η, outside-heat transfer outside the tubes, the rest data are for heat transfer inside the tubes.

According to the f/f_0, Nu/Nu_0, ψ and η values, the region for the best heat transfer enhancement inside TPT is observed at $Re \leq 3000$. The heat transfer enhancement gets poor with increasing Re from $Re \geq 3000$.

Heat transfer enhancement inside TPT

Most (≈81 %) of the investigations into heat transfer enhancement by TPTs have been focused on the heat transfer inside them. The work done so far is associated with basic thermal-hydraulic performance of TPT, effects of twist ratio, variable pitch, shape of twist axis on heat transfer enhancement under water or air flow conditions and the influence of twisted cross-sectional shape in the flow conditions of water, nanofluid and non-Newtonian fluids. The twist ratio is an important geometrical parameter, the curved twist axis, variable pitch and nanofluid can improve heat transfer enhancement further, the TPTs, especially twisted square tube (TST) and twisted hexagonal tube (THT) can generate heat transfer enhancement in non-Newtonian fluid flows.

Basic thermal-hydraulic performance. The forced convective heat transfer and turbulent flow characteristics of water through a TST were numerically predicted under isothermal boundary condition of the tube wall based on the 3D, steady, incompressible RANS equations, standard k-ε turbulence model and energy equation in Fluent at Re=10,000–120,000. The length of the square edge, twist angle and length of the TST were 10 mm, 360° and 200 mm, respectively. The results demonstrated that the Nusselt number and friction factor of the TST were greater by 14–38 % and 1.5–21 % than the plain square tube due to secondary flow, causing the heat transfer enhancement at the level of ψ=1.14–1.3. The best enhancement of ψ=1.3 occurred at Re=10,000 [114].

Effect of twist ratio. The twist ratio or twist number is defined as the ratio of the tube length to the twist pitch. The forced convective heat transfer in the TSTs with the twist ratios of 11.5 and 16.5 was tested in a counter-flow tube-in-tube heat exchanger at Re=600–70,000. The best heat transfer enhancement ψ=2.0 occurred at Re=3000 and the twist ratio of 11.5. It turned out that the TST had a better thermal-hydraulic performance in laminar flow regime and also to some extent in turbulent flow regime owing to the strong secondary flow inside the tube [115].

The forced convective heat transfer of air flowing in three twisted triangular tubes was simulated in ANSYS Fluent 17.1 based on the 3D, steady, incompressible RANS equations, standard k-ε turbulence model and energy equation at Re=5000–25,000. These twisted triangular tubes in a length of 1 m and a diameter of 30 mm had three different twist ratios of 5, 10 and 20, respectively. The inlet temperature of air was 25 °C and the tube wall temperature was fixed to 120 °C in the simulations. The results indicated that the twisted ratio was the key parameter

affecting heat transfer improvement and friction loss. The best heat transfer enhancement was reported at the twist ratio of 5 compared with the plain tube, however, ψ=0.85–1.0 was achieved only [116].

Effect of variable pitch. The effect of variable pitch on heat transfer enhancement was investigated numerically in a TST. Four variable pitch profiles along the tube axis were designed: (1) pitch increases steadily downstream; (2) pitch decreases steadily; (3) pitch increases steadily until the middle then reduces steadily; (4) pitch declines steadily until the middle then increases steadily. The forced convective heat transfer of water flowing in the TST with each pitch profile was predicted using the 3D, steady, incompressible Navier-Stokes equations and energy equation in the laminar flow regime (*Re*=600–1800) in Fluent. It was shown that the twist pitch profile had a remarkable effect on the thermal-hydraulic performance of the TST. In the studied range of Reynolds number, the TST with the steadily increasing pitch profile demonstrated the best heat transfer enhancement in comparison with the TST with a constant pitch in common [117].

Effect of shape of twist axis. The shape of twist axis may influence the heat transfer enhancement of a TPT. A sinusoidal wavy axis was specified by using wave amplitudes of 5, 10 and 15 mm (dimensionless amplitudes: 0.5, 1 and 1.5) and wavelengths of 0.15, 0.3 and 0.6 m (dimensionless wavelengths: 0.125, 0.25, 0.5), the square cross-sections of the tube were twisted with pitches of 0.15, 0.3 and 0.6 m (twist ratios: 0.125, 0.25, 0.5), respectively. The forced convective heat transfer of water in these twisted wavy square tubes was studied numerically using the 3D, steady, incompressible Navier-Stokes equations and energy equation in laminar flow regime (*Re*=500–2000) in Fluent. The numerical results showed that the heat transfer enhancement was improved with increasing wave amplitude. The thermal-hydraulic performance of the twisted wavy square tube was better than the twisted straight square tube at the similar geometrical parameters. For instance, the best heat transfer enhancement of ψ=2.42 in the twisted wavy square tube was obtained at *Re*=500 compared with ψ=1.79 in the untwisted wavy square tube and ψ=0.98 in the twisted straight square tube at the same Reynolds number [118].

A coil heat exchanger with TST was designed, where the helical coil centre line was used as the twist axis. The forced convective heat transfer of water in the heat exchanger was simulated using the 3D, steady, incompressible Navier-Stokes equations and energy equation in laminar flow regime (*Re*=600, 900, 1200) in Fluent when the tube wall temperature and inlet water temperature were given and the tube geometrical parameters such as helical diameter, helical pitch and twist pitch varied. It was shown that the helical diameter impacted the thermal-hydraulic performance most significantly, and then the twist pitch and helical pitch followed, respectively. The Nusselt number and friction factor were increased by 14.2 % and 7.7 %, however, just ψ=1.03–1.08 was achieved. It turned out that the twisted walls could prevent the development of thermal boundary layers and alter the location and strength of secondary flow and velocity profiles continuously, resulting in more uniform temperature profiles [119].

The coil, serpentine and spiral heat exchangers with TST were designed. The helical coil, serpentine and spiral centre lines were used as the twist axis, respectively. The forced convective heat transfer of water in these heat exchangers was analysed using the 3D, steady, incompressible Navier-Stokes equations and energy equation in laminar flow regime (*Re*=100, 300, 500, 700, 900) in Fluent when the tube wall temperature and inlet water temperature were prescribed and the coil pitch and twist pitch varied. It turned out the heat transfer coefficient was increased by up to 60 % in the serpentine heat exchanger compared with the exchanger with the plain tube, the coil and spiral heat exchangers with TST followed. Increasing coil pitch and twist pitch enhanced heat transfer coefficient but enlarged and pressure drop as well, especially increasing twist pitch. The heat transfer enhancement such as ψ=1.00–1.20, 0.96–1.45, 0.98–1.20 was gained in the coil, serpentine and spiral heat exchangers with TST [120].

Effect of cross-sectional shape in various fluid flows.

(1) Water flow

The THT was cooled by using counter flow in a shell and tube heat exchanger, and the thermal-hydraulic performance of water flowing in the THT was simulated using the 3D, steady, incompressible RANS equations, RNG *k*-ε turbulence model and energy equation in Fluent at *Re*=1000–100,000. The results revealed that the Nusselt number of the THT was higher in laminar flow regime but lower in turbulent flow regime than that of the TST. This matter of fact suggests that THTs should be applied in industry for laminar flow regime while TSTs for turbulent flow regime [121].

(2) Nanofluid flow

The effect of Al_2O_3/water nanofluid flow on heat transfer enhancement inside the TST was predicted by employing the 3D, steady solid-liquid two-phase mixture model with an algebraic slip formulation between the two phases in laminar flow regime in Fluent. The pitch of the twisted square tube was either constant or variable, the Al_2O_3 nanoparticle volume concentrations were set to be 1, 2, 3 and 4 %. The predicted PEC values are presented in Fig. 10 at 0, 1 and 4 % nanoparticle volume concentrations for the TSTs with constant and steadily increasing pitches, respectively. Obviously, ψ values rise with the increasing concentration and Reynolds number. Compared with the ψ values at 0 % concentration (water), the ψ values at the nanoparticle volume concentration of 1 % are increased by 1.30–1.78 % and 0.85–1.45 % for the TSTs with constant and variable pitches, respectively, depending on Reynolds number. At the concentration of 4 %, however, the ψ values are augmented by 14.04–17.21 % and 11.89–12.07 % for the TSTs with constant and variable pitches. This suggests the TST with constant pitch works better in the Al_2O_3/water nanofluid flow than the TST with variable pitch [117].

The heat transfer characteristics of Al_2O_3/water nanofluid (volume concentrations at 0.5–1 %) flowing in a TST were numerically investigated when the twist ratios were 7.5, 11.5 and 16.5 and the Prandtl number was ranged in 8 to 10 based on the 3D, steady solid-liquid two-phase mixture model with an algebraic slip formulation between the two

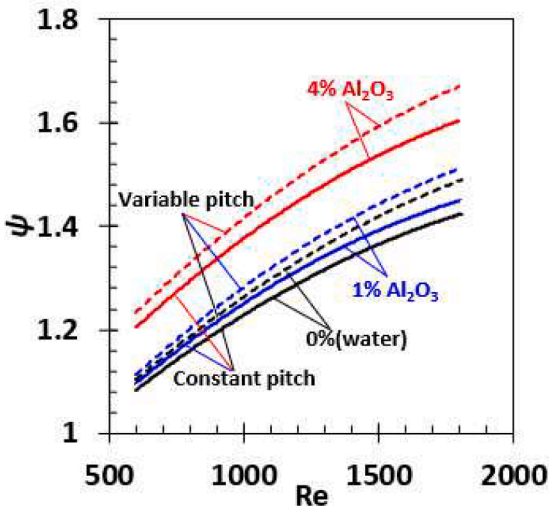

Fig. 10. PEC values of the TSTs with constant and steadily increasing pitch are plotted as a function of Reynolds number Re at 0(water), 1 and 4 % nanoparticle volume concentrations, the data after [117].

phases in laminar flow regime (Re=600–2000) in Fluent. It was shown that the Nusselt number rose with decreasing twist ratio and increasing Prandtl number. The nanoparticles at a volume concentration of 1 % in water could improve the Nusselt number by 1.2 to 1.45 % at the twist ratios considered compared with that of water. Once the concentration was smaller than 1 %, heat transfer enhancement did not occur [122].

The forced convective heat transfer of Al_2O_3/water nanofluid in the twisted mini channel (2.25 mm in diameter) with different geometrical parameters was simulated using the 3D, steady solid-liquid two-phase mixture model with an algebraic slip formulation between the two phases in laminar flow regime in Fluent. The elliptic, semi-circular, square, rectangular, and triangular cross-sections, three twist pitch ratios (5, 2, 1) and four nanoparticle volume concentrations (0, 1, 2, 3, 4 %) were selected to investigate their effects on heat transfer enhancement at Re=300–1500. The heat transfer enhancement by the various cross-sections was estimated to be ψ=1.04–1.51 compared with the plain circular tube. The twisted tube with square cross-section at a pitch ratio of 5 was the best in heat transfer enhancement. The heat transfer coefficient and pressure drop were enlarged with increasing pitch ratio. The nanoparticles resulted in a higher heat transfer coefficient and pressure drop than the pure water. The thermal-hydraulic performance of the mini channel was better than the pure water as soon as the nanoparticle volume concentration was at or above 1 % [123].

The forced convective heat transfer of CuO/organosilicone oil (Syltherm 800) nanofluid in the TPTs was investigated numerically by using the 3D, steady, incompressible RANS equations, k-ε dispersed turbulence model and energy equation based on the solid-liquid two-phase mixture model in laminar and turbulent flow regimes (Re=50–102,000) in Fluent 14.5, when the nanofluid inlet temperature was 450 K and the TPT wall temperature was 300 K to mimic the operational condition of parabolic trough solar collector. The TPTs had triangular, square, hexagonal and octagonal cross-sections and the twist angle per unit length varied from 0° to 360°, respectively. The volume concentrations of nanoparticles were 3 and 6 %. The heat transfer enhancement such as f/f_0=0.39–6.71, Nu/Nu_0=0.84–6.64, ψ=0.73–3.74, and η=0.60–3.80 was achieved at the nanoparticle concentration of 6 % compared with the plain circular tube. The TPT at a twist angle 360° had the best heat transfer enhancement at that concentration. Since the heat transfer of the fluid without nanoparticles was not simulated, the increment in heat transfer enhancement caused by the nanoparticles was unclear. Additionally, the numerical data are too scattered, further confirmation on them is needed [124].

(3) Non-Newtonian fluid flow

The forced convective heat transfer of the slurry from biogas plants in the twisted triangular, square, hexagonal, octagonal, decagonal tubes were simulated using the 3D, steady, incompressible RANS equations, RNG k-ε turbulence model and energy equation in Fluent 12.0 at the tube wall temperature of 328.15 K, Re=400–6000 and the total solid concentrations of 5.4 and 7.5 %. It was shown that the THT had the best thermal-hydraulic performance, and the maximum PEC was ψ=2 at Re=2000 but PEC was always higher than the other twisted tubes at Re≥2000, as shown in Fig. 11. The Reynolds number of 5000 was the best operational condition of the THT for the slurry with the total solid concentration of 7.5 % [125].

Corn straw slurry in biomethane process is non-Newtonian fluid with temperature-dependent and strongly shear-thinning rheological properties. The dynamic viscosity of the corn straw slurries at the total solid concentrations of 6 and 8 % was correlated to temperature and shear rate by using a power function based on the rheological experimental data. The thermal-hydraulic performance of the slurries flowing in the TST and THT was predicted numerically by using the 3D, steady, incompressible RANS equations, SST k-ω turbulence model and energy equation as well as the correlations of dynamic viscosity of the slurries in Fluent 12.0 when the tube wall temperature was 70 °C and the slurry inlet temperature was 10–55 °C at Re=3000–20,000. It was indicated that the THT had heat transfer enhancement with ψ=2.0 in the turbulent regime. The radial mixing and the near-wall shear effect could induce a strong and continuous shearing effect to enhance the heat transfer [126].

Food waste slurry is non-Newtonian fluid with highly viscous, temperature-dependent, and strongly shear-thinning rheological characteristics. The correlations of dynamic viscosity to temperature and shear rate for the food waste slurries at the total solid concentrations of 8 and 10 % by weight were best fitted by using a power function based on the rheological experimental data. Then, the forced convective heat transfer of the food waste slurries through the TET and THT was simulated based on the 3D, steady, incompressible Navier-Stokes equations and energy equation as well as the correlations of dynamic viscosity obtained in laminar flow regime (Re=1–1000) in Fluent. It was observed that the THT was more effective in heat transfer enhancement with the best heat transfer enhancement of ψ=2.75 than the TET at low-temperature difference across the tube wall. The TET showed certain heat transfer enhancement at high Reynolds number only. The low dynamic viscosity in the boundary layer induced by the strong and continuous shearing effect near the tube wall is responsible for the better heat-transfer enhancement achieved by the THT [127].

Heat transfer in annulus between TPT and outer tube

The forced convective heat transfer of water passing through the space between the shell and four TSTs in a counter-flow shell and tube heat exchanger was investigated numerically using the 3D, steady, incompressible RANS equations, SST k-ω turbulence model and energy equation in ANSYS CFX at Re=3000–20,000. The results indicated that the TST was more effective in heat transfer enhancement in the low

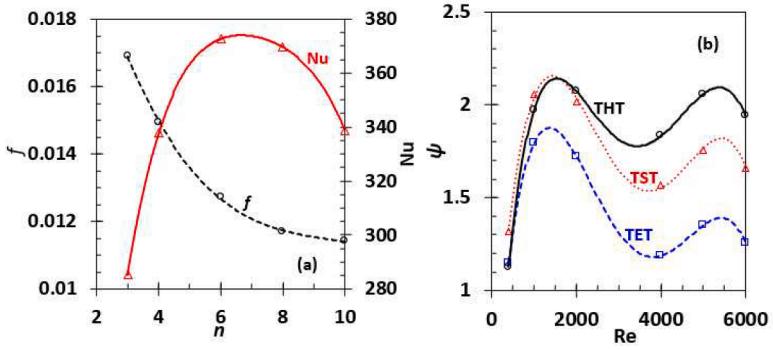

Fig. 11. Friction factor f and Nusselt number Nu of twisted polygonal tube are plotted as a function of number of edges of polygon n at Re=4000 (a), PEC values of twisted elliptical tube (TET), twisted square tube(TST) and twisted hexagonal tube(THT) are illustrated against Reynolds number Re, the total solid concentration of slurry is 7.5 %, the data in the figure after [125].

Reynolds number range (3000 to 5000) than the TET based on PEC values. The reason for this effect is that the TST can induce a weak whirl flow inside and outside the tube for the tube to achieve a better PEC at a lower Reynolds number. The TET, however, can create a strong whirl flow inside and outside the tube to enhance the heat transfer better in the high Reynolds number range [93].

The thermal-hydraulic performance of air flow in the annulus formed by an inner TST and an outer circular tube was tested at Re=400–60,000. The TSTs were at twist ratios of 10.6 and 15, respectively. The effect of the annulus parameters on the performance was exmined by altering the outer tube diameter. At a given twist ratio, a narrower annulus resulted in a larger friction factor and Nusselt number, especially at $Re \geq 3000$. The best heat transfer enhancement such as f/f_0=4.33–14.54, Nu/Nu_0=4.50–15.29, ψ=2.25–6.52, and η=0.56–1.43 was reached at the twist ratio of 10.6 and the area ratio of 0.19 (ratio of the inner cross-sectional area of the TST to the inner cross-sectional area of the outer tube). However, this excellent set of heat transfer enhancement needs to be confirmed in the future [112].

A counter-flow tube-in-tube heat exchanger, which consists of an outer TST and an inner circular pipe, was designed. The forced convective heat transfer of water streaming in the annulus between the TST and the inner tube was numerically studied using the 3D, steady, incompressible Navier-Stokes equations and energy equation in laminar flow regime (Re=220–1100) in Fluent 16.2 when the inner tube wall was at an inwards heat flux of 100 W/m^2 and water had a uniform inlet temperature. Three parameters such as edge length of twisted square (6.6, 8.2, 10.2,12.6 mm), diameter of the inner tube (19, 21, 23, 25 mm) and twist angle (0, 45, 60, 90°) varied. It was shown that the thermal-hydraulic performance of the annulus varied a little with Reynolds number, i.e., f/f_0=1.40–1.41, Nu/Nu_0=1.81–1.83, ψ=1.62–1.63, and η=1.29–1.30. The twisted outer tube created a swirl flow in the annulus, but also caused a boundary layer separation-reattachment on the inner tube wall [128].

Three wire coils with circular, equilateral triangular and square cross-sections were installed into a TET tube, respectively. The thermal-hydraulic performance of water through the annulus between the TET and the wire coils was simulated based on the 3D, steady, incompressible RANS equations, k-ω turbulence model and energy equation in Fluent at Re=5000–50,000 when the water inlet temperature was 300 K and the TET wall temperature was 373.15 K. The effects of the geometric shape, twist direction and cross-sectional orientation of the wire coil were investigated. The numerical results showed that the additional wire coil could enhance the heat transfer rate in the TET, but the PEC was decreased, resulting in increased pump consumption. The wire coil with the equilateral triangular cross-section led to the best thermal-hydraulic performance, e.g., Nusselt number was increased by 45.9 % along with an increment of 674.9 % in friction factor compared with the TET alone [113].

Twisted multi-lobe tube

Twisted multi-lobe tube (TMT) is the twisted tube along its central axis with a cross-section that has a base circle with a few outwards axisymmetric lobe-like projections. TMT has been one emerging technique for heat transfer enhancement since 2015. The most common multi-lobe cross-sections found in the literature are illustrated in Fig. 12. The lobes originate from the base circle and end on the envelope circle. The geometry of lobes can be either systematic or asymmetric, however, the lobes are always axisymmetric. Smooth connection is usually secured between the lobes, as shown in Fig. 12(b)-(d), but there is a cusp between the base circle and the lobes in Fig. 12(a) or between two lobes Fig. 12(e).

Existing investigations into heat transfer enhancement by TMTs have been devoted to effects of twist ratio, lobe shape and size on heat transfer enhancement and the thermal-hydraulic performance of helical coil heat exchanger with TMT. The plots f/f_0-Re, Nu/Nu_0-Re, η-Re and ψ-Re complied by the data found in the literature are illustrated in Fig. 13, and the plots Nu/Nu_0-f/f_0, η-f/f_0 and ψ-f/f_0 are given in Fig. 14. The parameters evaluating heat transfer enhancement achieved by TMTs exhibit a significant scatter: f/f_0=1.09–12.09, Nu/Nu_0=0.48–7.04, ψ=0.40–3.50, and η=0.12–2.39 in laminar flow regime (Re=100–2000). The scatter in the parameters is damped in turbulent

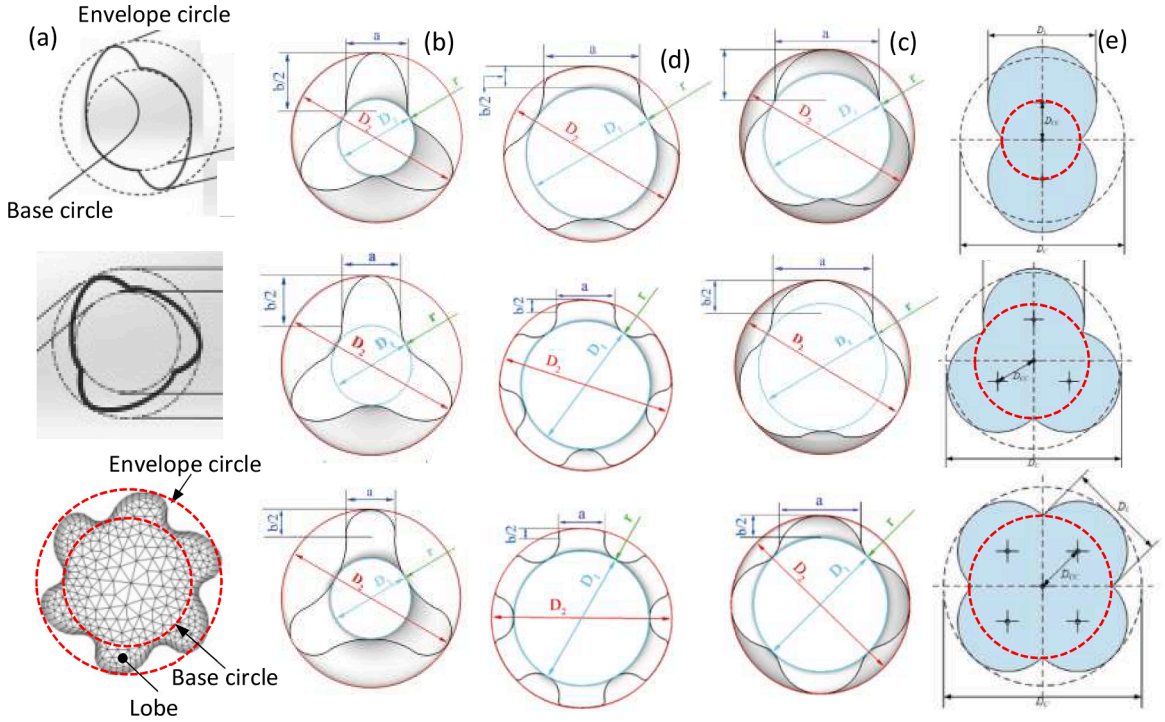

Fig. 12. Most common multi-lobe cross-sections found in the literature, columns (a)-(e) represent five types of multi-lobe, respectively, the pictures in column (a) adapted from [129,130,131], (b)-(d) from [74,132], (e) [133,134], respectively.

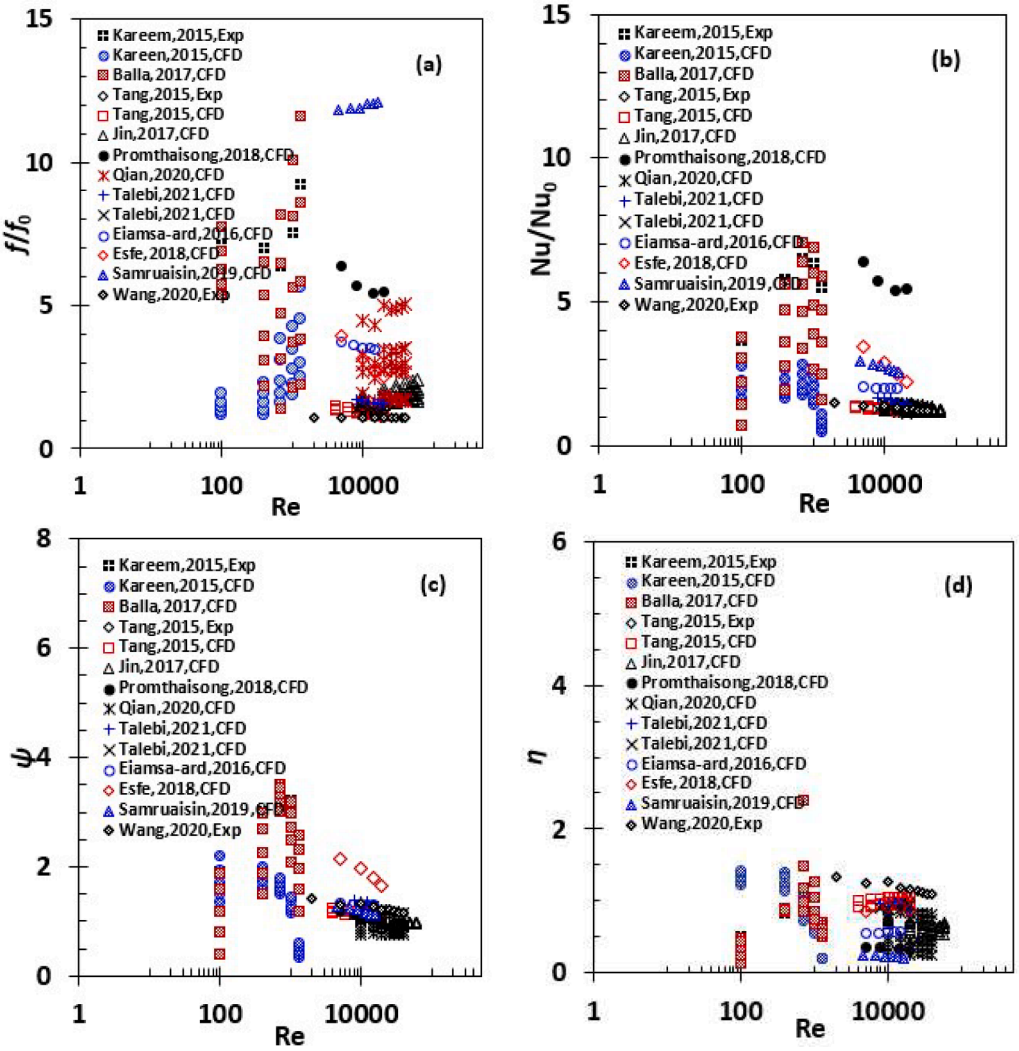

Fig. 13. Thermal-hydraulic parameters f/f_0, Nu/Nu_0, ψ and η are shown as a function of Reynolds number *Re* for twisted multi-lobe tubes, (a) f/f_0, (b) Nu/Nu_0, (c) ψ and (d) η, the data are for heat transfer inside the tubes.

flow regime (*Re*=2000–50,000), namely f/f_0=1.0–7.0, Nu/Nu_0=1.0–6.9, ψ=0.8–1.4 and η=0.4–1.5. The best heat transfer enhancement was ψ=1.6–2.2 with a sightly large f/f_0=2.5–3.9 in turbulent flow regime [135]. The heat transfer enhancement obtained by TMTs is better in laminar flow regime than in turbulent flow regime based on CFD simulations, but experimental confirmation is needed in the future.

Heat transfer enhancement inside TMT

The lobe height ratio, twist pitch ratio, severity index and number of lobes are major geometrical parameters of a TMT and have important impacts on the design and thermal-hydraulic performance of the TMT. The shape of lobe is another critical factor influencing the design and performance as well. Effects of those geometrical factors on the heat transfer enhancement inside TMTs have been clarified by using CFD simulations under water or air flow conditions in laminar or turbulent flow regime. Further, effects of shape and number of lobes on the heat transfer enhancement inside TMTs were examined in supercritical water flow conditions, too. The influence of twisted tape insert on the thermal-hydraulic performance of TMT was also investigated numerically. The effects of tape width ratio, pitch ratio or twist ratio on the heat transfer enhancement were explored. The thermal-hydraulic performance of helical coil heat exchanger with untwisted tube or TMT was evaluated numerically. It was suggested that TMTs could improve the thermal-hydraulic performance of helical coil heat exchangers slightly only.

Effects of lobe height ratio, pitch ratio, severity index and number of lobes. The important parameters of TMT are lobe height *e* (maximum radial distance of lobe profile to base circle) and twist pitch *s*. The corresponding lobe height ratio, pitch ratio and severity index are defined as e/d_n, s/d_n and e^2/sd_n, where d_n is the nominal diameter of TMT, d_n=0.5 (d_1 + d_2), d_1 and d_2 are the diameter of base and envelope circles, respectively [129]. The five twisted two-lobe tubes were designed with two asymmetrical lobes at e/d_n=0.053, 0.077, 0.095, 0.116, 0.1336, s/d_n=1.32, 1.08, 0.81, 0.60, 0.41, e^2/sd_n=0.0021, 0.0055, 0.011, 0.022, 0.045, as shown in Fig. 12(a). The forced convective heat transfer of water through those tubes was analysed numerically by employing the 3D, steady, incompressible Navier-Stokes equations and energy equation in laminar flow regime (*Re*=100–1300) in Fluent 14.0 when the inwards heat flux of 5 kW/m^2 and inlet temperature of 300 K were applied. The CFD results indicated the best thermal performance was ψ=1.8–2.3 in the twisted two-lobe tube with e^2/sd=0.045 at *Re*=100–700. The Nusselt number was increased by 21.7–60.5 % along with the increase of 19.2–36.4 % in friction factor [129].

The thermal-hydraulic performance of the twisted tri-lobe tube with asymmetrical lobes as shown in Fig. 12(a) was calculated numerically by using the 3D, steady, incompressible Navier-Stokes equations and energy equation in laminar flow regime (*Re*=100–1300) in Fluent 14.0

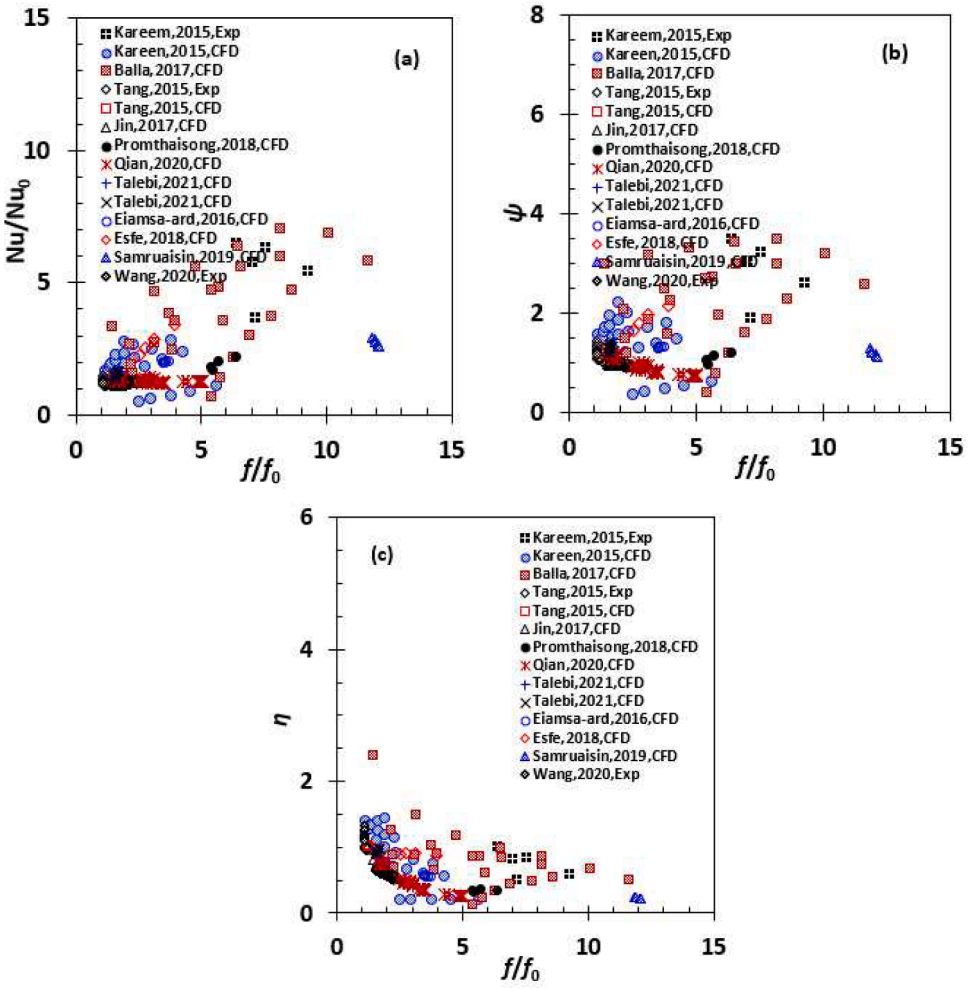

Fig. 14. Parameters Nu/Nu_0, ψ and η are demonstrated as a function of f/f_0 for twisted multi-lobe tubes, (a) Nu/Nu_0, (b) ψ and (c) η, the data are for heat transfer inside the tubes.

when the inwards heat flux of 5 kW/m^2 and inlet temperature of 300 K were specified. The geometrical parameters of five twisted tri-lobe tubes were prescribed by e/d_n=0.18, s/d_n=0.91, 1.82, 2.73, 3.64, 4.55, e^2/sd_n=0.036, 0.018, 0.012, 0.0091, 0.0072. The results showed the Nusselt number and friction factor were increased by 2.4–3.7 and 1.7–2.4 times compared with the plain tube at the same Reynolds number. The best heat transfer enhancement of ψ=1.8–3.4 was obtained at e^2/sd_n=0.036 [130].

Heat transfer and flow characteristics of water flow in a TET and twisted tri-lobe tube were studied experimentally at *Re*=8000–21,000. It turned out that the Nusselt number of the twisted tri-lobe tube was enhanced by 5.4 % and the friction factor was increased by 8.4 % compared with the TET at the same twist pitch [74]. Further, the influence of geometrical shape and parameters such as cross-section shape, twist pitch, twist direction and number of lobes on the heat transfer performance and flow characteristics were investigated numerically based on different TMTs in the cross-sections shown in Fig. 12(b)-(d) using the 3D, steady, incompressible RANS equations, SST *k*-ω turbulence model and energy equation in Fluent 6.3 at *Re*=4000–20,000, 350 K isothermal wall temperature and 300 K inlet water temperature. The geometrical parameters of six TMTs were ranged in e/d_n=0.15–0.38, s/d_n=11.11–12.42, e^2/sd_n=0.0021–0.012. The results revealed that the TMTs with a high e/d_n or e^2/sd_n and a small s/d_n could have a large Nusselt number and friction factor. The alternately right-hand and left-hand twisted multi-lobe tubes had better thermal-hydraulic performance (ψ=1.12–1.38) than the right- or left-hand twisted multi-lobe tubes. The better heat transfer enhancement of twisted tri-lobe tube was attributed to the helical flow and secondary flow induced by the twisted and curved tube wall [74].

Twisted tri-lobe tubes with cross-sections like Fig. 12(c) were designed and the influences of the lobe height ratio (e/d_2=0.02, 0.04, 0.06, 0.08, 0.1, 0.12, 0.14 and 0.16) and pitch ratio (s/d_2=0.5, 0.65, 0.75, 1.0, 1.5 and 2.0) on heat transfer enhancement in them were investigated in turbulent flow regime (*Re*=5000–20,000) based on the 3D, steady, incompressible RANS equations, realisable *k*-ε turbulence model and energy equation in ANSYS Fluent 18.0. Air was used as the heat transfer fluid in the tubes and the tube wall was subject a uniform inwards heat flux of 0.6 kW/m^2. The computational results demonstrated that twisted tri-lobe tubes could induce helical flow and secondary flow to reduce thermal boundary layer thickness and enhance heat transfer rate. The friction factor rose monotonically with increasing e/d_2 and decreasing s/d_2, but the maximum heat transfer rate occurred at e/d_2=0.08 and s/d_2=0.75. The Nusselt number and friction factor were 0.8–2.31 and 1.0–17.14 times the plain tube, respectively. The maximum PEC of 1.21 existed at e/d_2=0.06, s/d_2=0.75 and *Re*=5000 [136].

Five twisted six-lobe tubes with cross-sections shown in Fig. 12(c) were created at e/d_n=0.154, 0.231, 0.308, 0.385 and 0.462, s/d_n=1.538, 1.308, 1.077, 0.846 and 0.769, e^2/sd_n=0.0154, 0.0407, 0.0879, 0.175 and 0.277. The forced convective heat transfer of water flowing in these tubes was simulated using the 3D, steady, incompressible Navier-Stokes equations and energy equation in laminar flow regime (*Re*=100–1300)

in Fluent 14.0 when the inwards heat flux of 5 kW/m^2 and inlet temperature of 300 K were prescribed. The Nusselt number and friction factor were 2.4–3.7 and 1.7–2.3 times the plain tube, respectively. it was shown that the twisted six-lobe tube with e^2/sd_n=0.277 could produce the best heat transfer enhancement of ψ=1.8–3.4 at *Re*=100–1300 [137].

Two series of twisted six-lobe tube with the cross-sections shown in Fig. 12(a) were designed, in the first series the lobe height and envelope diameter remained fixed but the twist pitch varied, resulting in e/d_2=0.23, s/d_2=4.07–5.52, e^2/sd_2=0.0133–0.0098, in the second series, however, the pitch was fixed but the lobe height and envelope diameter varied, leading to e/d_2=0.28–0.061, s/d_2=4.38–2.85, e^2/sd_2=0.0181–0.0013. The forced convective heat transfer of water, air and T55 oil passing through these tubes was simulated at *Re*=10,000–60,000 as the inlet temperature and tube wall temperature were 363 K and 300 K. It was shown that the pressure drop and friction factor declined with increasing twist pitch, and increasing lobe height could lead to a large friction factor. The effect of fluid properties on friction factor was marginal. The twisted six-lobe tube had better heat transfer enhancement than the twisted four-lobe tube. The secondary flow velocity and longitudinal vortex vorticity became large with increasing lobe height [138,139]. Six twisted tubes with 2, 3, 4, 5, 6 and 8 lobes (e/d_2=0.14, s/d_2=1.59–6.36, e^2/sd_2=0.0123–0.0031) were generated, respectively, and the heat transfer enhancement of these twisted tubes were evaluated numerically using CFD method. the PEC value of the twisted eight-lobe tube is 1.10 times the twisted six-lobe tube, but the Nusselt number was 0.73–0.85 times the latter. The twisted eight-lobe tube in heat transfer enhancement was better than the twisted six-lobe tube in terms of PEC [131].

Effects of shape and number of lobes in supercritical water flow. The TMTs used in [74] were adopted to study their heat transfer enhancement under flow conditions of supercritical water at *Re*=8000–20,000. Effects of cross-section shape and number of lobes on the heat transfer performance were investigated. The results showed that the Nusselt number of the twisted tri-lobe tube was higher by 53 % and 41 % than the circular tube and TET, respectively. A larger radius of connecting arc and a smaller major axis length could improve heat flux by 4–6 % due to the intensification of swirling fluid flow in the tubes. Increasing the number of lobes could intensify the swirling flow rate through the lobes [132].

Effect of variable pitch. A twisted tri-lobe tube with the cross-sections in Fig. 12(e) was designed and its twist pitch was variable, i.e., steadily decreasing to the middle and then monotonically increasing towards downstream. The forced convective heat transfer of water flowing in the twisted tri-lobe tubes was simulated by using the 3D, steady, incompressible RANS equations, SST *k*-ω turbulence model and energy equation in ANSYS Fluent when the inlet temperature and tube wall temperature were 300 K and 350 K at *Re*=8000–20,000. The computational results were compared with those of the TET and twisted tri-lobe tube with a constant twist pitch. It was shown that the heat transfer coefficient of the TET and twisted tri-lobe tube with the constant and variable pitch was better by 18 %, 29 % and 63 % than the plain tube, respectively, but the pressure drop was increased by 65 %, 107 %, and 140 %. The PEC values were ranged in 1.12–1.03 for the TET, 1.18–1.05 for the twisted tri-lobe tube with the variable pitch, 1.39–1.20 as the Reynolds number varied from 8000 to 20,000. These results suggested that the twisted tri-lobe tube with variable twist pitch could improve thermal performance greatly but suffered from considerable pressure drop, causing a low PEC value. Thus, a twisted tri-lobe tube with a constant pitch has better heat transfer enhancement than that with a variable pitch in terms of PEC [82].

Effect of twisted tape insert

The twisted tri-tape insert with the tape width ratios w/d_2=0.1, 0.25, 0.34 and 0.5 was installed in a twisted tri-lobe tube with the cross-section shown in Fig. 12(e). The heat transfer enhancement by the tube and twisted tri-tape insert was simulated using the 3D, steady, incompressible RANS equations, realisable *k*-ε turbulence model and energy equation at *Re*=5000–15,000. Influences of relatively circumferential positions between the tube and twisted tri-tape insert on the heat transfer enhancement were investigated. It was shown that the Nusselt number and friction factor rose with increasing tape width ratio. The arrangement where the twisted tapes were towards the tube neck was better in the heat transfer enhancement than the arrangement where the tapes were towards the tube belly at the same width ratio. The Nusselt number of the twisted tri-lobe tube with the twisted tape insert in the tape-towards-neck arrangement at w/d_2=0.34 was larger by 36 % than the plain twisted tri-lobe tube compared with 17 % in the tape-towards-belly arrangement. As a result of this, the corresponding maximum PEC was ψ=1.32 at *Re*=5000 and w/d_2=0.34. This is because of the stronger interaction between the swirling flows generated by the twisted tri-lobe tube and by the tapes, respectively [140].

An untwisted tri-lobe tube with a cross-section shown in Fig. 12(e) was generated and three twisted tape inserts were installed in the tri-lobe tube, respectively. The forced convective heat transfer of water flowing in the tri-lobe tube was simulated using the 3D, steady, incompressible RANS equations, SST *k*-ω turbulence model and energy equation in Fluent at *Re*=5000–20,000. The twist pitch and tape width ratio varied in *s*=100, 150, 200 mm and w/d_2=0.15, 0.25, 0.34 and 0.4. It turned out that the Nusselt number, friction factor and PEC were increased when the tape width ratio rose from 0.15 to 0.4. The best PEC of ψ=2.05–1.60 was identified at w/d_2=0.4, twist pitch of 100 mm and *Re*=5000–20,000 [135].

A twisted tri-lobe tube with a cross-section shown in Fig. 12(b) was created and a twisted tape insert with four twist ratios of 2, 3, 4 and 5 was installed in the twisted tri-lobe tube. Experiments were conducted on forced convective heat transfer in the twisted tri-lobe tubes in turbulent flow regime (*Re*=4500–16,000) when water was adopted as the heat transfer fluid. The Nusselt number was improved with decreasing twist ratio. The largest PEC values were 1.28, 1.25, 1.23, and 1.21 at twist ratios of 2, 3, 4 and 5, respectively [141].

Helical coil heat exchanger with TMT

A helical coil heat exchanger with a twisted tri-lobe tube in the cross-section shown in Fig. 12(b) was designed and fabricated, the forced convective heat transfer of water in the heat exchanger was tested and simulated using the 3D, steady, incompressible RANS equations, realisable *k*-ε turbulence model and energy equation in Fluent at *Re*=2000–40,000. The helical coil heat exchangers with the circular tube, untwisted elliptical tube and the untwisted tri-lobe tube in the cross-sections in Fig. 12(b) were fabricated, tested and simulated, too. the results showed that the coil heat exchanger with the twisted tri-lobe tube exhibited better thermal-hydraulic performance than the coil heat exchanger with the circular tube, untwisted elliptical tube and untwisted tri-lobe tube, respectively. The Nusselt number and friction factor of the coil heat exchanger with the twisted tri-lobe tube were increased by 19–31 % and 24–38 % compared with the exchanger with the circular tube. As a result, when the Reynolds number rose from 2000 to 40,000, the PEC values reduced from 1.38 to 1.34 for the coil heat exchanger with the twisted tri-lobe tube, from 1.36 to 1.25 for the exchanger with the untwisted tri-lobe tube, from 1.24 to 1.20 for the exchanger with the untwisted elliptical tube, respectively [108].

Twenty-five helical coils with twisted two-lobe tubes in the cross-section shown in Fig. 12(e) were designed in terms of twist pitches in 20–100 mm and lobe heights in 0.4–2 mm, the forced convective heat transfer of propane flowing in the tubes was predicted numerically at *Re*=4000–16,000. The maximum PEC of ψ=1.13 was obtained at the lobe height of 2 mm, twist pitch of 20 mm, and *Re*=4000 for the twisted two-lobe tube. The PEC values of the coil with the twisted two-lobe tube were 0.94–1.13 times and 0.88–1.05 times the coil with the plain tube at

Re=400016,000, respectively. Additionally, the PEC value of the coil with the twisted two-lobe tube was higher than the helical coil with the TET [109].

The forced convective heat transfer of water in the helical coil heat exchangers with twisted two-, tri-, four- and five-lobe tubes in the cross-sections in Fig. 12(e) was simulated using the 3D, steady, incompressible Navier-Stokes equations and energy equation in laminar flow regime (*Re*=500–2000) with ANSYS Fluent at constant wall temperature. The effect of number of lobes, number of twists was evaluated. For the straight untwisted tubes with multi-lobe cross-sections, it was shown that increasing number of lobes had an insignificant impact on the thermal-hydraulic performance of the tubes. For the coil heat exchanger with the untwisted multi-lobe tubes, however, the twisted two- and four-lobe tubes could increase heat transfer coefficient with a minor impact on friction factor. As a result, the thermal performance of the helical coil heat exchanger with untwisted two- or four-lobe tubes was improved by 18.4 % compared with straight tube at *Re*=500–2000. The twisting of multi-lobe tube could improve the thermal-hydraulic performance of the straight tube but deteriorate the performance of the helical coil tube [133].

The forced convective heat transfer of water in the helical coil heat exchangers with twisted two-, tri-, four- and five-lobe tubes in the cross-sections in Fig. 12(e) was simulated using the 3D, steady, incompressible RANS equations, SST *k*-ω turbulence model and energy equation in turbulent flow regime (*Re*=8000–20,000) with ANSYS Fluent at constant wall temperature. It was revealed that the TMT enhanced the heat transfer in a straight tube by 6.76 % but generated a marginal improvement in heat transfer in the helical coil tube. The variable number of lobes could lead to a change in thermal performance as little as 2 % only. The PEC values of the helical coil tube with untwisted and twisted two-lobe cross-section were 1.08 and 1.00 only, comparison with ψ=1.037 for the coil tube with untwisted and twisted five-lobe cross-section [134].

Periodical convergent-divergent tube

Periodical convergent-divergent tubes make use of a periodical variation of their cross-sectional area or wall deformation along the flow path to enhance the heat transfer inside the tubes. This passive method has come to notice since the 1990s and has drawn more attention,

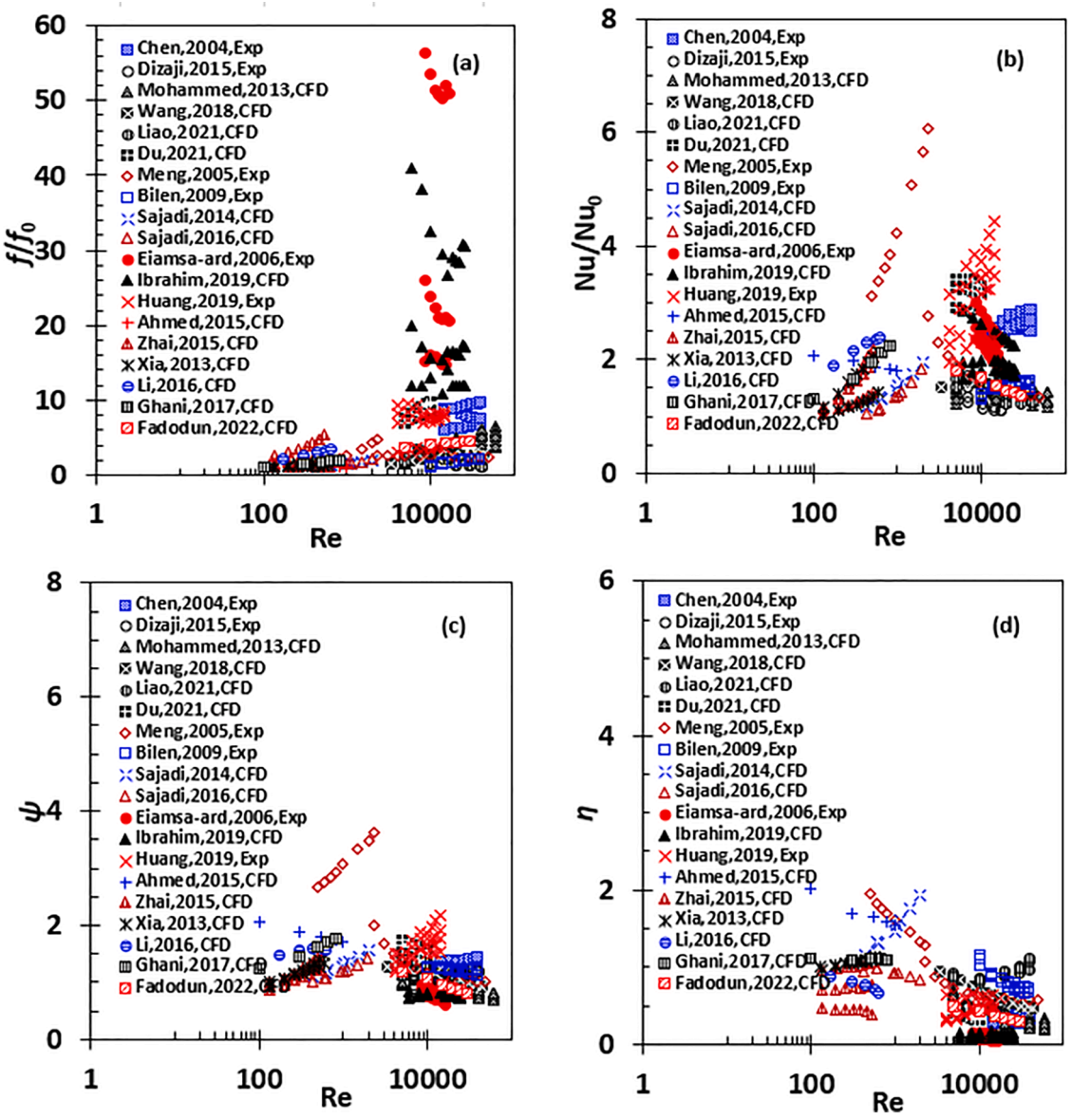

Fig. 15. Thermal-hydraulic parameters f/f_0, Nu/Nu_0, ψ and η are shown as a function of Reynolds number *Re* for periodically convergent-divergent tubes, (a) f/f_0, (b) Nu/Nu_0, (c) ψ and (d) η, the data are for heat transfer inside the tubes.

resulting in a large body of literature. Periodical convergent-divergent tubes can be divided into seven types: (1) two-dimensional (2D) sinusoidal convergent-divergent channel, (2) 3D periodical convergent-divergent channel, (3) transversely corrugated tube, (4) orthogonal ellipse tube, (5) periodical contraction-expansion tube, (6) alternating circle and ellipse tube, and (7) nozzles or inserts in series in tube.

The plots f/f_0-*Re*, Nu/Nu_0-*Re*, η-*Re* and ψ-*Re* based on the data extracted from the literature are demonstrated in Fig. 15, and the plots Nu/Nu_0-f/f_0, η-f/f_0 and ψ-f/f_0 are presented in Fig. 16. The situation: f/f_0=1.0–5.55, Nu/Nu_0=1.0–6.06, ψ=0.92–3.62, η=0.05–2.01 at *Re*=130–2300 and f/f_0=3.00–56.39, Nu/Nu_0=1.21–4.44, ψ=0.73–2.17, η=0.14–1.17 at *Re*=2200–60,000 is observed. The extremely large f/f_0 values were found in [142] in the experimental heat transfer enhancement of streamwise periodically fitted V-nozzles in a straight circular tube and in the numerical heat transfer enhancement of streamwise periodically inserted conical rings in a straight circular tube in [143], respectively. The best heat transfer enhancement such as f/f_0=1.60–4.70, Nu/Nu_0=3.12–6.06, ψ=2.66–3.62 and η=1.95–1.29 in laminar flow regime was credited to [144] in terms of experimental heat transfer on the orthogonal ellipse tubes when the Reynolds number varied from 500 to 2300. For the periodical contraction-expansion tubes the best heat transfer enhancement was achieved experimentally at f/f_0=6.06–9.88, Nu/Nu_0=2.49–2.68, ψ=1.12–1.44 and η=0.27–0.41 in turbulent flow regime at *Re*=14,000–40,000. This matter of fact suggests that periodically convergent-divergent tubes are most suitable to the heat transfer enhancement in laminar flow regime, they are not economical in turbulent flow regime, and suffer from considerable energy consumption.

2D periodical sinusoidal convergent-divergent channel

2D periodical sinusoidal convergent-divergent channel is a special periodical convergent-divergent channel with rectangular cross-section where the distance of two sinusoidal walls is much smaller than the distance between two flat walls. It is one simple case of 3D periodical sinusoidal convergent-divergent channel and has been investigated initially as a passive heat transfer enhancement technique. Effects of geometrical parameters of 2D periodical sinusoidal convergent-divergent channel have been studied under water, air, nanofluid and microfluid flow conditions so far.

Effect of geometrical parameters. Turbulent flow and heat transfer characteristics of air flow in a 2D periodical convergent-divergent channel were numerically studied by using the 2D, steady, incompressible RANS equations, standard *k*-ε turbulence model and energy equation at *Re*=40,000–100,000, wall temperature of 35.4 °C and inlet temperature of 23 °C. The channel is shown in Fig. 17 and its wall is sinusoidally shaped with amplitude 2a and wavelength ℓ=6.667 cm. The CFD simulations took place in the body-fitted orthogonal curvilinear mesh at two

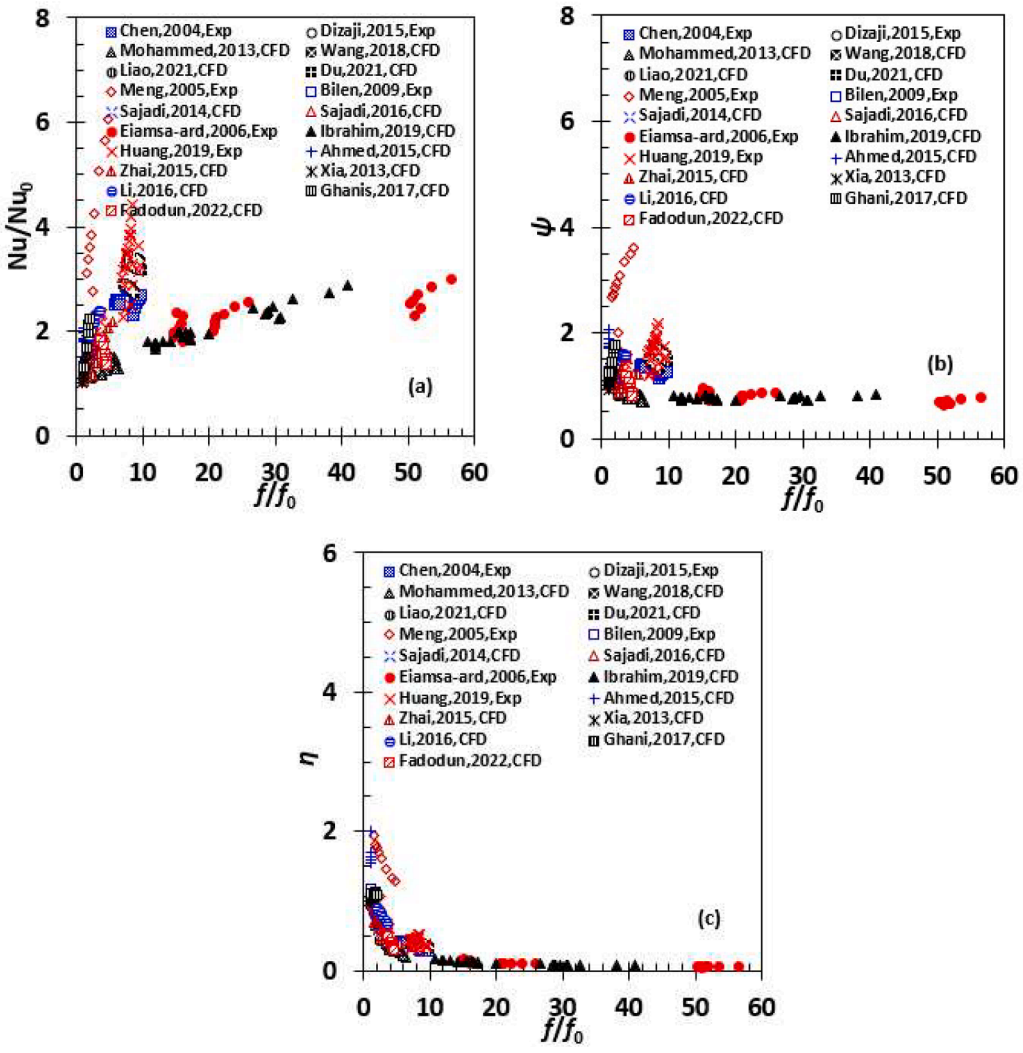

Fig. 16. Parameters Nu/Nu_0, ψ and η are demonstrated as a function of f/f_0 for periodically convergent-divergent tubes, (a) Nu/Nu_0, (b) ψ and (c) η, the data are for heat transfer inside the tubes.

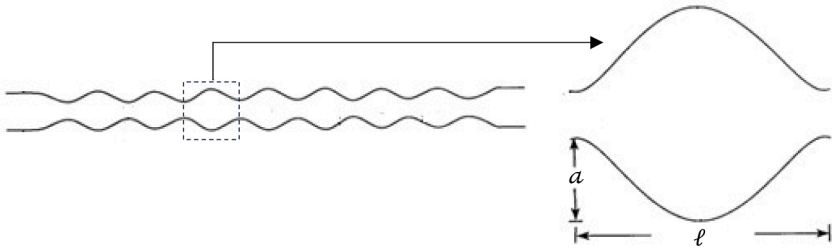

Fig. 17. Geometrical shape and parameters of a 2D symmetric periodical convergent-divergent channel, the picture after [145].

amplitude-wavelength ratios: $2a/\ell$=0.27, 0.34 by using a custom CFD code. The results showed that heat transfer was increased by around 15 % but pressure drop was enlarged by 40 % as the amplitude-wavelength ratio rose from 0.27 to 0.3, suggesting an ineffective channel in heat transfer enhancement [145].

Flow patterns of laminar and transitional flows of water in 2D sinusoidal wavy channels were conducted firstly in a water tunnel, and then the forced convective heat transfer in the channels was tested in a wind tunnel. The two wavy walls of the tested channels were in 12–14 wavelengths long, and the wave amplitude, phase angle, and wall-to-wall spacing varied. It was found that the onset of unsteady macroscopic mixing in the flow was directly relevant to the heat transfer enhancement. The location of the onset of mixing depended on Reynolds number and channel geometry. The onset of the macroscopic mixing in the whole channel occurred at a moderate Reynolds number (Re≈800) [146].

The forced convective heat transfer of incompressible fluid flowing through a 2D periodical, sinusoidal convergent-divergent channel was numerically analysed using the stream-vorticity method in laminar flow regime under constant wall temperature and uniform fluid inlet temperature. The effects of amplitude-wavelength ratio on Nusselt number and friction factor were clarified at Re=100–700. The numerical results showed that the Nusselt number and friction factor rose with increasing amplitude-wavelength ratio. The heat transfer enhancement was insignificant at a smaller amplitude-wavelength ratio than 0.2, and a sufficiently large amplitude-wavelength ratio (>0.2) was suggested for effective heat transfer enhancement [147].

The unsteady forced convective heat transfer of air flowing in a 2D periodical convergent-divergent channel with sinusoidal walls was simulated using the 2D, unsteady, incompressible Navier-Stokes equations and energy equation in laminar flow regime (Re=25–1000) based on an in-house computer program of finite volume method. It was shown that the heat transfer rate was very low for steady flow but increased for unsteady flow because of the increased mixing between the core and the near wall fluids [148].

Under nanofluid and micropolar fluid flow conditions. The forced convective heat transfer of Cu/water nanofluid in a 2D periodical sinusoidal convergent-divergent channel with a hot bottom wall was simulated in laminar flow regime (Re=300, 450, 600) at three nanoparticle volume fractions (0.01, 0.03, 0.05) and amplitude-channel height ratios (φ=0.1, 0.2, 0.3). The governing equations included the single-phase 2D steady Navier-Stokes equations and energy equations with effective density, thermal conductivity, and dynamic viscosity. A sensitivity analysis was performed on the CFD results by using response surface method to optimise the thermal-hydraulic performance. The maximum enhancement in Nusselt number was increased by 56 % but 24 % at Re=600 and φ=0.1 as the amplitude-channel height ratio rose from 0.1 to 0.3 and from 0.1 to 0.5, respectively. The dimensionless pressure drop was more sensitive to amplitude-channel height ratio than Reynolds number and nanoparticle volume fraction. The Nusselt number was more sensitive to Reynolds number and amplitude-channel height ratio. Increasing amplitude of the sinusoidal walls could enhance the mixing of fluid in the channel and increase the temperature gradient near wall [149].

An entropy generation analysis on the forced convective heat transfer of Cu/water nanofluid in a 2D periodical sinusoidal convergent-divergent channel with constant wall heat flux based on the simulated results in ANSYS Fluent in laminar flow regime (Re=300–900), three nanoparticle volume fractions (0.01, 0.03, 0.05), amplitude-channel height ratios (φ=0.1, 0.2, 0.3) and wavenumbers (2, 4, 6). The governing equations were the same as those in [149]. It was found that the thermal entropy generation was in everywhere in the channel and the viscous entropy generation rose with increasing Reynolds number and amplitude-channel height ratio [150].

Micropolar fluids are a kind of fluid in which molecules can rotate independently of local fluid flow and vorticity, and their flow characteristics are affected by the micro rotation. Numerical simulations of the laminar mixed convection of a cold micropolar fluid in a horizontal 2D periodical sinusoidal convergent-divergent channel with a hot bottom wall were launched. The governing equations included 2D steady Navier-Stokes equations formulated in both stream function and vorticity, micro motion equation and energy equation. The micropolar fluid thermo-physical properties were constant except its density, and the buoyancy effect was handled by the Boussinesq approximation. The governing equations were solved numerically by finite difference method. Effects of Rayleigh number, Reynolds number, Prandtl number, vortex viscosity parameter and wavenumber on velocity and temperature profiles as well as Nusselt number were clarified. It was found that the Nusselt number rose with increasing Rayleigh, Reynolds and Prandtl numbers but declined with decreasing wavenumber. However, the influence of vortex viscosity parameter on the Nusselt number was not monotonic [151].

3D periodical convergent-divergent channel

3D periodical convergent-divergent channels are a kind of 3D periodical convergent-divergent channels with a rectangular or square cross-section. The 3D periodical convergent-divergent channel is mainly used as a heatsink to cool electrical devices. They usually are subject to a high wall heat flux (400–1000 kW/m^2), low Reynolds number (100–1000) and small size (millimetre scale). The forced convective heat transfer of water in 3D periodical convergent-divergent channels with arc, triangle, trapezoid, and sinusoidal-shaped walls has been investigated numerically.

Arc, triangle and trapezoid shaped wall. A 3D microchannel with arc-shaped walls and rectangular cross-section as illustrated in Fig. 18 was proposed in [152]. The conjugate heat transfer of water in the channel was simulated by employing the 3D, steady, incompressible Navier-Stokes equations and energy equation in laminar flow regime (Re=132, 529, 926) in Fluent 6.2.16 when an inwards heat flux of 1000 kW/m^2 was applied at the channel bottom and the temperature of 293 K was prescribed to water at the channel inlet. The effects of wall geometrical parameters including length and width of the periodical structures on Nusselt number and pressure drop were presented. The PEC values for evaluating heat transfer enhancement were ranged in 1.10–1.55 when the wall geometrical parameters and Reynolds number varied. The optimised wall geometrical parameters were in the range of

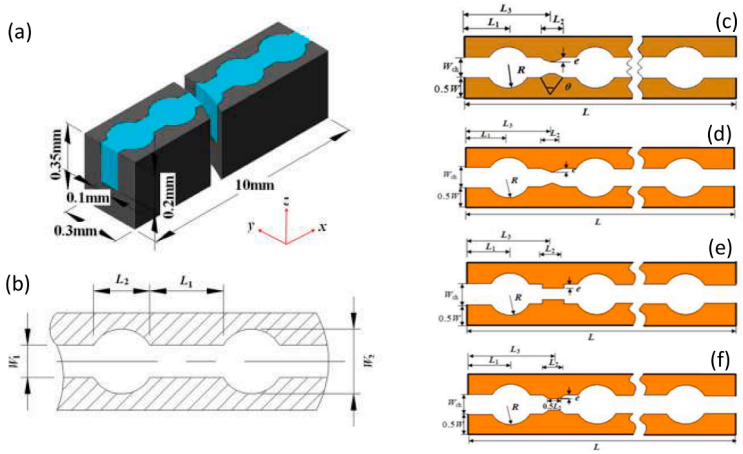

Fig. 18. 3D structure (a) and 2D profile of walls (b) of the periodical convergent-divergent channel proposed in [152], the wall shape (c) was proposed in [153], the shapes (d)-(f) were created in [154].

$0.15<L_1/L_2<2$ and $1.4<W_2/W_1<2.1$ [152].

To improve the heat transfer enhancement in the channel with the wall shape shown in Fig. 18(b) further, a pair of inwards arcs were added, making the channel even more narrowed locally, see Fig. 18(c). The conjugate heat transfer of water in that channel was predicted at Re=150–600 and six dimensionless arc heights (arc height to the hydraulic diameter of the channel) by using the same flow and heat transfer models and numerical methods as well as boundary conditions in [152]. The results showed that the Nusselt number of the channel was 1.3–1.6 times the plain channel when the dimensionless arc height varied in 0.074 to 0.217 at Re=600, but the friction factor was 6.5 times the latter, depending on the Reynolds number [153]. This work was extended by replacing the inwards arc with triangular, rectangular and trapezoidal elements/ribs as illustrated in Fig. 18(d)-(f) in [154]. The numerical results suggested the PEC of the channel with additional rectangular ribs was the lowest and the PEC value of the channel with trapezoidal ribs was better at Re<300, but the PEC values of the channels with arc and triangular ribs were the best at $Re\geq$300, especially the channel with arc ribs [154].

The 3D periodical convergent-divergent channel shown in Fig. 18(a) but with triangular-shaped wall or trapezoidal-shaped wall as well as arc, triangular and trapezoidal elements/ribs was proposed in [155]. The longitudinal cross-sections of the channel are illustrated in Fig. 19. CFD simulations of the conjugate heat transfer of water in the channels were performed in laminar flow regime (Re=100–600) at the known uniform wall heat flux on the channel bottom in six channels with different wall shapes and rib sizes. The results confirmed that the periodical convergent-divergent channel with triangular-shaped wall and triangular ribs exhibited the best heat transfer enhancement (ψ=1.25–1.45) at Re=300–600, while the channel trapezoidal-shaped wall and trapezoidal ribs had the best enhancement (ψ=1.03–1.18) at Re=100–300 [155].

The 3D periodical arc or triangular convergent-divergent microchannels for heat sink with rectangular cross-section were designed, and the conjugate heat transfer of water flowing in them was predicted based on the 3D, steady, incompressible Navier-Stokes equations and energy equation in laminar flow regime and the head conduction in the solid domain (water volume flow rate=100–200 ml/min, bottom wall heat flux=2000 kW/m^2, water inlet temperature=298 K). The numerical results suggested two types of microchannels enhanced the heat transfer compared with the plain microchannel in rectangular cross-section due to the jetting and throttling effect [156].

A number of CFD simulations of the conjugate heat transfer of water in the 3D periodical convergent-divergent channels with trapezoidal-shaped wall were conducted when the geometrical parameters of longitudinal trapezoidal cross-section varied at a fixed water inlet temperature and a 1000 kW/m^2 wall heat flux prescribed under the channel bottom in laminar flow regime (Re=100, 300, 550, 800, 1000). The geometrical parameters include base length ratio (top base length to bottom base length), height ratio (height to the channel length), pitch ratio (channel length to pitch/wavelength) and relative longitudinal position between trapezoids on the opposite walls (difference in the longitudinal positions between the trapezoids on the opposite walls to channel length). The best heat transfer enhancement such as ψ=2.06–1.72 at Re=100–1000 was achieved at the base length ratio of 0.5, height ratio of 0.4, pitch ratio of 3.33, and zero relative longitudinal position (i.e. symmetrical channel walls) [157].

A 3D periodical convergent-divergent channel with triangular-shaped wall and rectangular ribs was proposed as shown Fig. 20 and the conjugate heat transfer of water in the channel was simulated based on the 3D, steady, incompressible Navier-Stokes equations and energy equation in laminar flow regime (Re=173–635) as well as the heat conduction in the channel wall at a constant bottom wall heat flux of 1000 kW/m^2 and a water inlet temperature of 293 K in Fluent 6.3. The effects of wall and rib geometry on Nusselt number and friction factor were investigated. The best heat transfer enhancement of f/f_0=2.14–3.55, Nu/Nu_0=1.89–2.39, ψ=1.46–1.56, and η=0.88–0.67 was gained as the Reynolds number varied from 173 to 635. That enhancement was attributed to the interruption and redevelopment of the thermal boundary layer [158].

A 3D periodical convergent-divergent channel with rectangular ribs as shown in Fig. 20 was proposed by replacing the triangular profile with

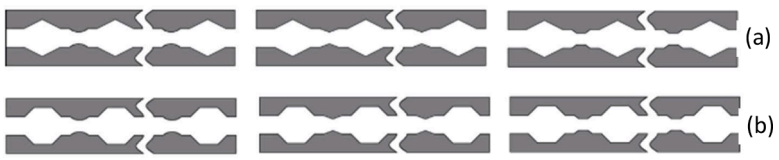

Fig. 19. Periodical convergent-divergent channel with triangular-shaped wall (a), and a periodical convergent-divergent channel with trapezoidal-shaped wall (b), both channels with arc, triangular and trapezoidal elements/ribs, respectively, the picture after [155].

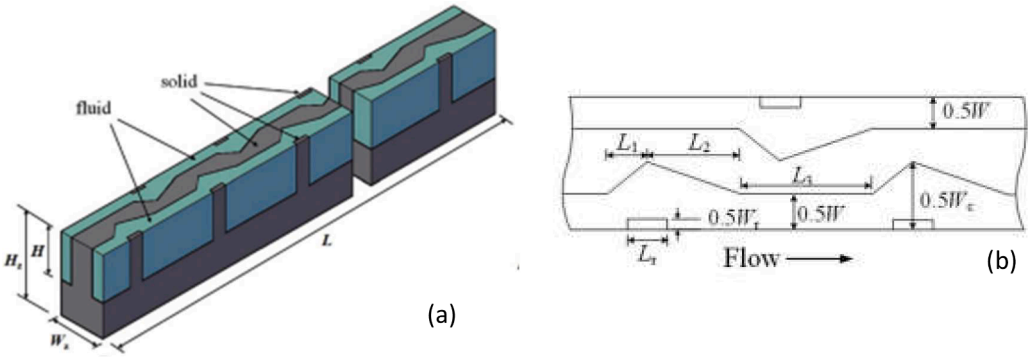

Fig. 20. 3D periodical triangular outwards convergent-divergent channel with rectangular cross-section and rectangular ribs, (a) 3D shape, (b) longitudinal cross-section, the pictures after [158].

a sinusoidal profile, and the conjugate heat transfer of water in the channel was predicted based on the 3D, steady, incompressible Navier-Stokes equations and energy equation in laminar flow regime (Re=100–800) as well as the heat conduction in the channel wall at a constant bottom wall heat flux of 1000 kW/m^2 and a water inlet temperature of 300 K in ANSYS Fluent 14.0. The effects of sinusoidal amplitude and rib geometry on Nusselt number and friction factor were analysed. The best heat transfer enhancement: f/f_0=1.18–2.06, Nu/Nu_0=1.30–2.24, ψ=1.23–1.76, and η=1.11–1.09 reached at Re=100–800 [159].

The work in [159] was extended by putting one 3D periodical convergent-divergent channel on top to form a counter-flow double--layer microchannel heat sink with sinusoidal expansion wall and rectangular ribs. the conjugate heat transfer of GNP–SDBS/water nanofluid in the sink was simulated based on the 3D, steady, incompressible Navier-Stokes equations and energy equation in laminar flow regime (Re=50–1000) as well as the heat conduction in the sink wall at a constant bottom wall heat flux of 500 kW/m^2 and a nanofluid inlet temperature of 293.15 K in Fluent. The results suggested that it was possible to increase the Nusselt number by nearly 20 % [160].

The 3D periodical trapezoidal convergent-divergent channels silicon wall as shown in Fig. 21, one with symmetrical cross-section and one with asymmetrical cross-section, were designed and the conjugate heat transfer of water in them was predicted at Re=443 with laminar flow models. Compared with the plain channel, the optimised channel could improve the Nusselt number by up to 1.15 times [161]. This work was extended to Re=187–715 in [162]. For the channel with symmetrical cross-section, the Nusselt number and friction factor were 1.03–2.01 and 1.06–9.09 times the plain channel. For the asymmetrical cross-section, however, the Nusselt number and friction factor were 1.01–2.16 and 0.04–7.43 times the plain channel [162].

3D sinusoidal-shaped wall. 3D convergent-divergent channels in rectangular cross-section with two sinusoidal-shaped top and bottom walls and two flat side walls were designed at ⁄=1.3, 2,2.6, 4 mm, 2𝛼=50, 100, 150, 200 μm, channel aspect ratio (height/width)=1, 1.25, 1.67, 2.5.

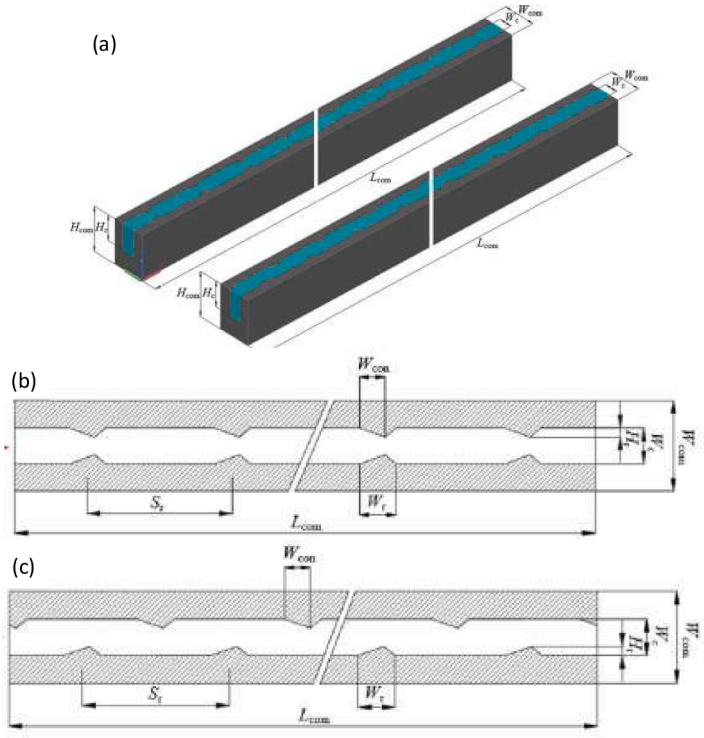

Fig. 21. 3D periodical trapezoidal convergent-divergent channels (a) and symmetrical longtudinal cross-section (b) and asymmetrical longitudinal cross-section (c), the pictures after [161].

The conjugate heat transfer of water in these channels was simulated by using the 3D, steady, incompressible Navier-Stokes equations and energy equation in laminar flow regime (Re=50, 100, 150) in Fluent when a wall heat flux of 470 kW/m^2 was given at the channel bottom and the temperature of 300 K was fixed at the channel inlet. The best heat transfer enhancement was ψ=1.45 at Re=150. Additionally, if the top and bottom sinusoidal walls were arranged in such a way that forms a serpentine/wavy channel, the thermal-hydraulic performance of the channel could be better than the channel with symmetrical sinusoidal top and bottom walls [163].

Effects of geometrical parameters (channel aspect ratio, amplitude-wavelength ratio and area expansion ratio, i.e. maximum cross-sectional area to minimum cross-sectional area) of the periodical converging-diverging microchannel with two sinusoidal side walls and flat top and bottom walls on heat transfer enhancement inside the channel were studied numerically by solving the 3D, steady, incompressible Navier-Stokes equations and energy equation of water in laminar flow regime (Re=200, 400, 600) in Fluent at a uniform bottom wall heat flux and the inlet temperature of 300 K. A performance factor was proposed to evaluate the heat transfer and pumping power characteristics of the periodical convergent-divergent microchannel. It was shown that the performance factor of the channel was improved by up to 20 % in comparison with the plain channel. Counter-rotating vortices having an adverse effect on heat transfer were identified. A large wall curvature resulted in chaotic advection to enhance the heat transfer rate, but a huge pressure drop was caused [164].

Alternating convergent-divergent channels with two perforated walls. Alternating convergent-divergent channels with perforated walls in rectangular cross-section were proposed to enhance convective heat transfer in heat exchangers at Re=500–3000. The convergent-divergent channels were stacked by many layers in an alternating manner, i.e., the convergent channel in one layer corresponds to the divergent channel in the next layer and so forth. Effects of wall geometry and perforation pattern on the heat transfer enhancement were studied experimentally. It turned out that the secondary flow induced by the suction and injection through perforated holes and frequent boundary layer interruptions at each convergent channel were responsible for the mechanism of the heat transfer enhancement [165].

Alternating convergent-divergent channels with slotted walls in rectangular cross-section were devised and fabricated on a heat sink. The conjugate heat transfer of air in the channels was simulated by using ANSYS Fluent 15.0 with the 3D, steady, incompressible RANS equations, RNG k-ε turbulence model and enhanced wall treatment as well as energy equation. It was observed that the channel sections induced secondary flows and repeatedly disturbed the boundary layer over the leading edges of the slots. Even though heat transfer enhancement was generated, the vortices generated by the secondary flow resulted in considerable pressure drop to limit further improvement in heat transfer enhancement [166].

Transversely corrugated tube

Transversely corrugated tubes are the tubes whose inner wall is periodically corrugated inwards or outwards along the tube axis with a geometrical element such as arc, triangle, rectangle, trapezoid and sinusoidal shape. As a result, the cross-sectional area of the corrugated tube exhibits a periodical contraction and expansion effect along the tube axis. When a fluid flows over the inwards or outwards geometrical elements, the orientation and magnitude of the fluid velocity will change, and vortices will be induced to enhance heat transfer. A few studies were devoted to heat transfer enhancement inside the transversely corrugated tubes when the critical geometrical parameters varied in turbulent flow regime.

Transversely rectangular inwards corrugated tube. The forced convective heat transfer of water in a transversely rough rectangular inwards corrugated circular tube was estimated numerically based on the 2D, steady, axisymmetric, incompressible RANS equations, standard k-ε turbulence model and energy equation when the inwards wall heat flux of 500 kW/m^2 was applied at Re=5000–60,000. The geometrical parameters of the rough rectangular elements were optimised based on 19 design cases when the dimensionless element height, pitch and width were ranged in 0.025–0.1, 0.5–1.5 and 0.05–0.2, respectively. The results showed that the Nusselt number was improved with increasing rough element height, width and Reynolds number and decreasing element pitch. The highest Nusselt number and best PEC were achieved when the dimensionless element heights were 0.1 and 0.025 at the dimensionless pitch and width of 0.5 and 0.2, respectively [167].

Transversely triangular inwards corrugated tube. A series of V-shaped nozzles were tightly inserted a circular tube to form the transverse triangular inwards corrugated tubes with pitch ratios of 2, 4 and 7, respectively. The forced convective heat transfer and friction characteristics of air flowing in the tubes was tested at a uniform inwards heat flux over the tube wall and Re=8500–16,500. The best heat transfer enhancement was achieved at the pitch ratio of 2, i.e., f/f_0=15.12–16.07, Nu/Nu_0=2.36–1.78, ψ=0.95–0.71, and η=0.16–0.11 as the Reynolds number increased from 8500 to 16,500 [142].

Three transverse triangular inwards corrugated tubes were designed and the forced convective heat transfer of air through the tubes was tested at a constant wall heat flux of 616 W/m^2 and Re=1500–8000. The wall shape was in periodical isosceles triangle, obtuse triangle and acute triangle with angles 27, 50 and 22/60° and the narrowest diameters 5 and 10 mm, respectively. The heat transfer enhancement rate (the product of heat transfer coefficient and heat transfer surface of the corrugated tube is divided the product of heat transfer coefficient and heat transfer surface area of the plain tube) varied in 1–11 at Re=2000–5000 [168].

Transversely arc inwards corrugated tube. Two transversely inwards corrugated tubes (inner diameter of 18 mm) with arc profile in the radii of 1.03 and 0.67 mm and a pitch of 15.95 mm were designed and the forced convective heat transfer of water in them was predicted based on the 3D, steady, incompressible RANS equations, realisable k-ε turbulence model and energy equation in Fluent at Re=12,000–57,000. The numerical results suggested that the corrugated tubes had a greater heat transfer coefficient than the plain tube but a lower coefficient than the helically inner finned tube [169].

Transversely S-shaped arc inwards corrugated tube. A transversely S-shaped arc inwards corrugated tube was proposed as heat transfer enhancement devices. The forced convective heat transfer of air turbulent flow in the tube was simulated when the arc pitch, height, width and circumferential wavenumber varied. It was showed that the heat transfer enhancement was improved by transverse vortex and longitudinal swirl flow. The increasing arc height and decreasing both pitch and width could enhance both Nusselt number and friction factor, and the circumferential wavenumber of 3 could result in the largest Nusselt number. The highest PEC=1.73 was achieved with the dimensionless pitch, height and width of 0.804, 0.065 and 0.217, and the wavenumber of 3 at Re=5000 [170].

Transversely arc, rectangular and trapezoidal outwards corrugated tube. Three transversely outwards corrugated tubes with semi-circle, rectangular and trapezoidal longitudinal cross-sections as shown in Fig. 22 were thermally tested to gain their thermal-hydraulic performance when the tubes were heated outside at a constant nominal power of 180 W and Re=10,000–38,000. In comparison with the plain tube, the heat transfer enhancement: f/f_0=1.15–2.26, Nu/Nu_0=1.34–1.63, ψ=1.28–1.24, and η=1.17–0.72 was obtained in the semi-circle

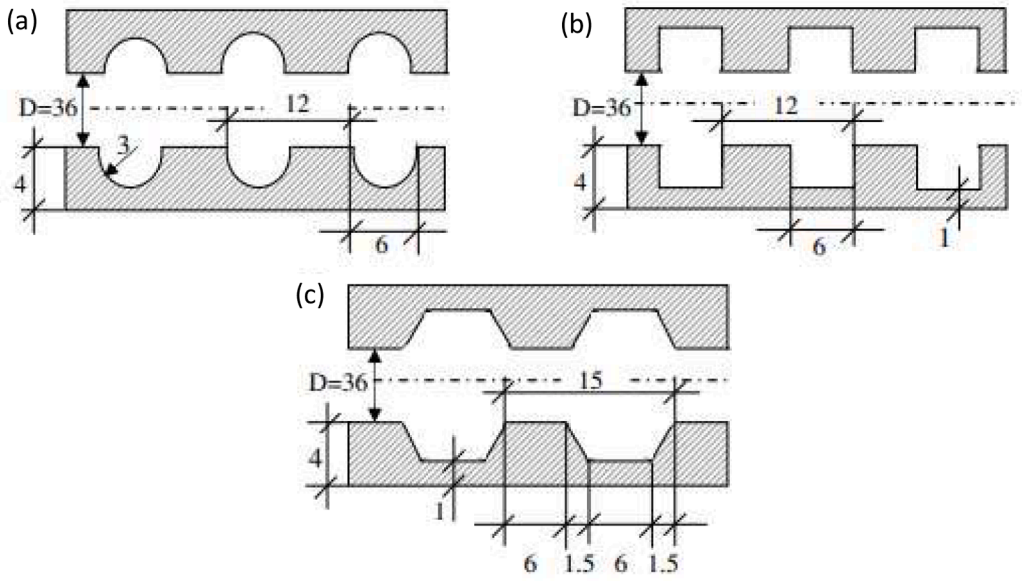

Fig. 22. Longitudinal cross-sections of the semi-circle, rectangular and trapezoidal corrugated tube proposed in [171], (a) semi-circle, (b) rectangular, and (c) trapezoidal, the pictures after [171].

outwards corrugated tube when the Reynolds number increased from 10,000 to 38,000. For the rectangular outwards corrugated tube, f/f_0=1.36–2.17, Nu/Nu_0=1.39–1.49, ψ=1.26–1.13, and η=1.03–0.68 were achieved, while f/f_0=1.19–2.19, Nu/Nu_0=1.32–1.58, ψ=1.24–1.22, and η=1.11–0.72 were presented for the trapezoidal outwards corrugated tube [171]. The semi-circle outwards corrugated tube shows the best but the rectangular outwards corrugated tube the poorest heat transfer enhancement, while the trapezoidal outwards corrugated tube is in between.

Twenty-five design cases were produced by using central composite design method based on four design parameters such as dimensionless arc pitch, height, radius and Reynolds number for the transversely arc outwards corrugated tube. The forced convective heat transfer characteristics of helium flowing inside these tubes were analysed using the 3D, steady, incompressible RANS equations, standard k-ε turbulence model and energy equation in ANSYS Fluent 13.0 when the helium inlet temperature and wall temperature were 663.15 K and 600 K at Re=26,250, 45,938, 65,626, respectively. The Nusselt number, friction factor and heat transfer coefficient were obtained and their correlations to the four design parameters were best fitted by employing response surface method. An optimisation took place against these correlations. It was revealed that the best heat transfer enhancement was ψ=1.42 and f/f_0=1.22 at Nu/Nu_0≥1.2 [172]. The same methodology was applied to the heat transfer enhancement of steam outside the transversely arc outwards corrugated tube when the steam inlet temperature and tube wall temperature were 603.15 K and 700 K at Re=26,250, 45,938, 65, 626, respectively. The best heat transfer enhancement ψ=1.12 at Nu/Nu_0≥1.2 was obtained when the dimensionless arc pitch, height, radius and Reynolds number were 0.82, 0.22, 0.23, and 26,263 [173].

The forced convective heat transfer of helium in a transversely arc outwards corrugated tube was simulated using the 3D, steady, incompressible RANS equations, Reynolds stress transport equations and energy equation in ANSYS Fluent 14.5 when the helium inlet temperature and tube wall temperature were 663.15 K and 603.15 K at Re=3800–43,800. The PEC varied from 1.28 to 0.92 when the Reynolds number increased from 3800 to 43,800 [174].

The forced convective heat transfer characteristics of air flow inside the transversely arc outwards corrugated tube was predicted using the 3D, steady, incompressible RANS equations, standard k-ε turbulence model and energy equation in Fluent 15.0 when the air inlet temperature and wall temperature were 300 K and 350 K at Re=5000–40,000, respectively, and the arc width, pitch and height varied. The effects of these parameters or roughness parameters such as skewness R_{sk} and kurtosis R_{ku} on the flow characteristic and heat transfer performance were analysed. It was showed that PEC was improved with increasing arc width and height and decreasing pitch, i.e. decreasing R_{sk} and R_{ku} [175].

The thermal-hydraulic characteristics of turbulent water flow in the transversely inwards or outwards corrugated tubes with arc, triangular, rectangular and trapezoidal profiles were predicted numerically based on the 2D, axisymmetric, steady, incompressible RANS equations, standard k-ε turbulence model and energy equation in ANSYS Fluent at an inwards wall heat flux of 500 kW/m^2 and Re=5000–61,000. The results revealed that the Nusselt numbers in the inwards corrugated tubes with trapezoidal, rectangular, arc and triangular profiles were higher by 52.61 %, 50.12 %, 47.82 %, and 44.96 % than the plain tube, respectively. In the outwards corrugated tubes, the Nusselt numbers were improved by 48.31 %, 40.94 %, 41.23 %, and 45.72 % for the trapezoidal, rectangular, arc, and triangular profiles, respectively. The best heat transfer enhancement ψ=1.10–0.95 (maximum ψ=1.18 at Re=10,000) was obtained in the inwards corrugated tubes with the arc profile, but ψ=1.05–1.07 (maximum ψ=1.25 at Re=10,000) in the outwards corrugated tubes with the triangular profile [176].

Flow and heat transfer characteristics of xanthan gum solutions were tested in a transversely semi-circle outwards corrugated tube as illustrated in Fig. 22(a) at different concentrations and bulk velocities of xanthan gum solutions. The results showed that the friction factor increment ratio in the corrugated tube rose then declined with increasing bulk velocity. The Nusselt number increment ratio and heat transfer enhancement efficiency (Nusselt number increment ratio is divided by friction factor increment ratio) increased with increasing concentration and decreasing bulk velocity, and ended up with the maximum Nusselt number increment ratio of 25 and the best heat transfer enhancement efficiency of 1600 [177].

Two transversely semi-circular corrugated tubes, one with inwards semi-circle and the other one with outwards semi-circle, were designed and the forced convective heat transfer of SCO2 flowing in them was predicted numerically by using the 3D, steady, compressible RANS equations, standard k-ε turbulence model and energy equation in ANSYS Fluent when the tubes were used as the receiver in a solar trough at a

non-uniform wall heat flux and SCO2 mass flow rate varied in 0.06–0.10 kg/s. The numerical results revealed that the inwards corrugated tube exhibited the best heat transfer performance, for example, the heat transfer coefficient of the tube was increased by 157.8 % and 169 % at the mass flowrate of 0.08 kg/s compared with the plain tube when both the tubes were installed horizontally and vertically, respectively [178].

The transversely inwards corrugated tubes with arc, triangular, trapezoidal and rectangular profiles were generated and the forced convective heat transfer of GNP-SDBS/water, Al_2O_3/water, and SiO_2/water nanofluids in them was analysed numerically based on the 2D, axisymmetric, steady, incompressible RANS equations, realisable k-ε turbulence model and energy equation for single phase flow in ANSYS Fluent 2019 R3 when the nanofluid inlet temperature was 300 K and a uniform inwards wall heat flux was 50 kW/m^2 at Re=5000–40,000. The results suggested that the corrugated tubes and nanofluids could improve heat transfer by around 20 % and 11 % compared with the plain tube, respectively, while both techniques used together could enhance the heat transfer by up to 37 % at Re=10,000. The corrugated tube with arc profile could achieve the best heat transfer enhancement at Re≥10,000 with the maximum ψ=1.37 at Re=10,000 [179].

Three transversely inwards corrugated tubes with semi-circular, triangular and trapezoidal profiles were generated and the forced convective heat transfer of single-walled carbon nanotube (SWCNT)/water nanofluid through these tubes was predicted numerically by using the 2D, axisymmetric, steady, incompressible RANS equations, SST k-ω turbulence model and energy equation in Fluent when the nanofluid inlet temperature was 300 K and a uniform wall heat flux was 10 kW/m^2 at Re=5000–30,000. The profile height ratio e/d, profile width ratio w/d and pitch ratio s/d were 0.38, 0.3, and 0.9; the nanoparticle volume concentration-dependent effective thermo-physical and transport properties were prescribed in the CFD simulations, and nanoparticle volume concentrations were given to be 0, 0.05, 0.1, and 0.25 %, respectively. The best heat transfer enhancement: f/f_0=3.63–4.53, Nu/Nu_0=1.81–1.35, ψ=1.18–0.82, and η=0.50–0.30 was predicted with trapezoidal profile when the Reynolds number varied from 5000 to 30,000 for water. This achievement seems unsatisfactory. Additionally, the ratio of the PEC in nanofluid flow condition ψ_{nano} to the PEC in water flow condition ψ can be correlated to the nanoparticle volume concentration φ linearly as shown in Fig. 23 [180].

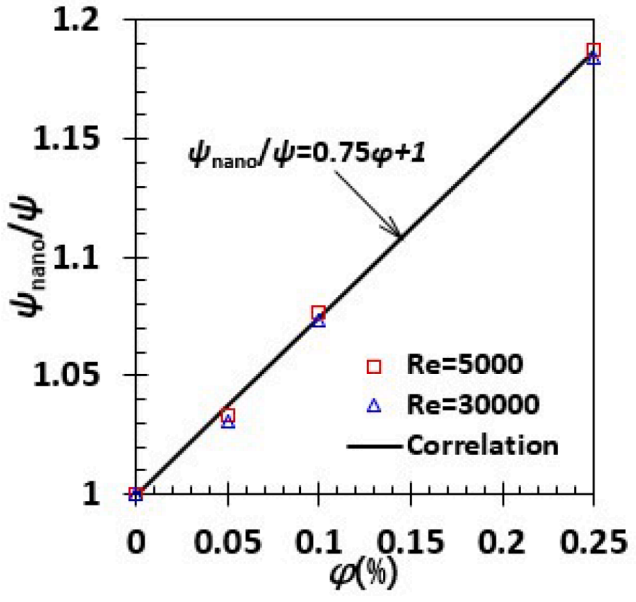

Fig. 23. Ratio of the PEC in nanofluid flow condition ψ_{nano} to the PEC in water flow condition ψ is correlated to nanoparticle volume concentration φ, the data after [180].

Three transversely outwards corrugated tubes with arc, triangular and trapezoidal profiles were generated and the forced convective heat transfer of Fe_3O_4/water nanofluid in them was investigated numerically by using the 3D, steady, incompressible RANS equations, SST k-ω turbulence model, two-phase mixture model and energy equation in ANSYS Fluent when the uniform wall heat flux was 10 kW/m^2 at Re=5000–30,000 and φ=0, 1, 2, 3 %. The numerical results suggested that the pressure drop and Nusselt number in the corrugated tube with trapezoidal profile were 2.92 and 1.66 times the plain tube at Re=30,000 and φ=2 %. The presence of corrugation could increase the viscous entropy generation rate but reduce the thermal entropy generation rate. The Bejan number decreased with increasing Reynolds number [181].

Transversely sinusoidal inwards and outwards corrugated tubes. Heat transfer, pressure drop and effectiveness in a tube-in-tube heat exchanger with sinusoidal inwards and outwards corrugated tubes were measured when hot water flowed in the inner tube at Re=3500–18,000 and 40 °C inlet temperature, and cold water passed through the outer tube at Re=5500 and 8 °C inlet temperature, respectively. The maximum heat transfer enhancement ψ=1.19–0.93 was gained in the heat exchanger with inwards corrugated outer tube and outwards corrugated inner tube at Re=7000–17,500 [182].

Transversely arc inwards corrugated tube with spring tape insert. The forced convective heat transfer of air in a transversely arc inwards corrugated tube with spring/coil tape insert in two corrugation pitch ratios and lead ratios (ratio of lead to spring/coil diameter) was tested at Re=10,000–50,000 under heating conditions. The results demonstrated that the heat transfer enhancement, i.e., f/f_0=1.62, Nu/Nu_0=3.17, ψ=2.70, and η=1.96 almost was independent of Reynolds number [183].

Periodical contraction-expansion tube. The periodical contraction-expansion tube is a tube that is composed of several venturis in series. Since the area expansion is quite large, a periodical contraction-expansion tube always suffers from a considerable flow resistance and low heat transfer enhancement efficiency. Three periodical contraction-expansion tubes with linear contraction wall shape and linear or nonlinear quick expansion wall shape were designed. The forced convective heat transfer of air passing through the tubes was measured at Re=14,000–40,000. In compassion with the plain tube, the heat transfer enhancement: f/f_0=6.06–6.68, Nu/Nu_0=2.49–2.51, ψ=1.36–1.38, and η=0.41–0.38 was achieved in the contraction-expansion tube with slowly linear expansion wall shape when the Reynolds number varied from 14,000 to 40,000. For the contraction-expansion tube with quick linear expansion wall shape, the heat transfer enhancement was f/f_0=8.89–7.65, Nu/Nu_0=2.53–2.85, ψ=1.22–1.44, and η=0.28–0.37. For the contraction-expansion tube with quick nonlinear expansion wall shape, f/f_0=8.63–9.88, Nu/Nu_0=2.31–2.68, ψ=1.12–1.25, and η=0.26–0.27 [184].

The forced convective heat transfer of Al_2O_3/water and CuO/water nanofluids in the periodical contraction-expansion tubes with linear contraction wall shape and quick linear expansion wall shape was simulated using the single-phase 3D steady RANS equations, realisable k-ε model and energy equations with effective density, thermal conductivity, and dynamic viscosity in ANSYS Fluent 18.2. When the CFD simulation took place, four geometrical parameters (two diameters, two axial lengths) of the periodical contraction-expansion tube varied at Re=10,000, 12,500, 15,000, 17,500 and 20,000, φ=2, 3, 4, 5 %, while the constant inwards wall flux of 500 kW/m^2, and nanofluid inlet temperature of 303 K and were held. It was showed that the thermal performance of Al_2O_3/water nanofluid was slightly superior to CuO/water nanofluid, for example, ψ=1.098–1.069 for Al_2O_3/water nanofluid and ψ=1.096–1.063 for CuO/water nanofluid at φ=3 % but ψ=1.097–1.073

for Al_2O_3/water nanofluid and ψ=1.088–1.058 for CuO/water nanofluid at φ=5 % when the Reynolds number varied from 10,000 to 20,000 [185]. This fact implied that the periodical contraction-expansion tubes with linear contraction wall shape and quick linear expansion wall shape was ineffective in heat transfer enhancement in Al_2O_3/water or CuO/-water nanofluid flow condition.

Orthogonal ellipse tube

The orthogonal ellipse tube or alternating elliptical axis tube is composed of a series of ellipses which are distributed along the tube axis in an orthogonal manner, or their major and minor axes are rotated alternatingly by 90° in different axial positions along the tube axis, as shown in Fig. 24. Even though the cross-sectional area of these ellipses is identical, the area experiences contraction and expansion in the orthogonal radial directions simultaneously when the major and minor axes are rotated by 90°, as demonstrated in Fig. 24(a). The variation of the cross-sectional area in the orthogonal radial directions can generate longitudinal vortices in the flow field to enhance convective heat transfer in the tube.

Experiments were performed on the forced convective heat transfer of water or 22# lubricating oil in the orthogonal ellipse tube at *Re*=500–50,000. The experimental data confirmed that the heat transfer enhancement was as great as f/f_0=1.60–4.69, Nu/Nu_0=3.11–6.06, ψ=2.66–3.62, and η=1.94–1.29 at *Re*=500–2300 but f/f_0=2.59–2.30, Nu/Nu_0=2.76–1.34, ψ=2.01–1.01, and η=1.07–0.58 at *Re*=2200–50,000. The mechanism for this heat transfer enhancement is basically because of the longitudinal vortices generated by the cross-sectional variation in the orthogonal ellipse tubes [144]. This outcome suggests that the orthogonal ellipse tube is more suitable to heat transfer enhancement in laminar flow regime than in turbulent flow regime.

The forced convective heat transfer of heat transfer oil in four orthogonal ellipse tubes with different aspect ratios and pitches was investigated numerically in Fluent 6.3 based on the 3D, steady, incompressible RANS equations, standard *k*-ε turbulence model and energy equation at *Re*=300–2000 under isothermal wall conditions. The results demonstrated that the decreasing aspect ratio and pitch could improve heat transfer coefficient but increase flow resistance. The best heat transfer enhancement f/f_0=1.16–1.91, Nu/Nu_0=1.16–1.94, ψ=1.10–1.56, and η=1.00–1.02 was obtained as the Reynolds number increased from 300 to 2000 [186].

A mathematical method was developed to orthogonal ellipse tubes analytically in [187]. In the method the lengths of the semi-major and semi-minor axes vary as a sinusoidal function of axial coordinate between two ellipse bases or two super-ellipse bases when the cross-sectional area or hydraulic diameter remains fixed. The analytical expression for an ellipse is written as [187]:

$$\left|\frac{z}{a}\right|^{\prime\prime} + \left|\frac{y}{b}\right|^{\prime\prime} = 1 \tag{4}$$

where *a* and *b* are the lengths of the semi-major and semi-minor axes of the ellipse, respectively, ″ is the shape factor of the ellipse, ″=2 is for an ordinary ellipse, ″>2 for a super ellipse, ″=2.5 was used in [187]. When the hydraulic diameter is fixed, the coordinates of a cross-section in the orthogonal ellipse tube based on the ellipse base are described by [187]:

$$\begin{cases} z = \frac{\mathscr{R}}{2}\left(\frac{a}{b}\right)^{\sin\frac{2\pi x}{s}} + \frac{R}{2} \\ y = \frac{\mathscr{R}}{2}\left(\frac{a}{b}\right)^{-\sin\frac{2\pi x}{s}} + \frac{R}{2} \end{cases} \tag{5}$$

where $\mathscr{R}$ is the equivalent diameter of the circle whose area is equal to the ellipse, *s* is the pitch of the tube, and *x* is the axial coordinate of the tube. A few orthogonal ellipse tubes with different aspect ratios and pitches were designed and the forced convective heat transfer of water in the tubes was simulated based on the 3D, steady, incompressible Navier-Stokes equations, and energy equation in laminar flow regime and at a constant wall temperature in COMSOL. Unfortunately, the numerical results indicated the best PEC values are ranged in 1.05–1.07 at *Re*=90–1400, as shown in Fig. 25 [187]. Further work on this kind of tube is needed in the future.

The transition between any two ellipses in an orthogonal ellipse tube is sharp. To remove this drawback and reduce friction factor, the

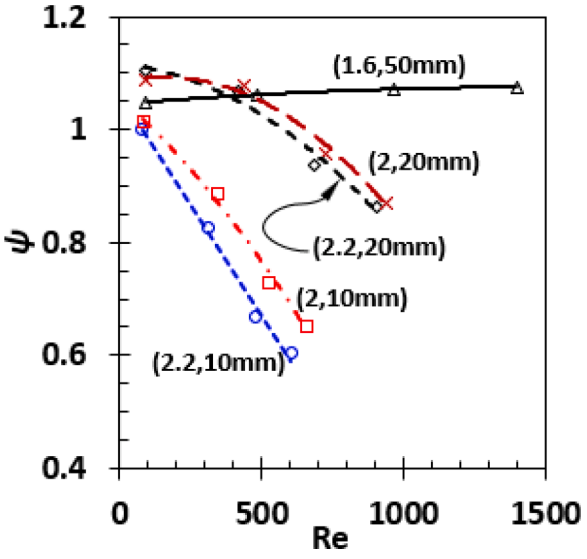

Fig. 25. PEC ψ is plotted as a function of Reynolds number *Re*, the data are based on constant hydraulic diameter and from [187], the first and second values in () are the aspect ratio and pitch of the orthogonal ellipse tubes.

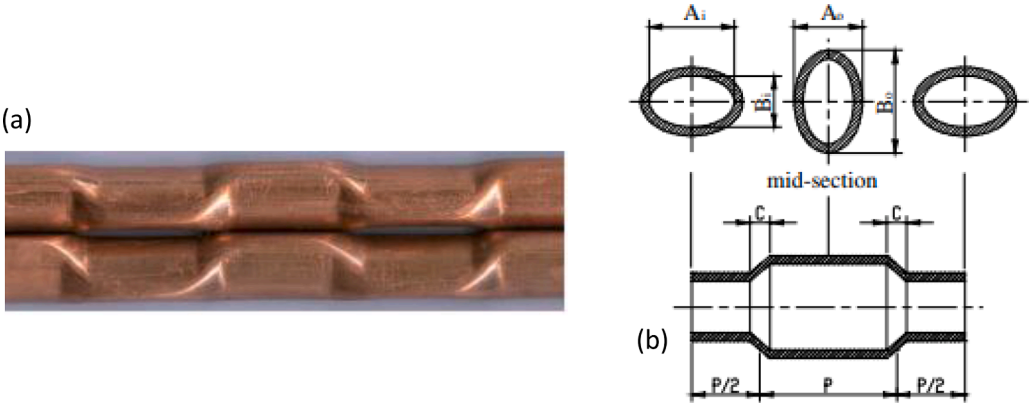

Fig. 24. Photo and three cross-sections of the orthogonal ellipse tube proposed in [144], (a) photo of the tube, (b) cross-sections, the pictures after [144].

transition segment was replaced with a smooth twisted ellipse tube, and a so-called alternative elliptical twisted tube was generated. The forced convective heat transfer of SCO2 flowing in the tube was simulated based on the 3D, steady, compressible RANS equations, standard k-ε turbulence model and energy equation when the tube served as the solar receiver in a solar trough at a non-uniform wall heat flux distribution. In the simulations, SCO2 mass flow rate at the tube inlet varied in 0.06–0.10 kg/s. The numerical results showed that the heat transfer coefficient of the alternative elliptical twisted tube was higher by 8 % and 8.3 % than the orthogonal ellipse tube when both the tubes were installed horizontally and vertically, respectively. Unfortunately, the thermal performance of the alternative elliptical twisted tube was poorer than the transversely semi-circular inwards corrugated tube [178].

Alternating circle and ellipse tube

The alternating circle and ellipse tube was proposed in [188]. The tube resembles the orthogonal ellipse tube shown in Fig. 24 but the ellipse between two horizontal two ellipses is replaced with a circle. The forced convective heat transfer of heat transfer oil in the alternating circle and ellipse tubes with different aspect ratios and pitches was estimated by using the 3D, steady, incompressible Navier-Stokes equations, and energy equation at Re=500–2000 and a constant wall temperature in Fluent 6.3. The best heat transfer enhancement f/f_0=1.10–2.21, Nu/Nu_0=1.05–1.83, ψ=1.01–1.49, and η=0.95–0.83 was gained when the Reynolds number varied from 500 to 2000 [188]. This heat transfer enhancement is slightly poorer than that in [186].

The alternating circle and ellipse tube in [188] was generated by using a manufacturing method, and the transition segment between the circle section and the ellipse is sharp and unsmooth. An analytical approach was developed in [189] to make the transition segment smooth. In the approach two semi-axis lengths of an ellipse vary as a sinusoidal function of axial coordinate between two circles when the cross-sectional area remains fixed. A few annular tubes were designed by using that approach and the forced convective heat transfer of water flowing those annular tubes was simulated based on the 3D, steady, incompressible Navier-Stokes equations, and energy equation in ANSYS Fluent 14.0 at Re=388 and a constant temperature on both walls. It was demonstrated that the heat transfer enhancement existed compared with the plain annular tube. A phase-shifting of one-eighth of a wavelength/pitch between the external and internal tube could improve ψ by 43 % [189].

Tube-in-tube heat exchanger with orthogonal ellipse tube

The forced convective heat transfer in a parallel- or counter-flow tube-in-tube heat exchanger with the inner tube being the orthogonal ellipse tube was simulated using the 3D, steady, incompressible Navier-Stokes equations, energy equation of water in laminar flow regime and heat conduction equation in the inner tube wall in a custom CFD code. Effects of velocity at the inner tube inlet and outer tube inlet and tube length on heat transfer enhancement were estimated. The results indicated that the orthogonal ellipse tube could generate longitudinal vortices in the inner and outer tube flows to enhance heat transfer performance. The counter-flow exhibited a higher overall heat transfer coefficient than the parallel-flow, but the heat transfer enhancement in the parallel-flow was slightly better than the counter-flow [190].

Nozzles or inserts in series in tube

A series of conical nozzle were tightly installed along the tube axis in a tube to form a periodical convergent-divergent tube [143]. Three tube configurations, i.e., convergent configuration, convergent-divergent configuration and divergent configuration with conical nozzle diameter ratios of 0.3, 0.4, 0.5, 0.6 and 0.7 and pitch ratios of 2, 3 and 4, respectively, were employed. The forced convective heat transfer of air flowing the tubes with a series of conical nozzles was numerically studied by using the 3D steady RANS equations, realisable k-ε model and energy equations in Fluent at a constant inwards wall heat flux and Re=6000–25,000. Both Nusselt number and friction factor increased with decreasing nozzle diameter ratio and pitch ratio. The best heat transfer enhancement was produced by the tube divergent configuration, namely f/f_0=40.96–30.54, Nu/Nu_0=2.86–2.23, ψ=0.83–0.71, and η=0.070–0.073, suggesting a poor heat transfer enhancement method [143].

A series of Y-shaped tee inserts were loosely placed in an arc-shaped inner finned tube to form a compound tube for further improvement of heat transfer enhancement [191]. The forced convective heat transfer in the compound tubes with different gaps between two inserts was tested at Re=4000–14,000. The best heat transfer enhancement: f/f_0=9.34–8.50, Nu/Nu_0=3.14–4.44, ψ=1.49–2.17, and η=0.34–0.52 reached at the gap of 10 mm when the Reynolds number varied from 4000 to 14,000 [191].

Helically corrugated tube

Helically corrugated tubes are the tubes with inwards or outwards screwed wall by employing various basic geometrical elements such as arc, elliptical, rectangular, trapezoidal, sinusoidal profiles and so on. This passive heat transfer enhancement method started to exist from the 1980s and grow up slowly right now. Helically corrugated tubes can be divided into three categories: (1) inwards corrugated tube, (2) outwards corrugated tube, and (3) inwards and outwards corrugated tube. The inwards or outwards corrugated tubes often have arc, rectangular, semi-elliptical profiles, while the inwards and outwards corrugated tubes are subject to sinusoidal profile. The helically corrugated tubes almost are in single thread currently.

The thermal-hydraulic performance in heat transfer enhancement by the existing helically corrugated tubes is summarised in Fig. 26 base on the plots f/f_0-Re, Nu/Nu_0-Re, ψ-Re and η-Re in Fig. 27 in terms of the plots Nu/Nu_0-f/f_0, ψ-f/f_0 and η-f/f_0. The values of f/f_0=1.29–14.80, Nu/Nu_0=0.65–4.28, ψ=0.36–1.70, and η=0.044–1.30 in laminar flow regime (Re=30–2300) and f/f_0=1.03–8.82, Nu/Nu_0=1.09–2.92, ψ=0.92–2.17, and η=0.22–1.85 in turbulent flow regime (Re=2300–90,000) are observed. The extremely large f/f_0 values were identified in experimental heat transfer enhancement of helically arc inwards corrugated tubes [192]. The best heat transfer enhancement: f/f_0=1.29–1.58, Nu/Nu_0=1.08–2.06, ψ=0.98–1.77 and η=0.79–1.30 in laminar flow regime was devote to [193] based on experimental heat transfer in the coil heat exchanger helically arc inwards corrugated tube at Re=30–800. For helically rectangular inwards corrugated tubes the best heat transfer enhancement: f/f_0=2.13–1.86, Nu/Nu_0=3.00–1.94, ψ=2.33–1.58 and η=1.40–1.04 was obtained at Re=5500–57,000 experimentally. Based on this outcome, helically rectangular inwards corrugated tube can be a reasonably good passive heat transfer enhancement method compared with periodically convergent-divergent tubes in turbulent flow regime.

The geometrical parameters describing helically corrugated tubes include the height, width and pitch of a geometrical profile which is used as a tool to corrugate the tube wall. The effects of these geometrical parameters on heat transfer enhancement generated have been studied experimentally and numerically. The effects mainly are associated with inwards or outwards corrugated tubes or both inwards and outwards corrugated tubes. The heat transfer enhancement inside or outside the helically corrugated tube or in coil heat exchangers or shell and tube heat exchangers with helically corrugated tubes are summarised in the following sections. Besides water, ethylene glycol, machine oil, Al_2o_3/water nanofluid, fluid foods of whole milk, cloudy orange juice, apricot puree and apple puree have been used as working fluids.

Geometrical effects inside helically corrugated tubes

Inwards corrugated tubes. Ten helically arc inwards corrugated tubes in

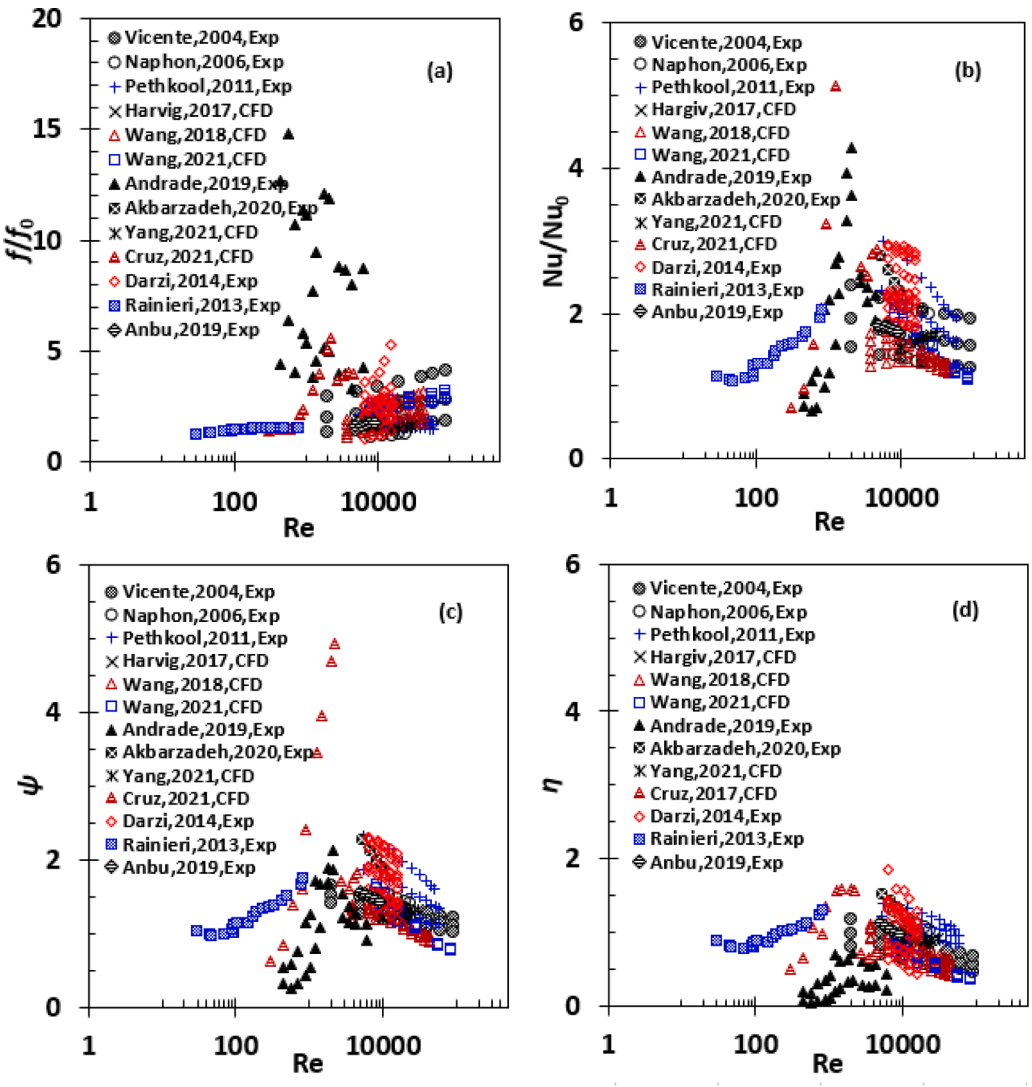

Fig. 26. Thermal-hydraulic parameters f/f_0, Nu/Nu_0, ψ and η are shown as a function of Reynolds number *Re* for periodically corrugated tubes, (a) f/f_0, (b) Nu/Nu_0, (c) ψ and (d) η, the data are for heat transfer inside the tubes.

single thread were manufactured by cold rolling, resulting in arc profile height ratios e/d=0.02–0.06 and pitch ratios s/d=0.6–1.2. The Reynolds number is ranged from 2000 to 90, 000 and Prandtl number from 2.5 to 100 by using of water and ethylene glycol, respectively. The severity index ($\varphi=e^2/sd$) was applied to describe geometrical effect of the tubes on heat transfer and pressure drop characteristics. For the optimal thermal-hydraulic performance, the severity index should meet φ>0.003 at low Reynolds numbers (*Re*<10,000), and φ=0.001–0.003 at high Reynolds numbers (*Re*=10,000–40,000) [194].

Nine helically rectangular inwards corrugated tubes in single thread with rectangular profile height ratios e/d=0.12, 0.15, 0.19, and pitch ratios s/d=1.05, 0.78, 0.63 were tested by using cold and hot water as heat transfer fluids. The best heat transfer enhancement: f/f_0=2.44–2.74, Nu/Nu_0=2.16–1.98, ψ=1.60–1.41 and η=0.88–0.72 was obtained as the Reynolds number rose from 8000 to 24,000 [195].

Helically rectangular inwards corrugated tubes in single thread with rectangular profile height ratios e/d=0.02, 0.04, 0.06, and pitch ratios s/d=0.18, 0.22, 0.27 were tested by using water under forced convective heat transfer conditions at *Re*=5500–60,000. The excellent heat transfer enhancement: f/f_0=2.14–1.86, Nu/Nu_0=3.00–1.94, ψ=2.33–1.58 and η=1.40–1.04 was achieved when the Reynolds number rose from 5500 to 60,000 [196].

The thermal-hydraulic performance of helically inwards corrugated tubes with arc profile, inwards dimpled tubes and inner wire coil tubes was analysed based on heat transfer and pressure drop experimental data in laminar, transitional and turbulent flow regimes. The results indicated that the plain tube was recommended at *Re*<200, the wire coil tube was more suitable to *Re*=200–2000, and the corrugated and dimpled tubes were more advantageous for *Re*>2000 [197].

Five helically inwards corrugated tubes with arc profiles in different heights and pitches were designed and the forced convective heat transfer in these tubes was simulated based on the 3D, steady, incompressible RANS equations, Reynolds stress model and energy equation in ANSYS Fluent 14.5 to obtain entropy generation characteristics at a constant wall temperature condition and *Re*=10,020–40,060. The numerical results indicated that the thermal entropy generation occurred in the viscous sub-layer and vortex region, but the viscous entropy generation was located in the windward of the corrugation and severely turbulent fluctuation region. The smallest Bejan number was 0.69 [198].

The forced convective heat transfer of water flowing in six helically inwards semi-elliptical profile corrugated tubes in single thread was numerically simulated at *Re*=25,000 and a constant inwards wall heat flux of 50 kW/m^2 by using the 3D, steady, incompressible RANS equations, realisable *k*-ε turbulence model and energy equation in ANSYS Fluent 17.0 to clarify the geometrical influences on heat transfer and flow patterns. A new dimensionless parameter, i.e., corrugation profile

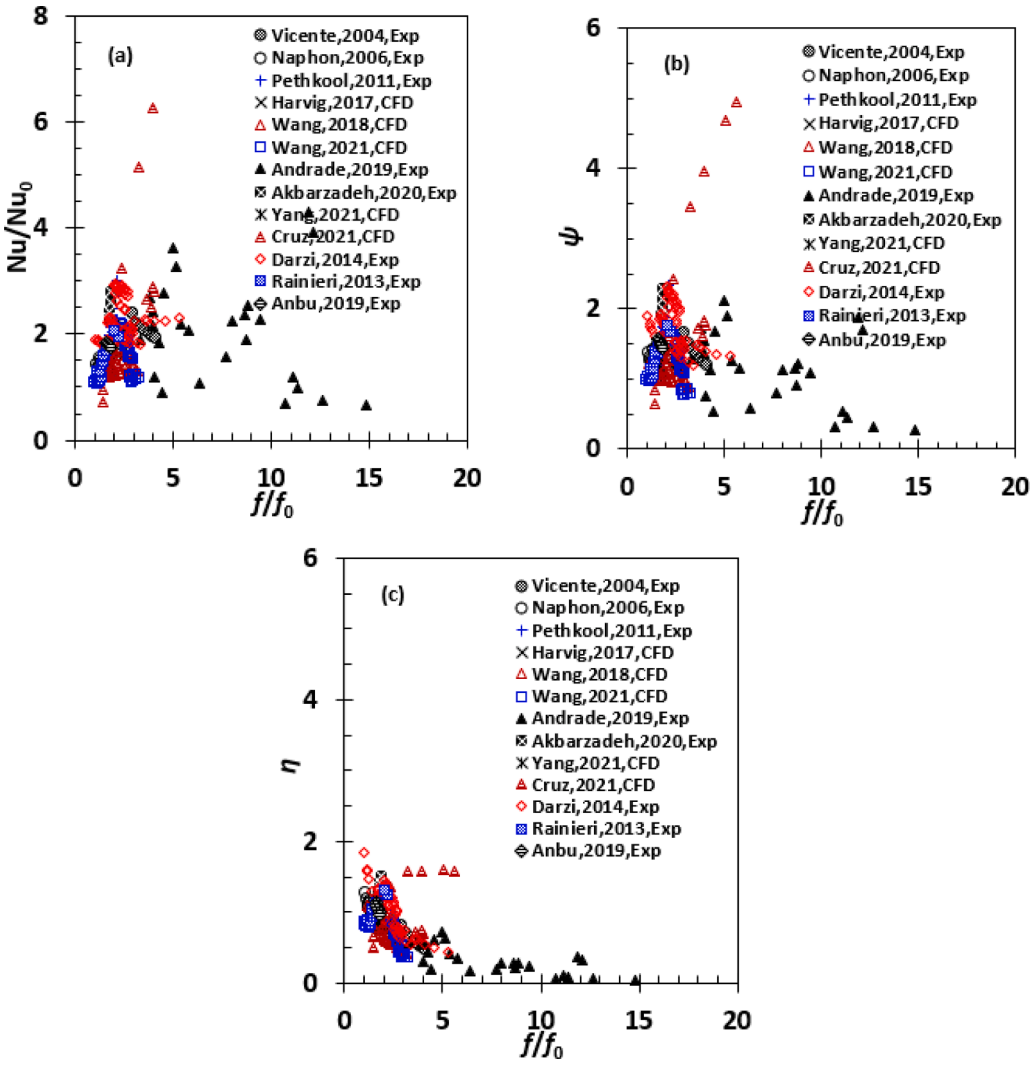

Fig. 27. Parameters Nu/Nu_0, ψ and η are demonstrated as a function of f/f_0 for helically corrugated tubes, (a) Nu/Nu_0, (b) ψ and (c) η, the data are for heat transfer inside the tubes.

shape factor ($e/d \times w/s$), which includes the width of the profile w, was proposed. The results showed that the Nusselt number ratio rose with increasing e/d until 0.05 then declined. The friction factor ratio f/f_0 and Nusselt number ratio Nu/Nu_0 decreased linearly with increasing s/d. The Nusselt number ratio Nu/Nu_0 and friction factor f/f_0 increased almost linearly with the profile shape factor (in the range of 4 to 18) [199].

The heat transfer and pressure drop of internal flow in the helically corrugated tubes with arc profile in different pitches were characterised experimentally by using water as heat transfer fluid. The experiments were performed with Reynolds numbers in the range from 429 to 6212 to cover laminar, transitional and turbulent flow regimes under adiabatic and diabatic (heat flux imposed on the tube wall varied from 5.5 kW/m^2 to 21.1 kW/m^2) conditions. The results suggested the heat transfer enhancement by the corrugated tubes was more effective in the transitional regime, for instance, f/f_0=4.99–4.00, Nu/Nu_0=3.63–2.16, ψ=2.16–1.36 and η=0.73–0.54 were obtained at Re=2000–3500 [192].

Three helically inwards corrugated tubes with arc profile in one thread was designed and the forced convective heat transfer of water flowing in the tubes was tested under heating condition (uniform wall heat flux from 4 to 33 kW/m^2) at Re=300–5000. Also, the heat transfer was simulation based on the 3D, steady, incompressible RANS equations, SST k-ω turbulence model and energy equation in Star-CCM. The results showed that the best heat transfer enhancement by the corrugated tubes was f/f_0=1.43–5.60, Nu/Nu_0=0.72–8.79, ψ=0.63–4.95 and η=0.50–1.57 at Re=300–2200 and f/f_0=3.64–3.93, Nu/Nu_0=2.64–2.89, ψ=1.72–1.83 and η=0.72–0.73 at Re=2750–4500, respectively. The critical Reynolds number for the transition between turbulent regime and laminar regime was 800–900. The optimal operating condition occurred at Re=1000–230o for the helically corrugated tubes investigated [200].

A helically semi-circular inwards corrugated tube (inner diameter of 27 mm) with a pitch of 60 mm and a profile height of 4.5 mm in six threads was generated and the forced convective heat transfer of water in the tube was simulated by using the 3D, steady, incompressible RANS equations, realisable k-ε turbulence model and energy equation in Fluent at the inlet temperature of 363K and a uniform wall temperature of 300 K as well as Re=10,000–30,000. The corrugated tube was composed of two segments in series, and two cases were investigated, the first one was the case where two segments shared the same helical direction, the second one was the case where two segments had opposite helical directions. The numerical results demonstrated that the case where two segments shared the same helical direction had better thermal-hydraulic performance. As a result, the best heat transfer enhancement such as f/f_0=1.40–1.59, Nu/Nu_0=1.54–1.71, ψ=1.21–1.33 and η=0.91–0.93 reached when the Reynolds number increased from 10,000 to 30,000. Also, a secondary flow pattern induced by the centrifugal force owing to the continuous helical structure was

discovered [201].

Nine helically inwards corrugated tubes of the diameter of 8.1 mm in rectangular profile with the pitches of 5, 7 and 8 mm, profile heights of 0.75, 1, 1.25 and 1.5 mm were tested when Al_2O_3/water nanofluid was used as heat transfer fluid at nanoparticle volume concentrations of 0.25, 0.5, and 1 % and Reynolds number varied from 5000 to 20,000. The results demonstrated that the Nusselt number and friction factor in the plain and helically corrugated tubes ascended with increasing nanoparticle concentration, especially in the corrugated tubes. This effect was intensified in the corrugated tubes with large profile height and small pitch. The best heat transfer enhancement: f/f_0=2.02–2.51, Nu/Nu_0=2.92–2.83, ψ=2.31–2.09 and η=1.44–1.13 at the profile height of 1.25 mm, pitch of 5 mm and nanoparticle concentration of 1 % was observed in comparison with f/f_0=2.06–2.57, Nu/Nu_0=2.76–2.46, ψ=2.17–1.80 and η=1.34–0.96 at zero nanoparticle concentration [202].

Five helically inwards corrugated tubes with three arc profile heights and three leads were designed and two rod inserts with spirally implanted short, inclined bars in two pitches were proposed. These rod inserts were installed into the five helically inwards corrugated tubes separately to produce five helically inwards corrugated tubes with the rod inserts. The forced convective heat transfer of TiO_2/water nanofluids in these helically corrugated tubes was tested at Re=4800–8900 and φ=0, 0.25, 0.5 %. The experimental results indicated the best heat transfer enhancement such as f/f_0=1.60–1.80, Nu/Nu_0=1.83–1.75, ψ=1.56–1.44 and η=1.14–0.97 was obtained at an arc height of 1 mm, a lead of 8 mm, a pitch of 30 mm for the bars and φ=0.5 % [203].

Outwards corrugated tubes. Five helically outwards corrugated tubes with arc profile were tested to determine the effects of arc height ratio and pitch ratio on heat transfer enhancement inside the tubes. Numerical simulations were also conducted to find the mechanism of heat transfer enhancement using the 3D steady incompressible RANS equations, Reynolds stress transport equations and energy equation at Re=3800–43,800 and a constant wall temperature. The best heat transfer enhancement: f/f_0=1.89–3.16, Nu/Nu_0=1.73–1.31, ψ=1.40–0.89 and η=0.91–0.41 was obtained at e/d=0.1 and s/d=1.0 when the Reynolds number varied from 3800 to 43,800. The heat transfer enhancement was due to a jet impingement heat transfer at windward side of the arc profile and the considerable turbulent fluctuation rather than swirling flo [174]

Nine helically corrugated tubes were designed for the absorber of a parabolic trough solar collector and the forced convective heat transfer of water in the tubes was tested at Re=5000–10,000. The results indicated that the heat transfer rate was increased by (85.7–107.2) % in the corrugated tubes, depending on the arc profile height and pitch ratio. The best heat transfer enhancement f/f_0=1.84–1.75, Nu/Nu_0=2.80–2.31, ψ=2.29–1.91 and η=1.52–1.32 was achieved at a pitch ratio of 0.12 and an arc height ratio of 0.06 when the Reynolds number varied from 5000 to 10,000 [204].

Inwards and outwards corrugated tubes. The forced convective heat transfer of flow in 28 helically inwards and outwards sinusoidal profile corrugated tubes in single thread was numerically investigated when the profile height ratio e/d and pitch ratio s/d varied in the ranges 0–0.16 and 0–2, respectively. The 3D, unsteady, incompressible RANS equations, SST k-ω turbulence model and energy equation were solved in ANSYS Fluent 16.2 using a representative computational domain at a constant wall temperature and Re=10,000. It was shown that the thermal-hydraulic performance was degraded with increasing sinusoidal profile height based on PEC value. This is because a large profile height results in a little increase in Nusselt number but a huge pressure drop [205].

Geometrical effects outside helically corrugated tube

The forced convective heat transfer of water flowing in the annulus between the outer circular tube and the helically outwards corrugated inner tube in arc profile and single thread was tested at Re=1700–13,000. The experimental results showed that both the pitch to arc height ratio (s/e) and the annulus diameter ratio (inner tube diameter to outer tube diameter) affected significantly Nusselt number. When the annulus diameter ratio was smaller than 0.5, the Nusselt number at s/e=10 was larger than at s/e=12.5. However, when the annulus diameter ratio was more than 0.5, the Nusselt number at s/e=14.2 was greater than at s/e=10. The best Nusselt number ratio such as Nu/Nu_0=1.03–1.78 was obtained [206].

The heat transfer enhancement generated by the helically outwards corrugated tubes with arc profile as the water with an inlet temperature of 303.15 K flowing in the shell side of a shell and tube heat exchanger was numerically predicted by using the 3D, steady, incompressible RANS equations, realisable k-ε model and energy equations in ANSYS Fluent 14.5 at a constant wall temperature of 333.15 K and Re=8900–89,400. The helically outwards corrugated tubes were arranged in three patterns of bundle, namely, circular bundle, square bundle and triangular bundle in four tube centre-to-centre spacings (1.25, 1.375, 1.5 and 1.625). The results suggested the best heat transfer enhancement: f/f_0=2.31–2.88, Nu/Nu_0=2.21–1.09, ψ=1.67–0.77 and η=0.95–0.38 at the centre-to-centre spacing of 1.625 in triangular bundle as the Reynolds number increased from 8900 to 89,400. The swirling flows with opposite rotating direction generated a strong mixing effect, and the secondary flow resulted in a better heat transfer in the boundary layer [207]

Coil heat exchanger with helically inwards corrugated tube

The plain tube in a coil heat exchanger was replaced with helically inwards corrugated tube in arc profile and single thread, and then the forced convective heat transfer of water-ethylene glycol mixture flowing in the coil was simulated by employing the 3D, steady, incompressible Navier-Stokes equations and energy equations in laminar flow regime (Re=360–1030) in ANSYS CFX 11.0 when the inlet temperature of the mixture was 20 °C and the wall temperature was 60 °C. It was shown that the heat transfer rate inside the coil with helically corrugated wall was improved by 80–100 % but the pressure drop was increased by 10–600 % due to the additional swirling flow developed in comparison with the plain coil [208].

The forced convective heat transfer in the coil heat exchanger was tested by using ethylene glycol as working fluid at Re=70–1200 and Dean number De=12–290 when the coil wall was smooth or helically inwards corrugated with arc profile. The experimental results confirmed that the heat transfer enhancement was achieved as follows: f/f_0=1.40–1.58, Nu/Nu_0=1.11–2.06, ψ=0.99–1.77 and η=0.79–1.30 as Reynolds number varied from 70 to 800 [193].

Shell and tube heat exchanger with helically inwards corrugated tube

An experimental study on heat transfer in a shell and tube heat exchanger with helically inwards corrugated tubes in w-shaped or trapezoidal profile was conducted in [209]. The cold machine oil with an inlet temperature of 35 °C flowed through the shell, and the hot water with an inlet temperature of 55 °C streamed inside the corrugated tube. The hot water velocity was alternated to change Reynolds number. The empirical correlations of Nusselt number and pressure drop in the hot and cold sides were established. The thermal-hydraulic performance of the heat exchanger with the helically inwards corrugated tubes in w-shaped profile was the best.

The forced convective heat transfer of four fluid foods, i.e., whole milk, cloudy orange juice, apricot puree and apple puree, flowing in helically inwards corrugated tubes with arc profile in a shell and tube heat exchanger was tested when the shell side was either heated or cooled by water. The whole milk and cloudy orange juice were Newtonian fluid, but apricot puree and apple puree were non-Newtonian

fluid. The experimental results indicated that helically corrugated tubes were quite effective in heat transfer enhancement when the generalised Reynolds number was above 800 and up to the limit of the transitional flow regime [210].

The thermal-hydraulic performance of a shell and tube heat exchanger with a helically corrugated tube bundle was predicted by using the empirical correlations of Nusselt number and friction factor proposed by [196] when water was used as heat transfer fluid at variable Reynold number (17,969–35,397) in the tube side and a fixed mass flow rate of 18 kg/s in the shell side. Entropy generation and second law analyses were performed as well. The results revealed that the overall heat transfer coefficient of the heat exchanger was improved up to 8 % compared with the exchanger with plain tube bundle. The energy and exergy efficiencies of the heat exchanger were increased up to 18 % and 16 %, respectively [211].

Tube-in-tube heat exchanger with helically corrugated inner tube

The thermal-hydraulic performance of a tube-in-tube heat exchanger with a helically outwards corrugated inner tube in non-symmetrical ridge profile and four threads was tested by using water as working fluid at *Re*=6000–20,000. There were nine helically outwards corrugated tubes, their profile height, helix angle and pitch varied. The heat transfer coefficient and friction factor in the inner tubes were determined and correlated to Reynolds number, profile height, helix angle and pitch. The ratio of the heat transfer coefficient of the corrugated tube to the coefficient of the plain tube was ranged in 1.07–1.72 and 1.31–1.46 in two flow directions in the inner tubes [212].

Either the outside surface or the inside surface of the inner tube in a tube-in-tube heat exchanger was helically corrugated in three helix angles of 15°, 20° and 25°, respectively. Then the forced convective heat transfer of the hot water in the hot side (inner tube) and the cold water in the cold side (annulus between the inner tube and the outer tube) was estimated numerically by using the 3D, steady, incompressible RANS equations, RNG *k*-ε model and energy equations in ANSYS Fluent 19.0 at *Re*=4000–20,000. The results suggested that the externally corrugated inner tube was in better heat transfer enhancement performance than the internally corrugated inner tube, further the PEC was the best and ranged in 1.18–1.00 at the helix angle of 15° when Reynolds number varied from 4000 to 20,000 compared with 1.00–0.70 in the internally corrugated inner tube at the same helix angle [213].

Helically corrugated tube with twisted tape insert

Heat transfer and isothermal friction factor were measured in two helically corrugated tubes (in three threads) with twisted tape inserts inside at *Re*=3000–60,000. The height to diameter ratios of corrugation were 0.0407 and 0.0569, and the pitch ratios were 15.3, 12.2, 7.7, 5.8,

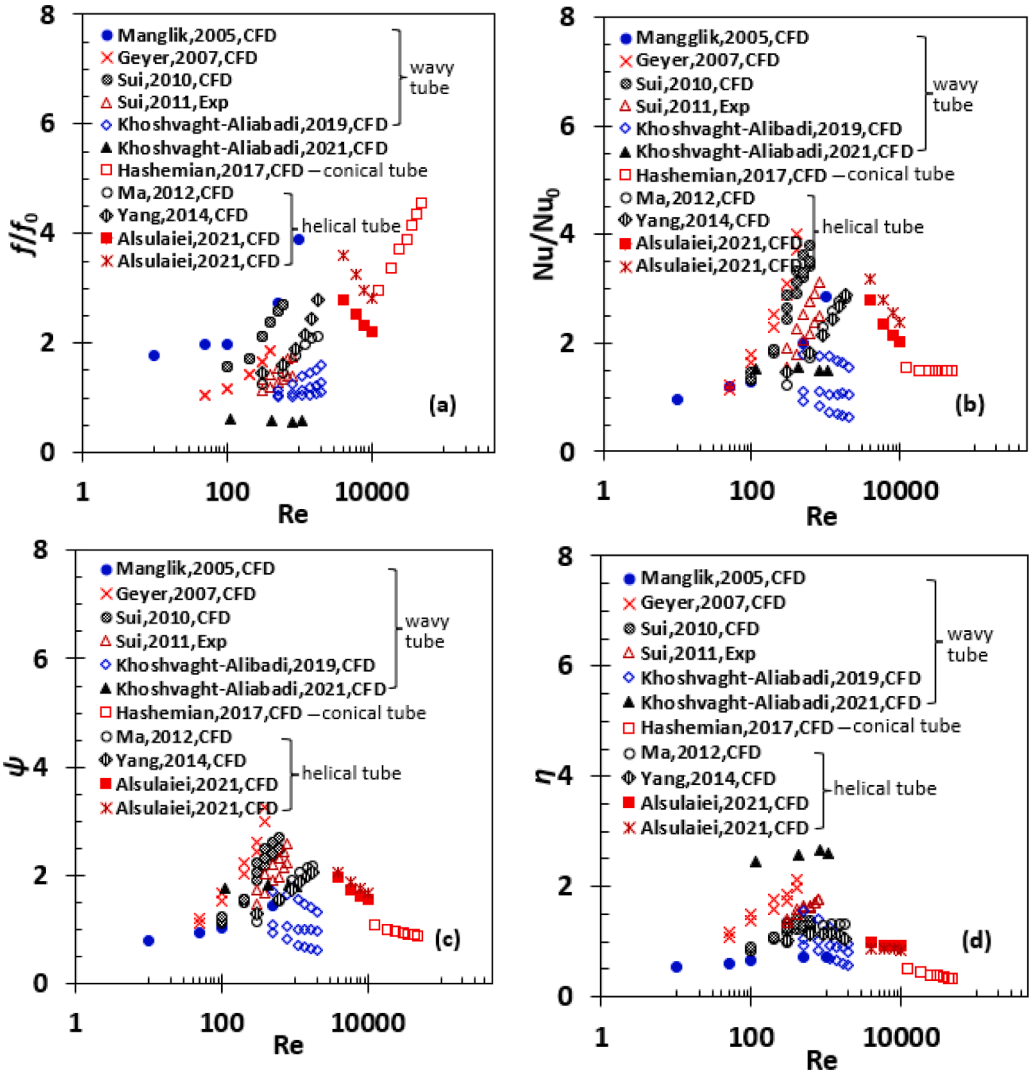

Fig. 28. Thermal-hydraulic parameters f/f_0, Nu/Nu_0, ψ and η are shown as a function of Reynolds number *Re* for wavy tubes, conical tubes and eccentrically helical tubes, respectively, (a) f/f_0, (b) Nu/Nu_0, (c) ψ and (d) η.

and 4.7. The friction factor ratio varied from 2.4 to 17.9. The Nusselt number ratio varied from 1.9 to 9.6 and approached the maximum at Re=3000–25,000, then gradually reduced [214].

Wavy tube or channel

The wavy tube or channel is one class of tubes or channels that has periodical varying walls with a certain large amplitude and wavelength in the lateral direction along the flow path. There are three types of wavy tube or channel: (1) periodical serpentine channel, (2) periodical sinusoidal wavy channel, (3) periodical channel with zigzag, curvy or step shape and so on. The Dean's vortices in the cross-section exist in the cross-section of a wavey tube or channel in laminar flow regime to enhance heat transfer. The study on heat transfer enhancement made by this kind of tubes has grown since the 2000's but still mainly is limited to laminar flow in microchannels of heat sinks for electronics cooling.

The thermal-hydraulic performance in heat transfer enhancement by the existing wavy channels is present in Fig. 28 by using the plots f/f_0-Re, Nu/Nu_0-Re, η-Re and ψ-Re and in Figs. 27 and 29 with the plots Nu/Nu_0-f/f_0, η-f/f_0 and ψ-f/f_0. The values of f/f_0=0.56–3.98, Nu/Nu_0=0.64–4.00, ψ=0.62–3.24, and η=0.55–2.67 in laminar flow regime (Re=10–2000) are observed. The largest f/f_0=4.00 was found in CFD simulation of heat transfer in 3D wavy-plate-fin compact channels in [215]. The best heat transfer enhancement: f/f_0=1.05–1.87, Nu/Nu_0=1.78–4.00, ψ=1.54–3.24 and η=1.09–2.14 in a periodic trapezoidal channel with semi-circular cross-section was predicted by using CFD simulations at Re=50–400 in [193]. Based on those results, it is concluded that the wavy channel or tube has better heat transfer enhancement than the corrugated tube and periodically convergent-divergent tubes in laminar flow regime.

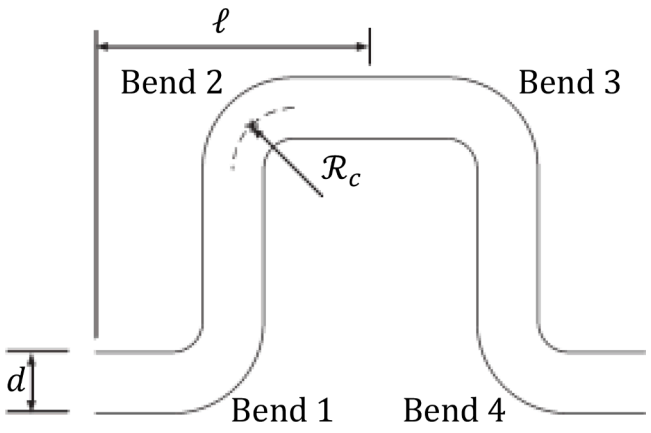

Fig. 30. Schematic of geometrical parameters of periodical serpentine.

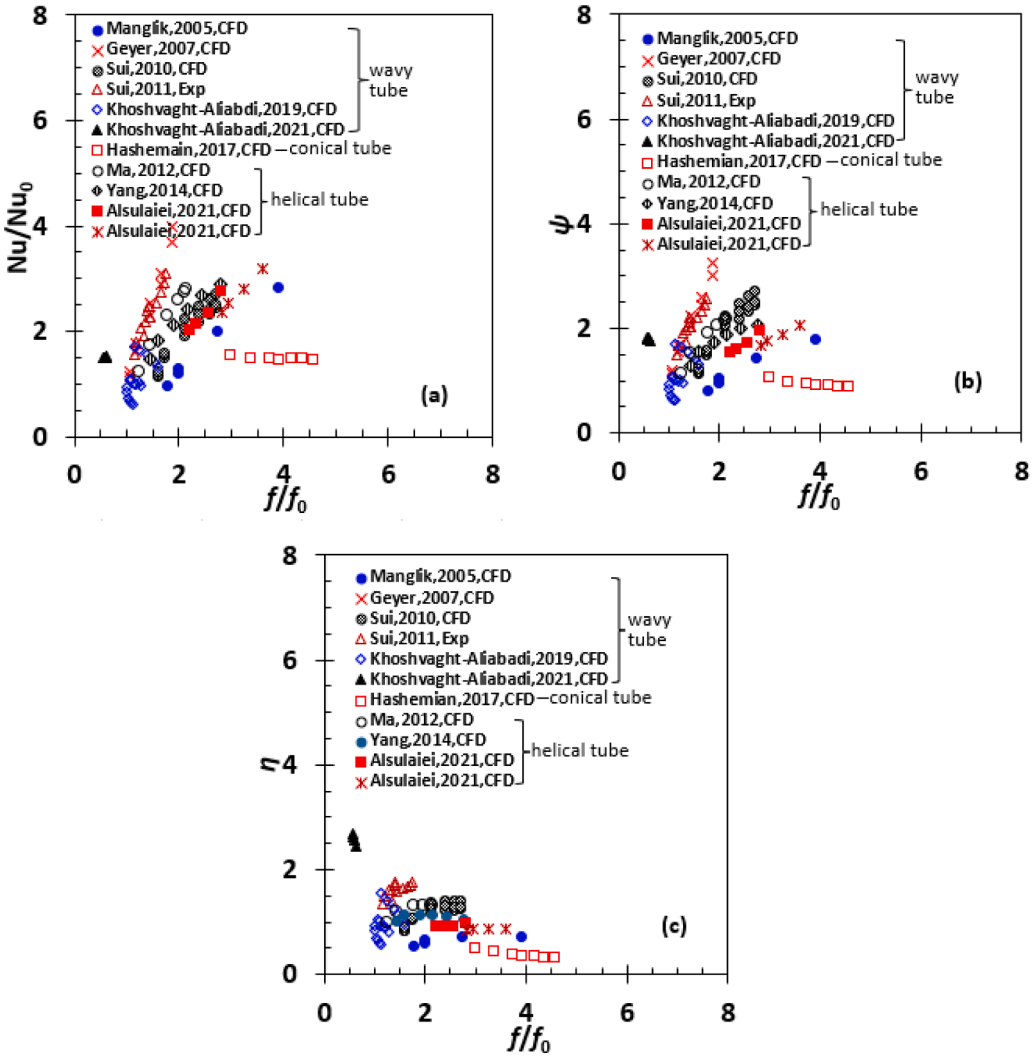

Fig. 29. Parameters Nu/Nu_0, ψ and η are demonstrated as a function of f/f_0 for wavy tubes, conical tubes and eccentrically helical tubes, respectively, (a) Nu/Nu_0, (b) ψ and (c) η.

Periodical serpentine channel

The forced convective heat transfer of incompressible Newtonian fluid in periodical serpentine channels with circular cross-section in laminar flow regime (Re=5–200) was simulated using a CFD program. The serpentine geometrical feature was characterised by the wavelength (2ℓ), channel diameter (d), and radius of curvature of bends ($\mathscr{R}_c$). The CFD simulations covered the geometrical parameters in the range of $3<\ell/d<12.5$ and $0.525<\mathscr{R}_c/d<2.25$, and Prandtl number was in a range of 0.7 and 100 under constant wall heat flux or constant wall temperature boundary condition. A single pair of Dean vortices was formed after each bend. At a higher Reynolds number ($De\approx150$), a second pair of vortices occurred. Dean vortices induced significant heat transfer enhancement compared with flow in a straight channel, especially at a large Prandtl number, but also inhibited flow separation to reduce pressure drop [216].

The forced convective heat transfer of incompressible Newtonian fluid in periodical serpentine channels with a semi-circular cross-section was simulated in laminar flow regime (Re=50–400) using a CFD program. The Dean vortices were found following each bend, resulting in a large heat transfer rate and low pressure drop [217].

The forced convective heat transfer of incompressible Newtonian fluid in periodical trapezoidal serpentine channels with a semi-circular cross-section in laminar flow regime (Re=50–400) was calculated by employing ANSYS CFX 10.0. The Dean vortices emerged following each bend. The intensity of the vortices was increased with increasing Reynolds number, leading to efficient fluid mixing and high heat transfer rate. The best heat transfer enhancement: f/f_0=1.05–1.87, Nu/Nu_0=1.21–4.00, ψ=1.20–3.24 and η=1.16–2.13 was predicted at Re from 50 to 400 [218].

The forced convective heat transfer of nanofluids of water and four types of nanoparticles such as Al_2O_3, CuO, SiO_2 and ZnO at five volume fractions (0, 1, 2, 3, 4 %) in the periodical trapezoidal serpentine mini channel with rectangular cross-section of a plate heat exchanger was simulated by using the 2D, steady, incompressible RANS equations, standard k-ε turbulence model and energy equations based on the single phase model at Re=6000–20,000 and a constant inwards wall heat flux (6 kW/m^2). The effects of wave amplitude and wavelength of the trapezoidal channel on the thermal-hydraulic performance and flow fields were investigated. The CFD results indicated that the nanofluid of SiO_2 had the largest Nusselt number. Nanoparticles at 20 nm diameter and 4 % volume fraction resulted in 10 % increase in the Nusselt number. The trapezoidal height of 2.5 mm and wavelength of 6 mm led to a better thermal-hydraulic performance for CuO nanofluid at a lower volume fraction [219].

Periodical sinusoidal wavy channel

The forced convective heat transfer of water flow in a periodical sinusoidal wavy microchannel with rectangular cross-section was predicted in laminar flow regime (Re=100–600) by using Fluent. The effect of wave amplitude and wavelength of wall on heat transfer was examined. The results showed that the Dean vortices were generated. The Nusselt number ratio and friction factor ratio rose with increasing wave amplitude and decreasing wavelength. The decreasing wavelength along the flow path could increase heat transfer enhancement. The best heat transfer enhancement: f/f_0=1.54–2.71, Nu/Nu_0=1.35–3.79, ψ=1.16–2.71 and η=0.85–1.39 was estimated at Re=100–600, constant wall temperature and a dimensionless wave amplitude of 0.125 [220].

Experiment was conducted on the forced convective heat transfer in the sinusoidal wavy microchannels with rectangular cross-sections in sizes of 205 μm(width), 404 μm(depth), of 2.5 mm (wavelength) and 0–259 μm (wavy amplitude) by using deionised water as working fluid at Re=300–800. The experimental results suggested the best heat transfer enhancement: f/f_0=1.34–1.75, Nu/Nu_0=1.90–3.11, ψ=1.73–2.57 and η=1.42–1.77 [221].

A sinusoidal wavy channel with rectangular cross-section was designed and the conjugate heat transfer of water in the channel was simulated by using the 3D, steady, incompressible Navier-Stokes equations and energy equation in laminar flow regime (Re=50, 100, 150) as well as the heat conduction equation in the solid domain in Fluent at an inwards wall heat flux and a given inlet temperature. At the same geometry parameters, the sinusoidal wavy channel had better heat transfer enhancement than the periodical sinusoidal convergent-divergent channel [163].

Three sinusoidal wavy channels with square cross-section in the wavelength-to-channel-length ratios of 0.125, 0.25 and 0.5 were designed, and the forced convective heat transfer of water through these channels was predicted based on the 3D, steady, incompressible Navier-Stokes equations and energy equation in laminar flow regime (Re=500–2000) at a constant inwards wall temperature in Fluent 6.0. The numerical results indicated the beast heat transfer enhancement: f/f_0=1.14–1.59, Nu/Nu_0=1.78–1.54, ψ=1.71–1.32 and η=1.56–0.97 existed in comparison with the straight square channel as Reynolds number varied from 500 to 2000. If the cross-section of the channel was twisted along the channel wavy axis, the heat transfer enhancement could be even better [118].

The forced convective heat transfer of SCO2 passing through a sinusoidal wavy channel (500 mm length) with square cross-section (1.31 mm side length) was simulated by employing the 3D, steady, compressible RANS equations, Lam and Bremhorst low Reynolds number k-ε turbulence model and energy equations in Fluent at the inlet mass flux of 127.1–400 kg/m^2 s, inlet temperature of 310–325 K, inlet pressure of 7–9 MPa and constant wall heat flux of 9–40 kW/m^2. The numerical results showed that the thermal performance of the sinusoidal wavy microchannels was better than the straight channel with the same cross-section but with a slight increase in pressure drop [222].

The thermal-hydraulic performance of CO2 flow inside a sinusoidal wavy mini-channel of heat sink at a uniform inwards wall heat flux of 1000 kW/m^2 was predicted based on the 3D, steady, compressible RANS equations, standard k-ε turbulence model and energy equations in Fluent. The effects of wall wave amplitude and wavelength on the performance were investigated at various CO2 inlet temperatures (305–310 K) and mass fluxes (500–2000 kg/m^{2}s). The numerical results illustrated that the thermal performance of the heat sink with the wavy channel was 1.86 times the performance of the plain channel but with 1.58 times pressure drop increment. The maximal PEC of ψ=4.41 was obtained at a wall wave amplitude of 1 mm, wavelength of 5 mm and inlet temperature of 305 K. A large wave amplitude and small wavelength and low inlet temperature could result in a large heat transfer coefficient [223].

Three printed circuit heat exchangers (PCHEs) with straight semicircle channel were modified by replacing the straight channel with sinusoidal wavy channel partially, i.e., the straight segment upstream was replaced with a segment of sinusoidal wavy channel, the middle part was replaced with the segment of sinusoidal wavy channel and the straight segment downstream was replaced with the segment of sinusoidal wavy channel. The conjugate heat transfer of SCO2 in the modified channels was simulated the 3D, steady, compressible RANS equations, SST k-ω turbulence model and energy equations in the fluid domain and the heat conduction equation in the solid domain in ANSYS Fluent 18.1. The numerical results indicated that the straight channel with downstream wavy channel had the best thermal-hydraulic performance, namely the largest pressure drop in the straight channel with downstream wavy channel was reduced by 23 % compared with the straight channel with upstream wavy channel, and the mean increment in local heat transfer coefficient in the wavy section is 1.56 kW/m^{2}K in the straight channel with downstream wavy channel in comparison with the straight channel segment [224].

Periodical sinusoidal wavy channel with slots

Two periodical sinusoidal wavy channels with slots aside every peak and valley of the channel wall at an angle of 45° against the wall were proposed and designed to establish cross-channel mixing. The forced

convective heat transfer of water in the channels was tested and simulated in laminar flow regime (Re=50–200). The thermal-hydraulic performance, and velocity and temperature fields of the two designs with different amplitude-to-wavelength ratios were compared with the reference wavy channel without slots to examine heat transfer enhancement. The results indicated that the sinusoidal wavy channels with properly designed slots could enhance heat transfer without pressure drop trade-off. Both the Dean's vortices and the cross-channel mixing were responsible for that property [225].

Air convective heat transfer enhancement in sinusoidal wavy-slot-fin channels was tested and simulated at Re=50–4000 in [226]. Effects of the cross-section aspect ratio (ratio of fin spacing to height), fin corrugation aspect ratio (ratio of corrugation amplitude to wavelength), and fin spacing ratio (ratio of fin spacing to wavelength) on heat transfer enhancement were simulated. New correlations for Fanning friction factor and Colburn factor were established. Additionally, more useful references on forced convective heat transfer and flow in sinusoidal wavy fin channels with and without slots are listed in [226]. Those studies are a bit out of the scope of the article; thus, their details are no longer described here.

Sinusoidal wavy channel with variable wave amplitude and length

A design of wavy microchannel heat sink with variable wavelength and amplitude along the flow path in rectangular cross-section was proposed and the conjugate heat transfer in the heat sink was predicted by using ANSYS Fluent 14.0 in laminar flow regime. The results showed that the decreasing wavelength or increasing amplitude could enhance heat transfer significantly. The heat transfer enhancement is attributed to the vortices in the cross sections caused by the sinusoidally curved walls [227].

Sinusoidal wavy-plate-fin compact channel

The forced convective heat transfer of air through a sinusoidal wavy-plate-fin compact channel with rectangular cross-section was simulated in laminar flow regime (Re=10–1000) by using a CFD program at a constant wall temperature or constant wall heat flux. The effects of wavy-fin density on the velocity and temperature fields, isothermal friction factor ratio and Nusselt number ratio were examined. Multiply pairs of counter-rotating vortices existed in the cross-section, resulting in high local heat transfer. These vortices could significantly improve the overall heat transfer coefficient but increase the pressure drop penalty compared with the straight plain channel with the identical cross-section. The best heat transfer enhancement: f/f_0=1.77–3.89, Nu/Nu_0=0.97–2.84, ψ=0.80–1.81 and η=0.55–0.73 at the fin gap to wave amplitude ratio of 0.303, cross-section width to height ratio of 0.240, and wave amplitude to wavelength ratio of 0.2667 was estimated as Reynolds number increased from 10 to 1000 [215].

Sinusoidal wavy channel with convergent or divergent cross-section

The sinusoidal wavy channels with convergent or divergent or convergent-divergent square cross-section along the flow path were designed, and the conjugate heat transfer of water in these channels was simulated based on the 3D, steady, incompressible Navier-Stokes equations and energy equation of water in laminar flow regime (Re=85–1145) and the heat conduction equation in the inner tube wall in a CFD code at a constant inwards wall heat flux on the channel bottom. The numerical results indicated that the convergent and divergent cross-sections along the flow path affected Nusselt number and friction factor significantly. The best heat transfer enhancement: f/f_0=0.62–0.57, Nu/Nu_0=1.51–1.50, ψ=1.77–1.80 and η=2.44–2.61 at Re=110–1000 was achieved by the wavy channel with a divergent cross-section along the flow path [228].

Effect of shape of channel

The effect of shape of the channel in microchannel heat sinks with a constant rectangular cross-section on their thermal-hydraulic performance was estimated by using three channels in zigzag, curvy, and step shapes, respectively, based on the 3D, steady, incompressible Navier-Stokes equations and energy equation of water in laminar flow regime (Re=100–1000) at a constant inwards wall heat flux. The numerical results demonstrated that the zigzag channel had the greatest heat transfer coefficient and pressure drop, and the curvy and step channels followed [229].

Cross-flow heat exchanger with sinusoidal wavy channels

A cross-flow micro heat exchanger with sinusoidal wavy channels (five channels on top for hot fluid, five channels on bottom for cold fluid) in rectangular cross-section was proposed and the conjugate heat transfer in the exchanger was simulated based on the 3D, steady, incompressible Navier-Stokes equations and energy equation of carbon nanotube (CNT)(20 % in volume)-Al_2O_3(80 % in volume)/water nanofluid in laminar flow regime and heat conduction equation in the solid domain by using a CFD code when the cold and hot channels inlet temperatures were 300 K and 360 K, respectively. The single-phase model was adopted with effective thermo-physical and transport properties, the hot fluid velocity varied in (5–100) mm/s, the wavenumber of the wall shape was ranged in 0–20, and the nanoparticle volume concentration was 0 and 5 % in volume. The highest heat exchanger efficiency was achieved at a wavenumber of 8, nanoparticle concentration of 5 % and inlet velocity of 50 mm/s [230].

Conical tube

The conical tube is a tube or channel with a gradual decreasing cross-sectional area from the inlet to the outlet. There are two flow conditions in the tube, one is converging flow where a fluid enters the tube from the large cross-section and leaves it from the small cross-section, and the other is diverging flow where the fluid enters the tube from the small cross-section and exits from the large cross-section. The simplest conical tube is a planar conical channel in which the cross-sectional area varies in one lateral direction only. The conjugate convective heat transfer in a planar conical channel was tested in converging and diverging flow conditions firstly in 2015 [231]. Since then, an analytical study was associated with heat transfer enhancement in a small conical tube when condensation or boiling took place [232] and a several numerical simulations have been conducted with an emphasis on forced convective heat transfer of SCO2 in conical tubes and heat transfer in tube-in-tube heat exchangers with conical tubes. However, there is only one set of data on heat transfer enhancement by conical tubes in the literature as shown in Figs. 28 and 29, respectively. The heat transfer enhancement: f/f_0=2.96–4.56, Nu/Nu_0=1.55–1.48, ψ=1.08–0.89 and η=0.52–0.32 in turbulent flow regime (Re=12,202–48,808) was achieved [233]. This fact suggests the conical tube is not good at heat transfer enhancement due to large f/f_0 and small Nu/Nu_0 values in turbulent flow regime.

Planar conical channel

The conjugate heat transfer in a 2D microchannel with 8° expansion angle and 156 μm hydraulic diameter was tested and simulated in both diverging and converging flow conditions when it was heated at the channel bottom and deionised water was used as heat transfer fluid at mass fluxes of 113–1200 kg/m^2 s (Re=30–274) and wall heat fluxes of 3–95 kW/m^2. The results showed that the heat transfer coefficient in the converging flow condition was larger by 35 % than in the diverging flow condition [231].

Two mini channels with divergence angles of 1.38°, 2.06°, respectively, were designed and the conjugate heat transfer of water flowing in them was tested at Re=235–1360 and inwards wall heat fluxes of 32, 40, 48 kW/m^2. The experimental results revealed that the divergent mini channel had a better thermal-hydraulic performance than the parallel mini channel [234].

Conical tube in SCO2 flow condition

The forced convective heat transfer of SCO2 in a conical tube was simulated by using the 3D, steady, compressible RANS equations, SST *k*-ω turbulence model and energy equation in turbulent flow regime with Fluent at constant outwards wall flux (cooling condition). The numerical results proved that the converging flow in the tube enhanced the heat transfer coefficient by 13.2 % compared with the cylindrical tube. However, the diverging flow in the conical tube reduced the heat transfer coefficient [235].

The forced convective heat transfer of SCO2 in a conical tube was numerically predicted by using the 3D, steady, compressible RANS equations, SST *k*-ω turbulence model and energy equation in turbulent flow regime with Fluent at constant inwards wall flux (heating condition). The numerical results suggested that the diverging flow in the tube improved the heat transfer rate by 19.3 % compared with the cylindrical tube. However, the converging flow in the tube reduced the heat transfer rate [236].

The forced convective heat transfer of SCO2 in two microtubes, one is convergent and the other is divergent, was simulated by using the 3D, steady, compressible RANS equations, SST *k*-ω turbulence model and energy equation in turbulent flow regime with Fluent under constant wall flux cooling conditions. The results showed that the heat transfer coefficient over the tube wall was relatively uniform. To obtain more uniform heat transfer coefficient, the expansion angle of the divergent microtube should be larger than the contraction angle of the convergent microtube. The buoyancy effect was responsible for different heat transfer coefficients in two microtubes [237].

Conical tube in nanofluid flow conditions

Three conical tubes were designed when the tube radius was described by the zero-order Bessel function, squared zero-order Bessel function and cubed zero-order Bessel function, respectively. The forced convective heat transfer of Al_2O_3/water nanofluid flowing in these tubes was simulated based on the single phase model by using the 2D, steady, axisymmetric, incompressible RANS equations, realisable *k*-ε turbulence model and energy equation in turbulent flow regime (Re=300–1200) with ANSYS Fluent at an inlet temperature of 300 K, uniform inwards wall heat flux of 1 kW/m^2 and φ=0, 1, 2, 3 %, respectively. The numerical results showed that the pressure drop profile along the flow path was parabolic, and the increasing convergence, Reynolds number and nanoparticle concentration could enhance convective heat transfer. However, the maximum PECs were 0.7, 0.525, and 0.43 only when the tube radius was in the form of the zero-order Bessel function, squared zero-order Bessel function and cubed zero-order Bessel function, respectively [238].

A similar work was conducted in [239] as well, but the forced convective heat transfer of CuO/water nanofluid flowing in those tubes was simulated based on the two-phase mixture model by using the 3D, steady, incompressible RANS equations, realisable *k*-ε turbulence model and energy equation in turbulent flow regime (Re=3000–50,000) with ANSYS Fluent at an inlet temperature of 300 K, uniform inwards wall heat flux of 2 kW/m^2 and φ=0, 1, 2, 5, 4 %, respectively. The results showed that the pressure drop, Nusselt number, and viscous entropy generation rate rose but the thermal entropy generation rate reduced when the tube radius was in the form of the zero-order Bessel function, squared zero-order Bessel function and cubed zero-order Bessel function, respectively [239].

Conical tube with protrusion

Four conical tubes with inlet-outlet diameter ratios of 1.5, 2, 3, and 5 were designed and their inner walls were roughened by using protrusion. The forced convective heat transfer of water in these tubes was simulated based on the 3D, steady, incompressible RANS equations, realisable *k*-ε turbulence model and energy equation in turbulent flow regime (Re=3000–40,000) with ANSYS Fluent 2021 R1 at a constant outwards wall flux of 40 kW/m^2 and an water inlet temperature of 300 K. The numerical results showed that the conical tubes protruded with the diameter ratios of 1.5, 2 and 3 had the lowest total entropy production rate. Unfortunately, there is no information about heat transfer enhancement [240].

Tube-in-tube-heat exchanger with conical tube

Two tube-in-tube heat exchangers with inner conical tube and outer conical or cylindrical tube were designed and the forced convective heat transfer of water through these heat exchangers was predicted based on eight cases (each has four cases: two parallel-flow cases and two counter-flow cases) by adopting the 3D, steady, incompressible RANS equations, standard *k*-ε turbulence model and energy equation when the cold water (outer tube) inlet temperature was 298 K and hot water (inner tube) inlet temperature was 325 K at Re=12,202–48,808. The numerical results exhibited 55 % increment in effectiveness in the tube-in-tube heat exchanger with inner conical tube and outer conical tube in parallel-flow when the cold water and hot water were in the diverging flow condition compared with the heat exchanger with cylindrical inner and outer tubes, and 40 % increase in heat transfer improvement number in the tube-in-tube heat exchanger with inner conical tube and outer cylindrical tube in parallel-flow when the cold water was in the diverging flow condition but the hot water was in converging flow condition [241]. Accordingly, 63 % increment in Nusselt number and 54 % increment in heat transfer rate were resulted but $\psi \leq 1.05$ [233].

Eccentrical helical tube

The eccentrical helical tube (EHT) was proposed in [242] for water firstly, then was followed by shell and tube heat exchanger with EHT bank in [243], and very recently by eccentrical helical tube with helical tape [244] for air and tube-in-tube heat exchangers with inner EHT for water in [245] and for Al_2O_3/water nanofluid [246]. Basically, an EHT is a helical coil since its centre line is a helix but under $R_{tube} > R_{helix}$ condition, see Fig. 31, where R_{helix} is the eccentricity of the helix. For a helical coil, however, the $R_{tube} \ll R_{helix}$ condition remains.

The data on heat transfer enhancement made by EHTs are rare, see Figs. 28 and 29. The numerical data in the two figures indicate that the heat transfer enhancement: f/f_0=1.25–2.14, Nu/Nu_0=1.23–2.81, ψ=1.14–2.18 and η=0.98–1.32 in laminar flow regime (Re=300–1800) was predicted [242], while the enhancement: f/f_0=2.80–2.21, Nu/Nu_0=2.78–2.03, ψ=2.07–1.56 and η=0.88–0.84 in turbulent flow regime (Re=4000–10,000) was demonstrated [244]. This information suggests that the EHT has a better performance in heat transfer enhancement than the conical tube in turbulent flow regime.

Heat transfer inside EHT

An EHT (length=480 mm, inner diameter=20 mm) with an eccentricity R_{helix}=3 mm (eccentricity ratio=3/20) and a pitch s=120 mm was designed, and the forced convective heat transfer of water transported in the tube was estimated numerically by employing the 3D, steady, incompressible Navier-Stokes equations and energy equation in laminar flow regime (Re=300–1800) in Fluent when the tube wall was subject to a uniform temperature of 350 K. The best heat transfer enhancement: f/f_0=2.14, Nu/Nu_0=2.81, ψ=2.18 and η=1.32 was obtained at Re=1800, and the enhancement became poor and poor with decreasing Reynolds number [242].

The thermal-hydraulic performance of an EHT(length=1000 mm, inner diameter=20 mm) with a twisted full-length tape attached to the inner wall of the tube, see Fig. 32, was predicted numerically as air was used as heat transfer fluid based on the 3D, steady, incompressible RANS equations, SST *k*-ω turbulence model and energy equation in turbulent flow regime (Re=4000–10,000) with ANSYS Fluent 17.0 at a uniform inwards wall flux of 1.7 kW/m^2 (heating condition). The tape height ratios 0.0, 0.125, 0.25, 0.375, 0.5 and 0.625 and the thickness of 1 mm were used to investigate effects of tape height on the thermal-hydraulic performance of the tube. The numerical results showed that a larger tape

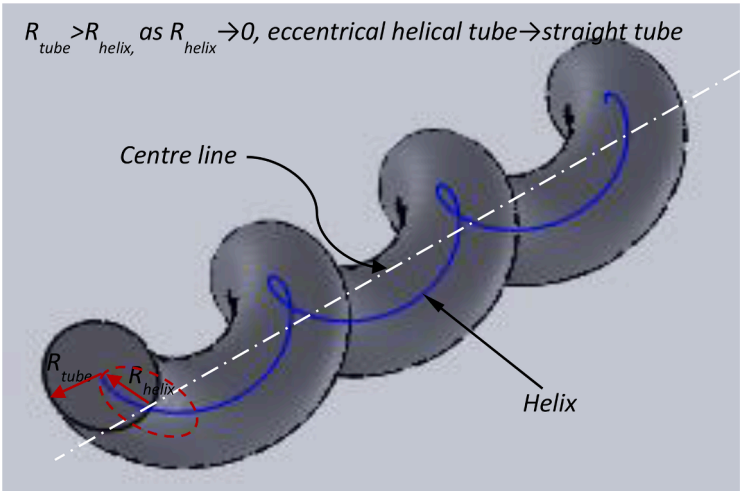

Fig. 31. Eccentrical helical tube with the radius of tube and the eccentricity of helix.

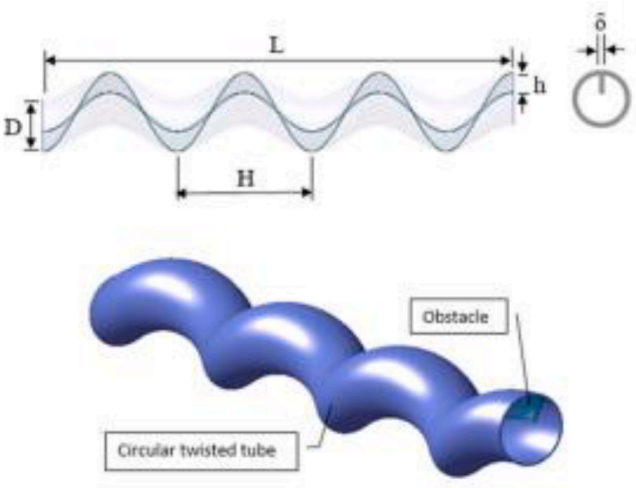

Fig. 32. Eccentrical helical tube with a full-length twisted tape attached to the tube wall along the tube, the picture after [244].

height resulted in a higher Nusselt number but induced a greater friction factor. The best PEC was obtained at the height ratio of 0.625, for instance, ψ=2.07 at *Re*=4000 and ψ=1.69 at *Re*=10,000 [244].

Shell and tube heat exchanger with EHT bank

A shell and tube heat exchanger for oil cooler was proposed and designed. The thermal-hydraulic performance of the tube side (hot oil) and shell side (cold water) was simulated separately in Fluent 6.3 under isothermal wall temperature conditions. The forced convective heat transfer of the oil (hot side) in the EHT was in laminar flow regime (*Re*=300–1800), but the heat transfer of the water (cold side) in the shell was in turbulent flow regime (*Re*=5000–14,000). The heat transfer enhancement inside the EHT was predicted as f/f_0=1.45–2.78, Nu/Nu_0=1.46–2.89, ψ=1.29–2.06, and η=1.01–1.04 compared with the plain tube. However, the heat transfer enhancement in the shell side was poorer than the shell and tube with rod baffles because of ψ=0.90–0.95 [243].

Tube-in-tube heat exchanger with inner EHT

Three tube-in-tube heat exchangers (length=1 m) with inner EHT (diameter=25 mm, pitch ratio=5, 10, and 15) and outer cylindrical tube (diameter=50 mm) were designed. The flow conditions in these exchangers were in counter-flow mode where hot water flowed in the inner EHT and cold air streamed in the outer tube. The forced convective heat transfer in these exchangers was simulated by using ANSYS Fluent 18.2 based on the 3D, steady, incompressible RANS equations, standard *k*-ε turbulence model and energy equation in turbulent flow regime when the hot water and cold air inlet temperatures were fixed at 343 K and 298 K but six pairs of the cold air and hot water mass flow rates were prescribed to cover *Re*=5000–30,000 in the inner EHT. The heat exchanger effectiveness and overall performance index (ratio of the effectiveness to the pressure drop in both the inner tube and the annulus) were determined. The results showed that the pitch ratio of 5 resulted in the best overall thermal-hydraulic performance, i.e., the effectiveness was increased by 14.8 % at the pitch ratio of 5 and *Re*=30,000 but the overall performance index was improved by 13 % at *Re*=5000 compared with the plain tube heat exchanger [245].

The tube-in-tube heat exchanger with the inner EHT at the pitch ratio of 5 in [245] was adopted to study the effect of Al_2O_3/water nanofluid on its thermal-hydraulic characteristics. The numerical methods and flow models were the same as [245] but the nanoparticle volume fraction-dependent effective thermophysical and transport properties were used for the nanofluid. The nanoparticle volume fraction was prescribed to be 0.05, 1, 2.5, and 4 % and Reynold number was ranged in 5000–30,000. The results indicated that the effectiveness and overall performance index of the heat exchanger were improved by 6 % and 10.7 % at the volume fraction of 4 % compared with the same heat exchanger under water flow conditions. However, the pressure drop was increased with increasing nanoparticle volume fraction [246].

Discussion

Assessment of the methods

When the heat transfer in a heat exchanger is enhanced by one of eight passive methods stated in Section 3, the pressure drop across the exchanger is increased inevitably because of the intensified swirling flow or secondary flow or vortex flow. Therefore, when these passive methods are assessed, the friction factor ratio f/f_0 must be taken into account [247]. As a first trial, it is proposed that f/f_0=5 is a critical condition. If f/f_0>5 is true for a passive method, the method will cause a severe pressure drop penalty, and caution should be alerted when it is adopted to enhance heat transfer in a heat exchanger. Otherwise, if $f/f_0 \leq 5$ is held for a passive method, the method will induce an acceptable pressure drop penalty and should be recommended to be applicable to the heat transfer enhancement in the exchanger. The ranges of variation of the ratios f/f_0, Nu/Nu_0, ψ and η were illustrated in Figs. 5, 8, 13, 15, 26, 28 and tabulated in Table 2. For four methods such as TOT, wavy

Table 2
Assessment of eight passive methods for heat transfer enhancement based on friction factor ratio, Nusselt number ratio, PEC and enhancement erfficiency.

Passive method	Heat transfer enhancement					
	Laminar regime	*Re*	$f/f_0 \leq 5$	Turbulent regime	*Re*	$f/f_0 \leq 5$
TOT	f/f_0=0.90–2.55, Nu/Nu_0=0.88–4.77, ψ=0.91–3.68, η=0.97–2.52	1000–2000	No	f/f_0=1.13–4.03, Nu/Nu_0=1.16–4.03, ψ=0.82–1.97, η=0.50–1.40	2000–65,000	No
TPT	f/f_0=0.39–9.81, Nu/Nu_0=0.83–13.44, ψ=0.73–6.00 η=0.40–1.76	90–2300	Yes	f/f_0=0.51–14.53, Nu/Nu_0=1.17–14.36, ψ=0.86–6.45, η=0.22–3.78	2400–12,000	Yes
TMT	f/f_0=1.09–12.09, Nu/Nu_0=0.48–7.04, ψ=0.40–3.50, η=0.12–2.39	100–2000	Yes	f/f_0=1.0–7.0, Nu/Nu_0=1.0–6.9, ψ=0.8–1.4, η=0.4–1.5	2000–50,000	Yes
Periodical convergent-divergent tube	f/f_0=1.0–5.55, Nu/Nu_0=1.0–6.06, ψ=0.92–3.62, η=0.05–2.01	130–2300	Yes	f/f_0=3.00–56.39, Nu/Nu_0=1.21–4.44, ψ=0.73–2.17, η=0.14–1.17	2200–60,000	Yes
Helically corrugated tube	f/f_0=1.29–14.80, Nu/Nu_0=0.65–4.28, ψ=0.36–1.70, η=0.044–1.30	30–2300	Yes	f/f_0=1.03–8.82, Nu/Nu_0=1.09–2.92, ψ=0.92–2.17, η=0.22–1.85	2300–90,000	Yes
Wavy tube or channel	f/f_0=0.56–3.98, Nu/Nu_0=0.64–4.00, ψ=0.62–3.24, η=0.55–2.67	10–2000	No	N/A		
Conical tube	N/A			f/f_0=2.96–4.56, Nu/Nu_0=1.55–1.48, ψ=1.08–0.89, η=0.52–0.32	12,202–48,808	No
EHT	f/f_0=1.25–2.14, Nu/Nu_0=1.23–2.81, ψ=1.14–2.18, η=0.98–1.32	300–1800	No	f/f_0=2.80–2.21, Nu/Nu_0=2.78–2.03, ψ=2.07–1.56, η=0.88–0.84	4000–10,000	No

tube, conical tube and EHT, clearly, the relation $f/f_0 \leq 5$ is true. Naturally, these methods should be recommended to be applied to heat transfer enhancement in a heat exchanger compared with the rest methods.

In our project, a tube-in-tube heat exchanger in cooling conditions for SCO2 will operate in a prototype test rig at the mass flux of 200–850 kg/m^{2}s with an inlet temperature of 30–70 °C through the inner tube with a diameter of 6 mm [5]. The corresponding operational Reynolds number is Re=1.9 × 10^4–2.55 × 10^5, suggesting SCO2 flow in turbulent flow regime. Based on the $f/f_0 \leq 5$ values illustrated in Table 2, the TET, conical tube and EHT potentially can be adopted in the tube-in-tube heat exchanger in cooling condition to enhance SCO2 heat transfer and make the exchanger more efficient and compact.

The typical thermal-hydraulic performance in heat transfer enhancement of the TETs [72,82], conical tube [233] and EHT [244] is shown by using the f/f_0-*Re*, Nu/Nu_0-*Re*, ψ-*Re* and η-*Re* in Fig. 33. The f/f_0-*Re* curve of the conical tube is much higher the curves of the TETs and EHT and rises but also approaches the f/f_0=5 criterion with increasing *Re*. The Nu/Nu_0-*Re* curve of the conical tube is comparable to that of two TETs but smaller than the EHT. Consequently, the ψ-*Re* and η-*Re* curves of the conical tube are below the curves of two TETs and the EHT. Obviously, the conical tube should be excluded from the candidate passive methods for heat transfer enhancement in the project. The TET and EHT should be the most suitable candidate passive methods for the SCO2 heat exchanger in the project.

Mechanism of heat transfer enhancement

The mechanism of heat transfer enhancement for the passive methods is essential to the design of heat exchanger. The identified mechanisms of heat transfer enhancement for the eight passive methods mentioned Section 3 are summarised in Table 3. It is shown that the secondary flow and swirling flow contribute to the mechanism of heat transfer enhancement for the methods based on twisted cross-section or helical corrugation along the flow path, namely TET, TPT and TMT as well as helically corrugated tube.

For periodical convergent-divergent tubes, however, a variety of mechanisms of heat transfer enhancement are available, depending on the tube and cross-section shapes. Macroscopic mixing or chaotic mixing, redevelopment of thermal boundary layer, and jetting and throttling effect are mainly responsible for the heat transfer enhancement in the tube/channel with contraction-expansion cross-sectional area. The mechanism of heat transfer enhancement in the orthogonal ellipse tube is attributed to the multi-longitudinal vortices induced by cross-sectional orientation change. The Dean vortices and the complex flow patterns caused by the vortices are responsible for the mechanism of heat transfer enhancement in the wavy tube or channel. There has not been the mechanism of heat transfer enhancement in the conical tube and EHT reported so far.

Theoretical analysis of heat transfer enhancement

After a CFD simulation on forced convective heat transfer in a heat exchanger is completed, two theoretical analyses, i.e., entropy generation analysis and field synergy analysis, can be performed based on velocity and temperature gradients in the flow and temperature fields just obtained. The status of application of two theoretical analyses in eight passive methods for heat transfer enhancement is present in Table 4. More applications of field synergy analysis are found in the TOT and conical tube than those of entropy generation analysis. This situation, however, is reversed in the periodical convergent-divergent tube. Neither entropy generation analysis nor field synergy analysis is applied in wavy tube presently.

In entropy generation analysis, the volume entropy generation/production rate in fluid domains needs to be determined from the specific entropy generation rate. The specific entropy generation rate includes the entropy generation rate by direct viscous dissipation s''_{DD},

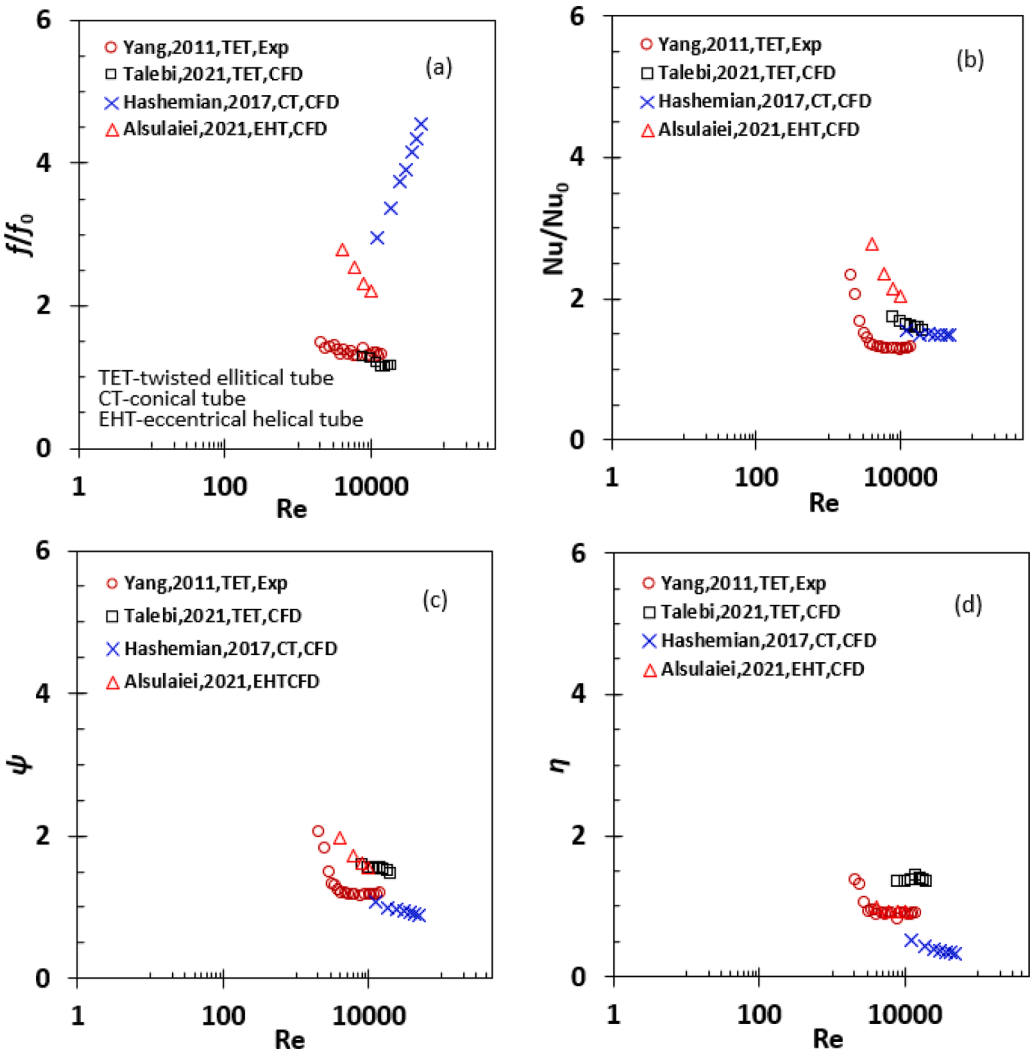

Fig. 33. Thermal-hydraulic parameters f/f_0, Nu/Nu_0, ψ and η are shown as a function of Reynolds number Re for three typical twisted elliptical tubes [72,82], conical tube [233] and eccentrical helical tube [244], respectively, (a) f/f_0, (b) Nu/Nu_0, (c) ψ and (d) η.

entropy generation rate by indirect (turbulent) dissipation $\dot{s}_{ID}$, entropy generation rate by heat conduction with mean temperature gradients $\dot{s}_{HC}$, and entropy generation rate by heat transfer with fluctuating temperature gradients $\dot{s}_{HT}$ [248]. Those specific entropy generation rates are expressed by [248]:

$$\begin{cases} \dot{s}''_{DD} = \dfrac{\mu}{T}\left[2\left(\dfrac{\partial u_i}{\partial x_i}\right)^2 + \left(\dfrac{\partial u_i}{\partial x_j}+\dfrac{\partial u_j}{\partial x_i}\right)^2\right] \\ \dot{s}''_{ID} = \dfrac{\rho\varepsilon}{T} \\ \dot{s}''_{HC} = \dfrac{\lambda}{T^2}\left(\dfrac{\partial T}{\partial x_i}\right)^2 \\ \dot{s}''_{HT} = \dfrac{\mu_t}{Pr_t}\dfrac{c_p}{T^2}\left(\dfrac{\partial T}{\partial x_i}\right)^2 \end{cases} \tag{6}$$

where μ is dynamic viscosity of fluid, T is time-averaged temperature of fluid, u_i and u_j are time-averaged velocities of fluid in coordinate directions i and j, indices i, j=1, 2, 3; x_i and x_j are coordinates in the directions i and j; ρ is density of fluid, ε is dissipation rate of turbulent kinetic energy, λ is thermal conductivity of fluid, μ_t is dynamic viscosity of turbulent eddy, Pr_t is turbulent Prandtl number, Pr_t=0.85; c_p is specific heat capacity of fluid. For laminar flows, $\dot{s}_{ID}=\dot{s}_{HT}=0$ is kept.

The specific entropy generation rate by direct and indirect dissipations is denoted by $\dot{s}_D=\dot{s}_{DD}+\dot{s}_{ID}$, and the specific entropy generation rate by head conduction and heat transfer is represented by $\dot{s}_H=\dot{s}_{HC}+\dot{s}_{HT}$. Then, the entropy generation rate by dissipations $\dot{S}_D$ and the entropy generation rate by heat conduction and heat transfer $\dot{S}_H$ in the fluid domain with a volume $\mathscr{V}$ are calculated by:

$$\begin{cases} \dot{S}_D = \displaystyle\int_0^{\mathscr{V}} \dot{s}_D d\mathscr{V} = \int_0^{V}\frac{\mu}{T}\left[2\left(\frac{\partial u_i}{\partial x_i}\right)^2 + \left(\frac{\partial u_i}{\partial x_j}+\frac{\partial u_j}{\partial x_i}\right)^2\right] d\mathscr{V} + \int_0^{\mathscr{V}}\frac{\rho\varepsilon}{T}d\mathscr{V} \\ \dot{S}_H = \displaystyle\int_0^{\mathscr{V}} \dot{s}_H d\mathscr{V} = \int_0^{\mathscr{V}}\frac{\lambda}{T^2}\left(\frac{\partial T}{\partial x_i}\right)^2 d\mathscr{V} + \int_0^{\mathscr{V}}\frac{\mu_t}{Pr_t}\frac{c_p}{T^2}\left(\frac{\partial T}{\partial x_i}\right)^2 d\mathscr{V} \end{cases} \tag{7}$$

Usually, Bejan number is employed to assess the importance of the entropy generation rate by heat conduction and heat transfer in a thermal and flow system. The Bejan number is defined as the ratio of the entropy generation rate by heat conduction and heat transfer to the total entropy generation rate, and expressed as:

$$Be = \frac{\dot{S}_D}{\dot{S}_D + \dot{S}_H} \tag{8}$$

where Be denotes to the Bejan number. For a better thermal-hydraulic

Table 3
Identified mechanisms of heat transfer enhancement for eight passive methods.

Passive method		Mechanism of heat transfer enhancement	Reference
TOT	Inside tube	Rotating fluid and secondary flow induced in the tube	[71]
		Longitudinal vortex induced by the tube wall	[72]
		Secondary flow in the form of spiral flow	[73]
		Secondary flow generated by the tube wall	[75]
		Secondary flow inside the tube	[77]
		Rotational motion produced in the flowing fluid	[79]
		Longitudinal vortex/ secondary flow in the tube	[81]
		Symmetrical secondary flow in the annulus	[89]
	Outside tube	Disturbance of flow condition and promotion of the mixing between hot and cold fluids	[103]
		Secondary flow strengthened by the centrifugal force of the helical streamlines and the swirling velocity induced by the twist	[111]
TPT	Square cross-section	1. Development of thermal boundary layer is avoided due to the continuous change in flow direction induced by the tube wall. 2. Secondary flow causes more uniform temperature profile,	[119]
	Triangular, square, hexagon, octagon cross-section	Centrifugal force generated by the rotating flow in the tube allows nanoparticles to move to proper locations and enhance heat transfer.	[124]
TMT	Tri-lobe	1. Helical flow and secondary flow induced by the twisted and curved tube wall. 2. Radial and tangential velocities generated by centrifugal force result in higher temperature gradients near the tube wall.	[74]
	Two-lobe	Harmony and orderly swirling flow in secondary flow region induced.	[129]
	Six-lobe	Secondary flow velocity and vorticity of longitudinal vortex	[138]
	Two-, tri-, five-, six-, eight-lobe	Secondary flow	[131]
	Tri-, four, five-, six-lobe	Swirling flow	[132]
	Tri-lobe with twisted tape insert	1. Secondary flow generated by the twisted tube wall. 2. Swirling flow along the core tube induced by the tape.	[141]
Periodical convergent-divergent tube	2D sinusoidal channel	Macroscopic mixing	[146]
	3D arc or triangular microchannel with rectangular cross-section	1. Increased heat transfer surface area. 2. Redeveloping boundary layers. 3. Jetting and throttling effect in contraction region. 4. Slipping over the expansion region.	[152]
		Jetting and throttling effect in contraction region	[153, 156]
	3D triangular microchannel with rectangular rib	1. Interruption and redevelopment of thermal boundary layer. 2. Intensified mainstream disturbance. 3. Chaotic mixing between cold and hot water.	[158]
		Mixing of fluid because of formation of secondary flows	[160]
	3D sinusoidal microchannel	Chaotic advection results in a higher heat transfer rate albeit with a larger pressure drop.	[164]
	Transversely arc outwards corrugated tube	1. Jet impingement heat transfer at windward side of the corrugation. 2. Considerable turbulent fluctuation. 3. Boundary-layer redevelopment.	[174]
	Orthogonal ellipse tube	Multi-longitudinal vortices induced by cross-sectional change.	[144]
	Tube-in-tube heat exchanger with orthogonal ellipse tube	Longitudinal/axial vortices in both the inner and outer tube flows	[190]
Helically corrugated tube	Outwards helically corrugated tube	1. Secondary flow. 2. Turbulent pulsation.	[207]
Wavy tube or channel	Periodical serpentine channel with circular cross-section	Dean vortices at a low Reynolds number and more complex vortical	[216]
	Periodic serpentine channel with semi-circular cross-section	flow patterns at an increased Reynolds number	[217]
	periodic trapezoidal channel with semi-circular cross-section		[218]
	3D sinusoidal microchannel with rectangular cross-section	1. Secondary flow (Dean vortices) generated. 2. Chaotic advection caused by the change in quantity and location of the vortices along flow direction.	[220]
	Wavy channel with slot	1. Dean vortices induced. 2. Cross-channel mixing and boundary layer disruption by slots.	[225]
	3D sinusoidal microchannel with variable wavelength and amplitude	Vortices in cross-section	[227]
	3D wavy-plate-fin compact channels	1. Periodical growth and disruption of pairs of counter-rotating vortices in the wall valley. 2. Periodical interruption of thermal boundary layers on the fin surface.	[215]

(*continued on next page*)

Table 3 (*continued*)

Passive method		Mechanism of heat transfer enhancement	Reference
Conical tube	N/A		N/A
EHT	Vortex is formed near the tube wall, but straight bulk flow is kept in the core region.		[243]

Table 4
Status of theoretical analysis in eight passive methods for heat transfer enhancement.

Passive method	Theoretical analysis	Reference
Twisted oval tube	Field synergy analysis	[72,75,77,79,96,103,108]
	Entropy generation analysis	[75,84]
	Second law analysis	[84]
Twisted polygon tube	Field synergy analysis	[125]
Twisted multi-lobe tube	Entropy generation analysis	[131]
	Field synergy analysis	[74]
Periodical convergent-divergent tube	Field synergy analysis	[154,155]
	Entropy generation analysis	[154,155,158,180,181,143]
	Exergy analysis	[155]
Helically corrugated tube	Entropy generation analysis	[198,211]
	Second law analysis	[211,214]
Wavy tube or channel	N/A	N/A
Conical tube	Field synergy analysis	[236,235]
	Entropy generation analysis	[239,241]
Eccentrical helical tube	Entropy generation analysis	[243]

performance, a heat exchanger should have $\dot{S}_D$ and $\dot{S}_H$ as small as possible.

Based on the predicted mean wall heat flux q_w, wall temperature T_w, outlet pressure p_2 and outlet temperature T_2 by CFD simulations, and the known inlet pressure p_1, inlet temperature T_1, and environment temperature T_0, the exergy (available energy) X_a, exergy destruction (loss) X_d and second law performance η_X can be estimated. This is so-called CFD-based second law analysis. If the working fluid is an incompressible liquid, the expressions for calculating the exergy X_a, exergy destruction X_d and second law performance η_X are written as [249]:

$$\begin{cases} X_a = q_w A\left(1-\dfrac{T_0}{T_w}\right) \\ X_d = \dot{m}c_p(T_1-T_2)+\dot{m}c_pT_0\ln\left(\dfrac{T_2}{T_1}\right)+\dot{m}\dfrac{p_1-p_2}{\rho}+X_a \\ \eta_X = \dfrac{X_a-X_d}{X_a} \end{cases} \tag{9}$$

where A is heat transfer area of the tube, $\dot{m}$ is the fluid mass flow rate in the tube, c_p is the specific heat capacity of fluid at constant pressure. If the tube cools the fluid, then $q_w<0$; if the tube heats the fluid, then $q_w>0$. Obviously, based on one-dimensional (1D) flow and heat transfer analysis and relevant empirical correlations of friction factor and Nusselt number, second law analysis also can be analysed on heat exchangers [211]. A comprehensive review of this kind of analysis is referred to [250].

The field synergy/coordination principle was proposed in [251,252] for enhancing convective heat transfer in tubes. The principle was explained by using a simplified energy equation for 2D, steady incompressible laminar flow of a fluid with constant thermo-physical properties over a flat plate. The original energy equation for 2D, steady, incompressible laminar flow over a flat plate is read as [253]:

$$\rho c_p\left(u\frac{\partial T}{\partial x}+v\frac{\partial T}{\partial y}\right)=\lambda\frac{\partial^2 T}{\partial y^2}+\mu\frac{\partial^2 u}{\partial y^2} \tag{10}$$

where u and v are the velocity in the primary flow direction x and the normal direction y to the plate wall, respectively. The viscous dissipation term in Eq, (10) was removed and the equation is simplified to [251,252]:

$$\rho c_p\left(u\frac{\partial T}{\partial x}+v\frac{\partial T}{\partial y}\right)=\lambda\frac{\partial^2 T}{\partial y^2} \tag{11}$$

Integrating Eq. (11) across the boundary layer thickness δ_T and considering two boundary conditions: $\lambda\partial T/\partial y|_0=-\ q_w$ and $\lambda\partial T/\partial y|_{\delta_T}=0$, Eq. (11) is expressed as:

$$\rho c_p\int_0^{\delta_T}\left(u\frac{\partial T}{\partial x}+v\frac{\partial T}{\partial y}\right)dy=q_w \tag{12}$$

The following dimensionless variables are introduced:

$$u^*=\frac{u}{u_e},v^*=\frac{v}{u_e},T^*=\frac{T-T_e}{T_w-T_e},Re_x=\frac{\rho u_e x}{\mu},Nu_x=\frac{q_w x}{\lambda(T_w-T_e)},Pr=\frac{\mu c_p}{\lambda} \tag{13}$$

where u_e and T_e are the velocity and temperature of fluid at edge of the boundary layer, respectively; Re_x and Nu_x are the local Reynolds number and Nusselt number at a location x, Pr is the Prandtl number of the fluid. Those dimensionless variables are involved into Eq. (12), and the equation is rewritten as:

$$Re_xPr\int_0^{\delta_T}\left(u^*\frac{\partial T^*}{\partial x}+v^*\frac{\partial T^*}{\partial y}\right)dy=Nu_x \tag{14}$$

Since

$$u^*\frac{\partial T^*}{\partial x}+v^*\frac{\partial T^*}{\partial y}=\boldsymbol{V}^*\cdot\nabla T^*=|\boldsymbol{V}^*||\nabla T^*|cos\beta \tag{15}$$

where $\boldsymbol{V}^*$ is the vector of the velocity with the components u^* and v^*, $\boldsymbol{V}^*=\boldsymbol{u}^*+\boldsymbol{v}^*$, $|\boldsymbol{V}^*|$ and $|\nabla T^*|$ are the modulus of $\boldsymbol{V}^*$ and ∇T^*, respectively; β is the angle between the vectors $\boldsymbol{u}^*$ and ∇T^*. Then, Eq. (14) is updated accordingly:

$$Re_xPr\int_0^{\delta_T}|\boldsymbol{V}^*||\nabla T^*|cos\beta dy=Nu_x \tag{16}$$

The equation suggests that the angle β between the vectors $\boldsymbol{V}^*$ and ∇T^* plays a critical role in the convective heat transfer in a tube. Under a given flow condition and wall heat flux, the angle β should be made small as possible to obtain a higher Nu_x. The smaller the angle β, the better the synergy/coordination between the temperature and velocity fields. That is so-called field synergy/coordinate principle for convective heat transfer proposed in [251,252]. The principle is attributed to the angle between the vectors $\boldsymbol{V}^*$ and ∇T^* only. After a 3D CFD simulation on forced convective heat transfer in a tube is completed, the angle β can be extracted by using the following expression:

$$\beta=cos^{-1}\frac{u\frac{\partial T}{\partial x}+v\frac{\partial T}{\partial y}+w\frac{\partial T}{\partial z}}{\sqrt{u^2+v^2+w^2}\sqrt{\left(\frac{\partial T}{\partial x}\right)^2+\left(\frac{\partial T}{\partial y}\right)^2+\left(\frac{\partial T}{\partial z}\right)^2}} \tag{17}$$

where w is the velocity in the spanwise direction z. For the forced convective heat transfer of water in a tube, β is ranged in 78.6–90° from the tube centre to the wall; for the TiO_2/water nanofluid of 1.5 wt. % concentration, however, β is reduced to 75.9–89.1° due to heat transfer enhancement [254].

Since the field synergy/coordination principle is as simple as finding

the angle between the velocity vector and the temperature gradient only, it has found more applications in explanation of various methods for heat transfer enhancement in Table 4. Unfortunately, this principle is unable to uncover the reasons why the angle between the velocity vector and the temperature gradients varied in each method for heat transfer enhancement in the table.

Most of the methods for heat transfer enhancement are relevant to vortices as shown in Table 3. However, the vortex kinematics and dynamics in tubes where the convective heat transfer is enhanced by eight methods in the table are not studied in the literature. As the first trial, the vortex kinematics in the tube with a twisted tape insert was investigated in [255]. Hopefully, vortex kinematics can be applied to the tubes where the convective heat transfer is enhanced by employing eight methods in Table 3 in the future.

Based on Table A1 in the supplemental material, the number and percentage of papers on eight passive methods achieved by using CFD or experiment or both are listed in Table 5. More than 2/3 papers were completed by using CFD method, demonstrating CFD has been a useful tool for dealing with heat transfer enhancement. However, experimental study is still needed in heat transfer enhancement to validate CFD results, especially for TPT, TMT, wavy tube, conical tube and EHT.

In these investigations completed by using CFD simulation, the heat transfer enhancement inside these tubes was a major concern, but the heat transfer enhancement outside the tubes received limited attention. The evidence suggested the heat transfer enhancement outside a TOT was stronger than that inside the tube [88]. Whether the heat transfer enhancement outside an EHT is stronger than inside the tube is worth being clarified in the future.

Conclusion

Passive heat transfer enhancement methods by using the tubes in various shapes were surveyed to seek mostly suitable methods for heat transfer enhancement of SCO2 heat exchangers in refrigeration systems. First, the existing tubes in various shapes for heat transfer enhancement were divided into eight groups: twisted oval tube, twisted polygon tube, periodical convergent-divergent tube, helically corrugated tube, wavy tube or channel, conical tube and eccentrical helical tube. Then, the overall thermal-hydraulic performance of each group and the thermal-hydraulic performance of individual tubes in the group were summarised in terms of friction factor ratio, Nusselt number ratio, PEC and enhancement efficiency in laminar and turbulent flow regimes, respectively. A threshold of friction factor ratio was proposed to evaluate those passive methods and the most suitable methods for heat transfer enhancement of SCO2 heat exchangers were secured. The mechanism of heat transfer enhancement in those groups, applications of entropy generation rate analysis, second law analysis and field synergy analysis in them were discussed. It is concluded that the twisted polygon tube, periodical convergent-divergent tube, helically corrugated tube and wavy tube belong to the passive methods with higher flow resistance and poorer PEC based on the f/f_0=5 criterion proposed, while the twisted oval tube, conical tube and eccentrical helical tube are subject to lower flow resistance and better PEC. The twisted elliptical tube and the eccentrical helical tube are the most suitable passive methods for enhancing heat transfer in the SCO2 heat exchanger in refrigeration systems due to lower flow resistance and better PEC. The vortex formation and development and pattern as well as thermal boundary layer disruption are relevant to the mechanism of heat transfer enhancement in the twisted oval tube, twisted polygon tube, periodical convergent-divergent tube, helically corrugated tube, wavy tube and eccentrical helical tube. CFD simulation-based entropy production rate is mainly applied to periodical convergent-divergent tubes, but the field synergy analysis is basically focused on twisted oval tubes.

The further work should be devoted to CFD and experimental study on heat transfer enhancement inside and outside twisted oval tube and eccentrical helical tube under SCO2 flow conditions, enhancement optimisation based on entropy generation rate or second law analysis or field synergy analysis as well as the study on vortex kinematics and kinetics inside and outside these tubes for even better understanding of the mechanism of heat transfer enhancement in them.

Table 5
Number and percentage of papers achieved by CFD, experiment and both.

Passive method	CFD	Exp	CFD & Exp	1D analysis
Twisted oval tube	21	9	7	0
Twisted polygon tube	13	0	5	0
Twisted multi-lobe tube	12	1	3	0
Periodical convergent-divergent tube	34	10	2	0
Helically corrugated tube	9	14	0	1
Wavy tube or channel	13	0	4	0
Conical tube	8	1	1	0
Eccentrical helical tube	3	0	0	0
Percentage (%)	67.8	20.3	11.3	0.6

Declaration of Competing Interest

The authors declare that they have no known competing financial interests or personal relationships that could have appeared to influence the work reported in this paper.

Data availability

publish the appendix as supplemental material attached.

Acknowledgement

The paper has financially benefited from EPSRC Investment (EP/T022701/1, EP/V042033/1, EP/P028829/1, EP/N020472/1, EP/N005228/1, EP/V030515/1, EP/W027593/1) in the UK.

Supplementary materials

Supplementary material associated with this article can be found, in the online version, at doi:10.1016/j.ijft.2023.100511.

References

[1] N.S. Sohoni, V.M. Kriplani, Review of heat transfer enhancement techniques in swirl flow using active and passive methods, Int. J. Eng. Res. Technol. 6 (1) (2013) 86–94.
[2] M. Jadhav, R. Awari, D. Bibe, A. Bramhane, M. Mokashi, Review on enhancement of heat transfer by active method, Int. J. Curr. Eng. Technol. (2016) 221–225. Special issue-6.
[3] M.H. Mousa, N. Miljkovic, K. Nawaz, Review of heat transfer enhancement techniques for single phase flows, Renew. Sustain. Energy Rev. 137 (2021), 110566.
[4] F. Illán-Gómez, J.R. García-Cascales, F.J. Sánchez-Velasco, V. Sena-Cuevas, R. Otón-Martínez, Numerical study on the influence of internal heat exchanger in transcritical CO2 heat pumps under optimal pressure conditions, in: 8th European Thermal Sciences Conference, The Netherlands, 2021.
[5] W. Li, Z. Yu, Heat exchangers for cooling supercritical carbon dioxide and heat transfer enhancement: a review and assessment, Energy Rep. 7 (2021) 4085–4105.
[6] S.S.M. Ajarostaghi, M. Zaboli, H. Javadi, B. Badenes, J.F. Urchueguia, A review of recent passive heat transfer enhancement methods, Energies 15 (2022) 986.
[7] S. Bhattacharyya, D.K. Vishwakarma, A. Srinivasan, M.K. Soni, V. Goel, M. Sharifpur, M.H. Ahmadi, A. Issakhov, J. Meyer, Thermal performance enhancement in heat exchangers using active and passive techniques: a detailed review, J. Therm. Anal. Calorim. 147 (2022) 9229–9281.
[8] M. Habibishandiz, M.Z. Saghir, A critical review of heat transfer enhancement methods in the presence of porous media, nanofluids, and microorganisms, Therm. Sci. Eng. Progress 30 (2022), 101267.
[9] H. Li, Y. Wang, Y. Han, W. Li, L. Yang, J. Guo, Y. Liu, J. Zhang, M. Zhang, F. Jiang, A comprehensive review of heat transfer enhancement and flow characteristics in the concentric pipe heat exchanger, Powder Technol. 397 (2022), 117037.
[10] X. Li, Y. Tan, J.Yuan T, Z. Wang, L. Wang, Research progress and application of heat transfer enhancement of twisted oval tubes, Chin. J. Process Eng. 22 (5) (2022) 561–572.

[11] A. Rukruang, N. Chimres, J. Kaew-On, M. Mesgarpour, O. Mahian, S. Wongwises, A critical review on the thermal performance of alternating cross-section tubes, Alexandria Eng. J. 61 (2022) 7315–7337.
[12] E. Tavousi, N. Perera, D. Flynn, R. Hasan, Heat transfer and fluid flow characteristics of the passive method in double tube heat exchangers: a critical review, Int. J. Thermofluids 17 (2023), 100282.
[13] A.K.A. Razzaq, K.S. Mushatet, A review study for a twisted tube heat exchanger, J. Nanofluids 12 (2023) 299–317.
[14] R. Kumar, Varun, A. Kumar, Thermal and fluid dynamic characteristics of flow through triangular cross-sectional duct: a review, Renew. Sustain. Energy Rev. 61 (2016) 123–140.
[15] J.C. Kurnia, A.P. Sasmito, Heat transfer performance of non-circular coiled tubes - Research summary, challenges and directions, Int. J. Autom. Mech. Eng. 13 (3) (2016) 3710–3727.
[16] A.P.C. Sarmiento, V.H.T. Soares, F.H. Milanez, M.B.H. Mantelli, Heat transfer correlation for circular and non-circular ducts in the transition regime, Int. J. Heat Mass Transf. 149 (2020), 119165.
[17] A. Gupta, M. Uniyal, Review of heat transfer augmentation through different passive intensifier methods, J. Mech Civil Eng. 1 (4) (2012) 14–21.
[18] S. Gulia, L. Punia, R. Kamboj, S. Dahiya, Review of heat transfer enhancement using passive techniques in different type of twisted tapes in circular tube, Int. J. Sci. Res. Dev. 2 (5) (2014) 609–612.
[19] M.S. Kamel, Heat transfer enhancement and fluid flow across tube banks heat exchanger with passive control technique by using vortex generator (a review), Int. J. Sci. Res. 3 (12) (2014) 363–367.
[20] S. More, D. Shelke, Review on heat transfer enhancement analysis of flow over the bumps on divergent channel, Int. J. Innov. Res. in Sci. Eng. Technol. 3 (12) (2014) 17994–17998.
[21] L. Wang, Y.F. Li, C.C. Zhang, K. Xu, J.X. Wu, Review heat exchanger: research development of self-rotating inserts in heat exchanger tubes, Int. J. Eng.-Trans. A: Basics 27 (10) (2014) 1503–1510.
[22] N. Patil, M. Tandale, A review on some passive techniques of heat transfer enhancement using inserts, Int. J. Des. Manuf. Technol. 9 (1) (2015) 16–22.
[23] R.R. Prajapati, P.A. Mane, S. Mane, D. Gaikwad, Review of recent techniques of heat transfer enhancement and validation of heat exchanger, J. Emerg. Technol. Innov. Res. 2 (2) (2015) 349–361.
[24] M. Sheikholeslami, M. Gorji-Bandpy, D.D. Ganji, Review of heat transfer enhancement methods: focus on passive methods using swirl flow devices, Renew Sustain. Energy Rev. 49 (2015) 444–469.
[25] A.V. Thakare, J.A. Hole, Review of heat transfer enhancement in plate heat exchanger with non-conventional shapes of rib, Int. J. Eng. Res. Technol. 4 (2) (2015) 1081–1084.
[26] T. Sonawane, P. Patil, A. Chavhan, B.M. Dusane, A review on heat transfer enhancement by passive methods, Int. Res. J. Eng. Technol. 3 (9) (2016) 1567–1574.
[27] A. Agrawal, S. Saha, N.K. Sharma, A review on tube and shell heat exchanger with elliptical twisted geometry, Int. J. Res. Appl. Sci. Eng. Technol. 5 (6) (2017) 2393–2398.
[28] J.S. Gulave, P.S. Desale, Review of heat transfer enhancement techniques of w ribs, Int. J. Sci. Eng. Res. 5 (5) (2017) 175–178.
[29] R. Gugulothu, V.K. Reddy, N.S. Somanchi, E.L. Adithya, A review on enhancement of heat transfer techniques, Mater. Today: Proc. 4 (2017) 1051–1056.
[30] K. Joshi, V.S. Bisht, Heat transfer enhancement by twisted tape inserts: a review, Int. J. Sci. Eng. Res. 10 (8) (2017) 143–145.
[31] A.D. Mokashi, D.G. Mohite, A. Manthale, D. Lad, M.A. Mane, Review paper on heat transfer enhancement in heat exchanger with rotating twisted inserts, Int. J. Curr. Eng. Sci. Res. 4 (12) (2017) 46–49.
[32] M. Omidi, M. Farhadi, M. Jafari, A comprehensive review on double pipe heat exchangers, Appl. Therm. Eng. 110 (2017) 1075–1090.
[33] M.A. Parmar, C.K. Desai, A review study of passive methods for enhancement of heat transfer by twisted tape and wire coil turbulator, Int. J. Sci. Dev. Res. 2 (3) (2017) 13–27.
[34] R.M. Ghogare, V.G. Gore, A.S. Shaikh, A review of passive technique used for heat transfer enhancement in heat exchanger, Int. Res. J. Eng. Technol. 5 (2) (2018) 571–576.
[35] D. Shriwas, J. Saini, Heat transfer enhancement technique in heat exchanger: an overview, Int. J. Res. Trends Innov. 3 (9) (2018) 12–15.
[36] R. Thejaraju, K.B. Girish, A comprehensive review on design and analysis of passive enhancement techniques in double pipe heat exchanger, Int. J. Sci. Technol. Res. 8 (8) (2019).
[37] A.H. Yousif, M.R. Khudhair, Enhancement heat transfer in a tube fitted with passive technique as twisted tape insert - a comprehensive review, Am. J. Mech Eng. 7 (1) (2019) 20–34.
[38] R. Datt, A. Kumar, M.S. Bhist, A.D. Kothiyal, R. Maithani, Hydrodynamic and thermal performance of twisted tape insert provided in heat exchanger tubes: a review, Front. Heat Mass Transf. 12 (2019) 26.
[39] A. Kaggwa, J.K. Carson, Developments and future insights of using nanofuids for heat transfer enhancements in thermal systems: a review of recent literature, Int. Nano Lett. 9 (2019) 277–288.
[40] M.S. Ahmed, M.Z. Abedin, Review on heat transfer enhancement by insert devices, Int. J. Eng. Mater. Manuf. 5 (4) (2020) 130–147.
[41] C.P. Vora, V.H. Oza, N. Bhatt, A detailed review on passive methods of heat transfer enhancement, Int. Adv. Res. J. Sci. Eng. Technol. 7 (5) (2020) 41–49.
[42] A.R. Akeedy, H. Alias, S.D. Salman, Heat transfer enhancement using passive technique: review, J. Teknol. 83 (2) (2021) 151–162.
[43] H.R. Kulkarni, P. Rathnakumar, C. Dhanasekaran, F. Akthar, Review on thermal analysis of helical coil heat exchanger using nanofluid, Int. J. Creat. Res. Thoughts 9 (5) (2021) 249–255.
[44] M. Sharma, R. Jilte, A review on passive methods for thermal performance enhancement in parabolic trough solar collectors, Int. J. Energy Res. 45 (2021) 4932–4966.
[45] A. Kumar, S. Birl, Review over the effects of baffle orientation and shape factor over pressure drop and heat transfer coefficient in tube heat exchangers, Int. Res. J. Eng. Technol. 9 (12) (2022) 685–690.
[46] S. Kumar, A.R. Jaurker, Review on heat transfer enhancement in helical tube heat exchanger, Int. J. Multidiscipl. Res. 8 (7) (2022) 297–304.
[47] F.T. Akyildiz, D.A. Siginer, L. Khezzar, Energy losses and heat transfer enhancement in transversally corrugated pipes, Int. J. Heat Mass Transf. 54 (2011) 3801–3806.
[48] Y. Chen, C. Zhang, M. Shi, J. Wu, Three-dimensional numerical simulation of heat and fluid flow in noncircular microchannel heat sinks, Int. J. Heat Mass Transf. 36 (2009) 917–920.
[49] P. Gunnasegaran, H.A. Mohammed, N.H. Shuaib, R. Saidur, The effect of geometrical parameters on heat transfer characteristics of microchannels heat sink with different shapes, Int. J. Heat Mass Transf. 37 (2010) 1078–1086.
[50] A.A. Alfaryjat, H.A. Mohammed, N.M. Adam, M.K.A. Ariffin, M.I. Najafabadi, Influence of geometrical parameters of hexagonal, circular, and rhombus microchannel heat sinks on the thermohydraulic characteristics, Int. J. Heat Mass Transf. 52 (2014) 121–131.
[51] H. Wang, Z. Chen, J. Gao, Influence of geometric parameters on flow and heat transfer performance of micro-channel heat sinks, Appl. Therm. Eng. 107 (2016) 870–879.
[52] D. Jing, L. He, Numerical studies on the hydraulic and thermal performances of microchannels with different cross-sectional shapes, Int. J. Heat Mass Transf. 143 (2019), 118604.
[53] L. Chai, S.A. Tassou, Effect of cross-section geometry on the thermohydraulic characteristics of supercritical CO_2 in minichannels, Energy Proc. 161 (2019) 446–453.
[54] M. Yang, G. Li, F. Liao, J. Li, X. Zhou, Numerical study of characteristic influence on heat transfer of supercritical CO2 in helically coiled tube with non-circular cross section, Int. J. Heat Mass Transf. 176 (2021), 121511.
[55] C.W. Leung, T.T. Wong, H.J. Kang, Forced convection of turbulent flow in triangular ducts with different angles and surface roughnesses, Heat Mass Transf. 34 (1998) 63–68.
[56] Y.S. Muzychka, M.M. Yovanovich, Laminar forced convection heat transfer in the combined entry region of non-circular ducts, J. Heat Transf. 126 (2004) 54–61.
[57] X. Yang, J. Bai, T. Lu, T. Kim, Experimental investigation of chimney-enhanced natural convection in hexagonal honeycombs, Theoret. Appl. Mech. Lett. 4 (2014), 032005.
[58] A. Fopah-Lele, C. Rohde, K. Neumann, T. Tietjen, T. Ronnebeck, K.E. N'Tsoukpoe, T. Osterland, O. r Opel, W.K.L. Ruck, Lab-scale experiment of a closed thermochemical heat storage system including honeycomb heat exchanger, Energy 114 (2016) 225–238.
[59] H. Liu, Q.N. Yu, Z.C. Zhang, Z.G. Qu, C.Z. Wang, Two-equation method for heat transfer efficiency in metal honeycombs: an analytical solution, Int. J. Heat Mass Transf. 97 (2016) 201–210.
[60] B. Pei, Z. Chen, F. Li, B. Bai, Flow and heat transfer of supercritical CO2 in the honeycomb ultra-compact plate heat exchanger, J. Supercrit. Fluids 148 (2019) 1–8.
[61] Z. Wang, G. Li, Y. Zhang, F. Wang, X. Jiang, Z. Ma, Flow and heat transfer investigation of supercritical carbon dioxide in a novel biomimetic honeycomb fractal gas cooler of transcritical CO2 heat pumps, Therm. Sci. Eng. Progress 37 (2023) 101533.
[62] W.T. Ji, J.F. Fan, C.Y. Zhao, W.Q. Tao, A revised performance evaluation method for energy saving effectiveness of heat transfer enhancement techniques, Int. J. Heat Mass Transf. 138 (2019) 1142–1153.
[63] H. Schilichting, Boundary-Layer Theory, 7th edition, McGraw-Hill, Inc., New York, 1979.
[64] K. Rehme, Simple method of predicting friction factors of turbulent flow in non-circular channels, Int. J. Heat Mass Transf. 16 (1973) 933–950.
[65] V.M. Ievlev, B.V. Dzyubenko, G.A. Dreitser, Y.V. Vilemas, In-line and cross-flow helical tube heat exchangers, Int. J. Heat Mass Transf. 25 (3) (1982) 317–322.
[66] L.A. Ashmantas, B.V. Dzyubenko, G.A. Dreitser, M.D. Segal, Unsteady-state heat transfer and mixing of a heat carrier in a heat exchanger with flow twisting, Int. J. Heat Mass Transf. 28 (4) (1985) 867–877.
[67] B.V. Dzyubenko, G.A. Dreitser, Heat transfer and fluid friction in bundles of twisted tubes, J. Eng. Phys. 50 (6) (1986) 611–618.
[68] B.V. Dzyubenko, V.N. Stetsyuk, Effect of flow-twisting intensity on the mixing of a heat-transfer agent in bundles of twisted tubes, J. Eng. Phys. 55 (5) (1988) 1195–1200.
[69] V.M. Iyevlev, B.V. Dzyubenko, G.A. Dreitser, V.V. Balashov, Unsteady-state heat and mass transfer in complex-shaped channels, Int. J. Heat Mass Transf. 32 (8) (1989) 1389–1400.
[70] L. Liang, Characteristics of sprial-flat tube heat exchanger and its commerical application, Petrol. Ref. Eng. 31 (8) (2001) 28–33.
[71] L. Yang, Z. Li, Numerical analysis of laminar flow and heat transfer in twisted elliptic tubes, Eng. Mech. 20 (5) (2003) 144–148.
[72] S. Yang, L. Zhang, H. Xu, Experimental study on convective heat transfer and flow resistance characteristics of water flow in twisted elliptical tubes, Appl. Therm. Eng. 31 (2011) 2981–2991.

[73] X.H. Tan, D.S. Zhu, G.Y. Zhou, L.D. Zeng, Experimental and numerical study of convective heat transfer and fluid flow in twisted oval tubes, Int. J. Heat Mass Transf. 55 (2012) 4701–4710.
[74] X. Tang, X. Dai, Z. D, Experimental and numerical investigation of convective heat transfer and fluid flow in twisted spiral tube, Int. J. Heat Mass Transf. 90 (2015) 523–541.
[75] A. Ebrahimi, E. Roohi, Numerical study of flow patterns and heat transfer in mini twisted oval tubes, Int. J. Modern Phys. C 26 (12) (2015), 1550140.
[76] H.R. Kim, S.K. Kim, M.S. Kim, S.H. Park, J.K. Min, M.Y. Ha, Numerical study of fluid flow and convective heat transfer characteristics in a twisted elliptic tube, J. Mech. Sci. Technol. 30 (2) (2016) 719–732.
[77] J. Cheng, Z. Qian, Q. Wang, Analysis of heat transfer and flow resistance of twisted oval tube in low Reynolds number flow, Int. J. Heat Mass Transf. 109 (2017) 761–777.
[78] Z.Y. Guo, H.Y. Zhu, X.G. Liang, Entransy-A physical quantity describing heat transfer ability, Int. J. Heat Mass Transf. 50 (2007) 2545–2556.
[79] C.C. Wu, C.K. Chen, Y.T. Yang, K.H. Huang, Numerical simulation of turbulent flow forced convection in a twisted elliptical tube, Int. J. Therm. Sci. 132 (2018) 199–208.
[80] X. Dong, Q. Bi, M. Gui, Experimental research on forced convective heat transfer titanium alloy twisted tube, Chin. J. Process Eng. 18 (2) (2018) 274–279.
[81] P. Promthaisong, W. Jedsadaratanachai, S. Eiamsa-ard, Numerical simulation and optimization of enhanced heat transfer in helical oval tubes: effect of helical oval tube modification, pitch ratio, and depth ratio, Heat Transf. Eng. 39 (19) (2018) 1665–1685.
[82] M. Talebi, F. Lalgani, Assessment of thermal behavior of variable step twist in the elliptical spiral tube heat exchanger, Int. J. Therm. Sci. 170 (2021), 107126.
[83] T. Dagdevir, Numerical analysis on heat transfer and flow characteristic through elliptical twisted tube, EURAS-J. Eng. Appl. Sci. 2 (2) (2022) 119–131.
[84] T. Dagdevir, Second law analysis on an elliptical twisted tube for a heat exchanger, J. Therm. Eng. 8 (6) (2022) 349–362.
[85] W. Yan, X. Gao, W. Xu, C. Ding, Z. Luo, Z. Zhang, Heat transfer performance of epoxy resin flows in a horizontal twisted tube, Appl. Therm. Eng. 127 (2017) 28–34.
[86] A.N. Guo, L.B. Wang, The mechanism of laminar convective heat transfer enhancement enforced by twisting of elliptical tube, Int. J. Heat Mass Transf. 157 (2020), 119961.
[87] C. Yu, Y. Cui, H. Zhang, B. Gao, M. Zeng, L. Han, Comparative study on turbulent flow characteristics and heat transfer mechanism of a twisted oval tube with different twisted tapes, Int. J. Therm. Sci. 174 (2022), 107455.
[88] P. Guan, F. An, M. Lu, Numerical simulation on heat transfer performance of laminar flow outside twisted oval tube, Light Indust. Mach. 34 (6) (2016) 15–20.
[89] C. Luo, K.W. Song, T. Tagawa, T.F. Liu, Heat transfer enhancement in a novel annular tube with outer straight and inner twisted oval tubes, Symmetry 12 (2020) 1213.
[90] C. Luo, K.W. Song, Thermal performance enhancement of a double-tube heat exchanger with novel twisted annulus formed by counter-twisted oval tubes, Int. J. Therm. Sci. 164 (2021), 106892.
[91] X.H. Tan, D.S. Zhu, G.Y. Zhou, L. Yang, 3D numerical simulation on the shell side heat transfer and pressure drop performances of twisted oval tube heat exchanger, Int. J. Heat Mass Transf. 65 (2013) 244–253.
[92] D.R. Shaver, L.B. Carasik, E. Merzari, N. Salpeter, E. Blandford, Calculation of friction factors and Nusselt numbers for twisted elliptical tube heat exchangers using Nek5000, J. Fluids Eng. 141 (2019), 071205.
[93] R.S. Misbakhov, V.M. Gureev, N.I. Moskalenko, A.M. Ermakov, I.Z. Bagautdinov, Numerical studies into hydrodynamics and heat exchange in heat exchangers using helical square and oval tubes, Biosci. Biotech. Res. Asia 12 (2015) 719–724.
[94] H.S. Chen, D.S. Zhu, E.X. Chen, X. Mo, L.Y. Tan, Numerical study on shell-side heat transfer enhancement of twisted oval tube heat exchanger, Adv. New Renew. Energy 10 (6) (2022) 519–525.
[95] H. Gu, Y. Chen, J. Wu, B. Sunden, Performance investigation on twisted elliptical tube heat exchangers with coupling-vortex square tube layout, Int. J. Heat Mass Transf. 151 (2020), 119473.
[96] X. Gu, Z. Zheng, X. Xiong, E. Jiang, T. Wang, D. Zhang, Heat transfer and flow resistance characteristics of helical baffle heat exchangers with twisted oval tube, J. Therm. Sci. 31 (2) (2022) 370–378.
[97] S. Wang, L. Sun, C. Song, Z. Zhang, J. Wen, Multi-objective optimization on shell-side performance of rod-baffle heat exchangers with twisted oval tubes, CIESC Journal 70 (9) (2019) 3353–3362.
[98] X. Duan, J. Xiao, L. Sun, S. Wang, Performance enhancement and optimization for rod-baffle heat exchangers with twisted oval tubes, Can. J. Chem. Eng. 101 (2023) 1700–1712.
[99] Q. Si, Q. Xia, L. Liang, D. Li, Investigation of heat transfer and flow resistance on twisted tube heat exchanger, J. Chem. Indust. Eng. 46 (5) (1995) 601–608.
[100] B. Vestergaard, R.L. Jorgensen, O. Kusch, Fluid to fluid heat exchanger: an improved design using a twisted flat oval tube. Advanced Computational Methods in Heat Transfer VI, Southampton, WIT Press, UK, 2000, pp. 497–506.
[101] X.H. Tan, D.S. Zhu, G.Y. Zhou, L.D. Zeng, Heat transfer and pressure drop performance of twisted oval tube heat exchanger, Appl. Therm. Eng. 50 (2013) 374–383.
[102] X. Dong, X. Jin, P. Li, Q. Bi, M. Gui, T. Wang, Experimental research on heat transfer and flow resistance properties in spiral twisted tube heat exchanger, Appl. Therm. Eng. 176 (2020), 115397.
[103] X. Gu, C. Chen, N. Li, G. Wang, Q. Zhang, Y. Wang, Torsional flow heat exchanger with twisted oval tube, J. Thermophys. Heat Transf. 37 (1) (2023) 1–15.
[104] V.P. Thawkar, H.S. Farkade, Experimental and CFD analysis of twisted tube heat exchanger under forced convection, Int. J. Sci. Res. 4 (5) (2015) 137–142.
[105] N.B. Dahare, M. Basavaraj, Experimental analysis and performance characteristic of heat transfer in shell and twisted tube heat exchanger, Int. Res. J. Eng. Technol. 2 (7) (2015) 1142.
[106] X. Li, D. Zhu, J. Sun, X. Mo, S. Liu, Heat transfer and pressure drop for twisted oval tube bundles with staggered layout in crossflow of air, Appl. Therm. Eng. 148 (2019) 1092–1098.
[107] M.S. Khan, R. Zou, A. Yu, Computational simulation of air-side heat transfer and pressure drop performance in staggered mannered twisted oval tube bundle operating in crossflow, Int. J. Therm. Sci. 161 (2021), 106748.
[108] G. Wang, T. Dbouk, D. Wang, Y. Pei, X. Peng, H. Yuan, S. Xiang, Experimental and numerical investigation on hydraulic and thermal performance in the tube-side of helically coiled-twisted trilobal tube heat exchanger, Int. J. Therm. Sci. 153 (2020), 106328.
[109] J. Yu, J. Chen, X. Mi, Y. Jiang, X. Fan, Z. Zhu, Study on flow and heat transfer characteristics for propane in twisted oval and the two-start twisted helically wound tube, Adv. Mech. Eng. 13 (12) (2021) 1–24.
[110] J. Wang, Y. Liu, R. Ding, Analysis of heat transfer and flow characteristics of a helically coiled tube with twisted elliptical in a low Reynolds number flow, Processes 10 (2022) 2229.
[111] S. Wahlquist, A. Ali, S.J. Yoon, P. Sabharwall, Laminar flow heat transfer in helical oval-twisted tube for heat exchanger applications, Front. Heat Mass Transf. 18 (2022) 35.
[112] R. Bhadouriya, A. Agrawal, S.V. Prabhu, Experimental and numerical study of fluid flow and heat transfer in an annulus of inner twisted square duct and outer circular pipe, Int. J. Therm. Sci. 94 (2015) 96–109.
[113] C. Yu, H. Zhang, Y. Wang, M. Zeng, B. Gao, Numerical study on turbulent heat transfer performance of twisted oval tube with different cross sectioned wire coil, Case Stud. Therm. Eng. 22 (2020), 100759.
[114] N. Uğurlubilek, Numerical investigation of heat transfer and flow in a twisted-shaped square duct, J. Therm. Sci. Technol. 32 (2) (2012) 121–131.
[115] R. Bhadouriya, A. Agrawal, S.V. Prabhu, Experimental and numerical study of fluid flow and heat transfer in a twisted square duct, Int. J. Heat Mass Transf. 82 (2015) 143–158.
[116] K.S. Mushatet, H.M. Hmood, Numerical investigation for heat transfer enhancement in a triangular twisted tube, ARPN J. Eng. Appl. Sci. 16 (5) (2021) 593–599.
[117] M. Khoshvaght-Aliabadi, Z. Arani-Lahtari, Proposing new configurations for twisted square channel (TSC): nanofluid as working fluid, Appl. Therm. Eng. 108 (2016) 709–719.
[118] M. Khoshvaght-Aliabadi, A. Feizabadi, S.F. Khaligh, Empirical and numerical assessments on corrugated and twisted channels as two enhanced geometries, Int. J. Mech. Sci. 157-158 (2019) 25–44. Vols.
[119] M. Farnam, M. Khoshvaght-Aliabadi, M.J. Asadollahzadeh, Intensified single-phase forced convective heat transfer with helical-twisted tube in coil heat exchangers, Ann. Nucl. Energy 154 (2021), 108108.
[120] M. Khoshvaght-Aliabadi, S. Deldar, S. Rehman, A. Alimoradi, Comparative study of heat transfer and pressure drop for curved-twisted tubes utilized in chemical engineering, Chin. J. Chem. Eng. 40 (2021) 53–64.
[121] S.K. Mahato, S.C. Rana, R.N. Barman, S. Goswami, Numerical analysis of heat transfer and fluid flow through twisted hexagonal and square duct and their comparisons, Chem. Eng. Trans. 71 (2018) 1351–1356.
[122] S.K. Mahato, S.C. Rana, R.N. Barman, S. Goswami, Numerical analysis of heat transfer and fluid flow through the twisted square duct (TSD): nanofluid as working fluid, J. Mech. Sci. Technol. 33 (11) (2019) 5507–5514.
[123] M. Khoshvaght-Aliabadi, Z. Arani, F. Rahimpour, Influence of Al_2O_3–H_2O nanofluid on performance of twisted minichannels, Adv. Powder Technol. 27 (2016) 1514–1525.
[124] Y. Wang, J.J. Zhou, Z.G. Jin, X.H. Yang, Performance investigation of the organosilicone conduction oil with CuO nanoparticles filled in twist tube flow for solar energy storage, J. Energy Storage 41 (2021), 102911.
[125] J. Chen, X. Ji, X. Lu, C. Wang, Mechanism study of heat transfer enhancement using twisted hexagonal tube with slurry from biogas plant, Energy Proc. 142 (2017) 880–885.
[126] J. Chen, Z. Hai, X. Lu, C. Wanga, X. Ji, Heat-transfer enhancement for corn straw slurry from biogas plants by twisted hexagonal tubes, Appl. Energy 262 (2020), 114554.
[127] J. Chen, M. Risberg, L. Westerlund, U. Jansson, C. Wang, X. Lu, X. Ji, Heat-transfer performance of twisted tubes for highly viscous food waste slurry from biogas plants, BioTechnol. Biofuels Bioproducts 15 (2022) 74.
[128] M.K. Rashed, K.A. Jehhef, F.A. Badawy, Numerical study on thermal performance of water flow in a twisted duct heat exchanger, Int. J. Appl. Mech. Eng. 27 (2) (2022) 199–216.
[129] Z.S. Kareen, M.N.M. Jaafar, T.M. Lazim, S. Abdullah, A.F. AbdulWahid, Heat transfer enhancement in two-start spirally corrugated tube, Alexandria Eng. J. 54 (2015) 415–422.
[130] Z.S. Kareem, S. Abdullah, T.M. Lazim, M.N.M. Jaafar, A.F.A. Wahid, Heat transfer enhancement in three-start spirally corrugated tube: experimental and numerical study, Chem. Eng. Sci. 134 (2015) 746–757.
[131] J.Y. Qian, C. Yang, M.R. Chen, Z.J. Jin, Thermohydraulic performance evaluation of multi-start spirally corrugated tubes, Int. J. Heat Mass Transf. 156 (2020), 119876.
[132] M. Najafian, A. Esmaeili, A. Nikkhoo, H. Jin, M.R. Soufivand, Numerical study of heat transfer and fluid flow of supercritical water in twisted spiral tubes, Energy Sources Part A 44 (3) (2022) 6433–6455.

[133] K.L. Liaw, J.C. Kurnia, A.P. Sasmito, Laminar convective heat transfer in helical twisted multilobe tubes, Case Stud. Therm. Eng. 39 (2022), 102459.
[134] K.L. Liaw, J.C. Kurnia, Z.A. Putra, M. Aziz, A.P. Sasmito, Enhanced turbulent convective heat transfer in helical twisted multilobe tubes, Int. J. Heat Mass Transf. 202 (2023), 123687.
[135] M.H. Esfe, H. Mazaheri, S.S. Mirzaei, E. Kashi, M. Kazemi, M. Afrand, Effects of twisted tapes on thermal performance of tri-lobed tube: an applicable numerical study, Appl. Therm. Eng. 144 (2018) 512–521.
[136] P. Promthaisong, W. Jedsadaratanachai, S. Eiamsa-ard, Effect of geometrical parameters on turbulent flow and heat transfer behaviors in triple-start corrugated tubes, J. Therm. Sci. Technol. 13 (1) (2018) 1–18.
[137] H.H. Balla, Enhancement of heat transfer in six-start spirally corrugated tubes, Case Stud. Therm. Eng. 9 (2017) 79–89.
[138] Z.J. Jin, F.Q. Chen, Z.X. Gao, X.F. Gao, J.Y. Qian, Effects of pitch and corrugation depth on heat transfer characteristics in six-start spirally corrugated tube, Int. J. Heat Mass Transf. 108 (2017) 1011–1025.
[139] Z.J. Jin, F.Q. Chen, Z.X. Gao, X.F. Gao, J.Y. Qian, Effects of pitch and corrugation depth on heat transfer characteristics in six-start spirally corrugated tube, Int. J. Heat Mass Transf. 108 (2017) 1011–1025.
[140] S. Eiamsa-ard, P. Promthaisong, C. Thianpong, M. Pimsarn, V. Chuwattanakul, Influence of three-start spirally twisted tube combined with triple-channel twisted tape insert on heat transfer enhancement, Chem. Eng. Process. 102 (2016) 117–129.
[141] P. Samruaisin, S. Kunlabud, K. Kunnaraka, V. Chuwattanakul, S. Eiamsa-ard, Intensification of convective heat transfer and heat exchanger performance by the combined influence of a twisted tube and twisted tape, Case Stud. Therm. Eng. 14 (2019), 100489.
[142] S. Eiamsa-ard, P. Promvonge, Experimental investigation of heat transfer and friction characteristics in a circular tube fitted with V-nozzle turbulators, Int. Commun. Heat Mass Transf. 33 (2006) 591–600.
[143] M.M. Ibrahim, M.A. Essa, N.H. Mostafa, A computational study of heat transfer analysis for a circular tube with conical ring turbulators, Int. J. Therm. Sci. 137 (2019) 138–160.
[144] J.A. Meng, X.G. Liang, Z.J. Chen, Z.X. Li, Experimental study on convective heat transfer in alternating elliptical axis tubes, Exp. Therm. Fluid Sci. 29 (2005) 457–465.
[145] M.A. Habib, I. Ul-Haq, H.M. Badr, S.A.M. Said, Calculation of turbulent flow and heat transfer in periodically converging-diverging channels, Comput. Fluids 27 (1) (1998) 95–120.
[146] T.A. Rush, T.A. Newell, A.M. Jacobi, An experimental study of flow and heat transfer in sinusoidal wavy passages, Int. J. Heat Mass Transf. 42 (1999) 1541–1553.
[147] C.C. Wang, C.K. Chen, Forced convection in a wavy-wall channel, Int. J. Heat Mass Transf. 45 (2002) 2587–2595.
[148] A.G. Ramgadia, A.K. Saha, Numerical study of fully developed flow and heat transfer in a wavy passage, Int. J. Therm. Sci. 67 (2013) 152–166.
[149] M. Akbarzadeh, S. Rashidi, M. Bovand, E. R, A sensitivity analysis on thermal and pumping power for the flow of nanofluid inside a wavy channel, J. Mol. Liq. 220 (2016) 1–13.
[150] J.A. Esfahani, M. Akbarzadeh, S. Rashidi, M.A. Rosen, R. Ellahi, Influences of wavy wall and nanoparticles on entropy generation over heat exchanger plate, Int. J. Heat Mass Transf. 109 (2017) 1162–1172.
[151] I.V. Miroshnichenko, M.A. Sheremet, I. Pop, A. Ishak, Convective heat transfer of micropolar fluid in a horizontal wavy channel under the local heating, Int. J. Mech. Sci. 128-129 (2017) 541–549.
[152] G. Xia, L. Chai, M. Zhou, H. Wang, Effects of structural parameters on fluid flow and heat transfer in a microchannel with aligned fan-shaped reentrant cavities, Int. J. Therm. Sci. 50 (2011) 411–419.
[153] G. Xia, Y. Zhai, Z. Cui, Numerical investigation of thermal enhancement in a micro heat sink with fan-shaped reentrant cavities and internal ribs, Appl. Therm. Eng. 58 (2013) 52–60.
[154] Y.L. Zhai, G.D. Xia, X.F. Liu, Y.F. Li, Heat transfer in the microchannels with fan-shaped reentrant cavities and different ribs based on field synergy principle and entropy generation analysis, Int. J. Heat Mass Transf. 68 (2014) 224–233.
[155] Y.L. Zhai, G.D. Xia, X.F. Liu, Y.F. Li, Exergy analysis and performance evaluation of flow and heat transfer in different micro heat sinks with complex structure, Int. J. Heat Mass Transf. 84 (2015) 293–303.
[156] G.D. Xia, J. Jiang, J. Wang, Y.L. Zhai, D.D. Ma, Effects of different geometric structures on fluid flow and heat transfer performance in microchannel heat sinks, Int. J. Heat Mass Transf. 80 (2015) 439–447.
[157] H.E. Ahmed, M.I. Ahmed, Optimum thermal design of triangular, trapezoidal and rectangular grooved microchannel heat sinks, Int. Commun. Heat Mass Transf. 66 (2015) 47–57.
[158] Y.F. Li, G.D. Xia, D.D. Ma, Y.T. Jia, J. Wang, Characteristics of laminar flow and heat transfer in microchannel heat sink with triangular cavities and rectangular ribs, Int. J. Heat Mass Transf. 98 (2016) 17–28.
[159] I.A. Ghani, N. Kamaruzaman, N.A.C. Sidik, Heat transfer augmentation in a microchannel heat sink with sinusoidal cavities and rectangular ribs, Int. J. Heat Mass Transf. 108 (2017) 1969–1981.
[160] E. Khodabandeh, S.A. Rozati, M. Joshaghani, O.A. Akbari, S. Akbari, D. Toghraie, Thermal performance improvement in water nanofluid/GNP–SDBS in novel design of double-layer microchannel heat sink with sinusoidal cavities and rectangular ribs, J. Therm. Anal. Calorim. 136 (2019) 1333–1345.
[161] L. Chai, L. Wang, X. Bai, Thermohydraulic performance of microchannel heat sinks with triangular ribs on sidewalls – Part 1: local fluid flow and heat transfer characteristics, Int. J. Heat Mass Transf. 127 (2018) 1124–1137.
[162] L. Chai, L. Wang, X. Bai, Thermohydraulic performance of microchannel heat sinks with triangular ribs on sidewalls – Part 2: average fluid flow and heat transfer characteristics, Int. J. Heat Mass Transf. 128 (2019) 634–648.
[163] L. Gong, K. Kota, W. Tao, Y. Joshi, Parametric numerical study of flow and heat transfer in microchannels with wavy walls, J. Heat Transf. 133 (5) (2011), 051702.
[164] H. Ghaedamini, P.S. Lee, C.J. Teo, Developing forced convection in converging–diverging microchannels, Int. J. Heat Mass Transf. 65 (2013) 491–499.
[165] M. Fujii, Y. Seshimo, G. Yamanaka, Heat transfer and pressure drop of perforated surface heat exchanger with passage enlargement and contraction, Int. J. Heat Mass Transf. 31 (1) (1988) 135–142.
[166] O.B. Kanargi, P.S. Lee, C. Yap, A numerical and experimental investigation of heat transfer and fluid flow characteristics of a cross-connected alternating converging–diverging channel heat sink, Int. J. Heat Mass Transf. 106 (2017) 449–464.
[167] H.A. Mohammed, A.K. Abbas, J.M. Sheriff, Influence of geometrical parameters and forced convective heat transfer in transversely corrugated circular tubes, Int. Commun. Heat Mass Transf. 44 (2013) 116–126.
[168] H. Pehlivan, I. Taymaz, Y. İslamoğlu, Experimental study of forced convective heat transfer in a different arranged corrugated channel, Int. Commun. Heat Mass Transf. 46 (2013) 106–111.
[169] Ö. Ağra, H. Demir, Ö. Atayılmaz, F. Kantaş, A.S. Dalkılıç, Numerical investigation of heat transfer and pressure drop in enhanced tubes, Int. Commun. Heat Mass Transf. 38 (2011) 1384–1391.
[170] J. Du, Y. Hong, Numerical simulation on fluid flow and heat transfer characteristics in inward sinusoidal rib enhanced tube heat exchangers for waste heat recovery: comparisons and parametric studies, Int. J. Therm. Sci. 167 (2021), 107030.
[171] K. Bilen, M. Cetin, H. Gul, T. Balta, The investigation of groove geometry effect on heat transfer for internally grooved tubes, Appl. Therm. Eng. 29 (2009) 753–761.
[172] H. Han, B. Li, W. Shao, Multi-objective optimization of outward convex corrugated tubes using response surface methodology, Appl. Therm. Eng. 70 (2014) 250–262.
[173] H.Z. Han, B.X. Li, H. Wu, W. Shao, Multi-objective shape optimization of double pipe heat exchanger with inner corrugated tube using RSM method, Int. J. Therm. Sci. 90 (2015) 173–186.
[174] W. Wang, Y. Zhang, B. Li, Y. Li, Numerical investigation of tube-side fully developed turbulent flow and heat transfer in outward corrugated tubes, Int. J. Heat Mass Transf. 116 (2018) 115–126.
[175] W. Liao, Y. Luo, T. Chen, Thermal-hydraulic performance analysis of outward convex corrugated tubes based on skewness and kurtosis, Int. J. Therm. Sci. 165 (2021), 106970.
[176] A. Kaood, T. Abou-Deif, H. Eltahan, M.A. Yehia, E.E. Khalil, Numerical investigation of heat transfer and friction characteristics for turbulent flow in various corrugated tubes, Proc. IMechE Part A: J. Power Energy 233 (4) (2019) 457–475.
[177] Y. Zhang, F. Zhou, J. Kanga, Flow and heat transfer in drag-reducing polymer solution flow through the corrugated tube and circular tube, Appl. Therm. Eng. 174 (2020), 115185.
[178] Y. Liu, Y. Dong, T. Li, C.Z. Zhang, Performance analysis and comparison of different corrugated structures and a novel alternative elliptical twisted tube in supercritical CO_2 tower solar receivers, Renew. Energy 199 (2022) 1523–1533.
[179] A. Kaood, M.A. Hassan, Thermo-hydraulic performance of nanofluids flow in various internally corrugated tubes, Chem. Eng. Process.: Process Intensif. 154 (2020), 108043.
[180] O.G. Fadodun, D.R.E. Ewim, S.M. Abolarin, Investigation of turbulent entropy production rate with SWCNT/H_2O nanofluid flowing in various inwardly corrugated pipes, Heat Transf. 51 (2022) 7862–7889.
[181] O.G. Fadodun, A. Kaood, M.A. Hassan, Investigation of the entropy production rate of ferrosoferric oxide/water nanofluid in outward corrugated pipes using a two-phase mixture model, Int. J. Therm. Sci. 178 (2022), 107598.
[182] H.S. Dizaji, S. Jafarmadar, F. Mobadersani, Experimental studies on heat transfer and pressure drop characteristics for new arrangements of corrugated tubes in a double pipe heat exchanger, Int. J. Therm. Sci. 96 (2015) 211–220.
[183] S. Bhattacharyya, A.C. Benim, H. Chattopadhyay, A. Banerjee, Experimental investigation of heat transfer performance of corrugated tube with spring tape inserts, Exp. Heat Transf. 32 (5) (2019) 411–425.
[184] Y. Chen, X. Deng, X. Ding, Y. Wang, Z. Li, Augmentation heat transfer of convergent-divergent tube, J. Chem. Indust. Eng.(China) 55 (9) (2004) 1528–1531.
[185] F.A. Hamedani, S.S.M. Ajarostaghi, S.A. Hosseini, Numerical evaluation of the effect of geometrical and operational parameters on thermal performance of nanofluid flow in convergent–divergent tube, J. Therm. Anal. Calorim. 140 (2020) 1483–1505.
[186] A.R. Sajadi, S.Y.D. Sorkhabi, D. Ashtiani, F. Kowsari, Experimental and numerical study on heat transfer and flow resistance of oil flow in alternating elliptical axis tube, Int. J. Heat Mass Transf. 77 (2014) 124–130.
[187] K. Navickaite, L. Cattani, C.R.H. Bahl, K. Engelbrecht, Elliptical double corrugated tubes for enhanced heat transfer, Int. J. Heat Mass Transf. 128 (2019) 363–377.
[188] A.R. Sajadi, F. Kowsary, M.A. Bijarchi, S.Y.D. Sorkhabi, Experimental and numerical study on heat transfer, flow resistance, and compactness of alternating flattened tubes, Appl. Therm. Eng. 108 (2016) 740–750.
[189] J.A. Zambaux, J.L. Harion, S. Russeil, P. Bouvier, The effect of successive alternating wall deformation on the performance of an annular heat exchanger, Appl. Therm. Eng. 90 (2015) 286–295.

[190] W.L. Chen, W.C. Dung, Numerical study on heat transfer characteristics of double tube heat exchangers with alternating horizontal or vertical oval cross section pipes as inner tubes, Energy Convers. Manage. 49 (2008) 1574–1583.

[191] S. Huang, H. Zhu, Y. Zheng, Z. Wan, Y. Tang, Compound thermal performance of an arc-shaped inner finned tube equipped with Y-branch inserts, Appl. Therm. Eng. 152 (2019) 475–481.

[192] F. Andrade, A.S. Moita, A. Nikulin, A.L.N. Moreira, H. Santos, Experimental investigation on heat transfer and pressure drop of internal flow in corrugated tubes, Int. J. Heat Mass Transf. 140 (2019) 940–955.

[193] S. Rainieri, F. Bozzoli, L. Cattani, G. Pagliarini, Compound convective heat transfer enhancement in helically coiled wall corrugated tubes, Int. J. Heat Mass Transf. 59 (2013) 353–362.

[194] P.G. Vicente, A. García, A. Viedma, Experimental investigation on heat transfer and frictional characteristics of spirally corrugated tubes in turbulent flow at different Prandtl numbers, Int. J. Heat Mass Transf. 47 (2004) 671–681.

[195] P. Naphon, M. Nuchjapo, J. Kurujareon, Tube side heat transfer coefficient and friction factor characteristics of horizontal tubes with helical rib, Energy Convers. Manage. 47 (2006) 3031–3044.

[196] S. Pethkool, S. Eiamsa-ard, S. Kwankaomeng, P. Promvonge, Turbulent heat transfer enhancement in a heat exchanger using helically corrugated tube, Int. Commun. Heat Mass Transf. 38 (2011) 340–347.

[197] A. García, J.P. Solano, P.G. Vicente, A. Viedma, The influence of artificial roughness shape on heat transfer enhancement: corrugated tubes, dimpled tubes and wire coils, Appl. Therm. Eng. 35 (2012) 196–201.

[198] W. Wang, Y. Zhang, J. Liu, Z. Wu, B. Li, B. Sundén, Entropy generation analysis of fully-developed turbulent heat transfer flow in inward helically corrugated tubes, Numer. Heat Transf., Part A: Applic. 73 (11) (2018) 788–805.

[199] J.I. Córcoles, J.F. Belmonte, A.E. Molina, J.A. Almendros-Ibáñez, Influence of corrugation shape on heat transfer performance in corrugated tubes using numerical simulations, Int. J. Therm. Sci. 137 (2019) 262–275.

[200] G.G. Cruz, M.A.A. Mendes, J.M.C. Pereira, H. Santos, A. Nikulind, A.S. Moita, Experimental and numerical characterization of single-phase pressure drop and heat transfer enhancement in helical corrugated tubes, Int. J. Heat Mass Transf. 179 (2021), 121632.

[201] C. Yang, M.R. Chen, J.Y. Qian, Z. Wu, Z.J. Jin, B. Sunden, Heat transfer study of a hybrid smooth and spirally corrugated tube, Heat Transf. Eng. 42 (3–4) (2021) 242–250.

[202] A.A.R. Darzi, M. Farhadi, K. Sedighi, Experimental investigation of convective heat transfer and friction factor of Al_2O_3/water nanofluid in helically corrugated tube, Exp. Therm. Fluid Sci. 57 (2014) 188–199.

[203] S. Anbu, S. Venkatachalapathy, S. Suresh, Convective heat transfer studies on helically corrugated tubes with spiraled rod inserts using TiO_2/DI water nanofluids, J. Therm. Anal. Calorim. 137 (2019) 849–864.

[204] S. Akbarzadeh, M.S. Valipour, Experimental study on the heat transfer enhancement in helically corrugated tubes under the non uniform heat flux, J. Therm. Anal. Calorim. 140 (2020) 1611–1623.

[205] J. Hærvig, K. Sørensen, T.J. Condra, On the fully-developed heat transfer enhancing flow field in sinusoidally, spirally corrugated tubes using computational fluid dynamics, Int. J. Heat Mass Transf. 106 (2017) 1051–1062.

[206] S.W. Ahn, Experimental studies on heat transfer in the annuli with corrugated inner tubes, KSME Int. J. 17 (8) (2003) 1226–1233.

[207] W. Wang, Y. Shuai, L. Ding, B. Li, B. Sunden, Investigation of complex flow and heat transfer mechanism in multi-tube heat exchanger with different arrangement corrugated tube, Int. J. Therm. Sci. 167 (2021), 107010.

[208] A. Zachár, Analysis of coiled-tube heat exchangers to improve heat transfer rate with spirally corrugated wall, Int. J. Heat Mass Transf. 53 (2010) 3928–3939.

[209] Z. Yao, H. Cui, Y. Yang, Study of enhanced heat transfer of eddying tube type heat exchangers with oil as medium, China Petrol. Mach. 28 (8) (2000) 26–27.

[210] S. Rozzi, R. Massini, G. Paciello, G. Pagliarini, S. Rainieri, A. Trifiro, Heat treatment of fluid foods in a shell and tube heat exchanger: comparison between smooth and helically corrugated wall tubes, J. Food Eng. 79 (2007) 249–254.

[211] A. Celen, Energy and exergy analysis of a shell and tube heat exchangers having smooth and corrugated inner tubes, Süleyman Demirel Univ.y J. Nat. Appl. Sci. 26 (1) (2022) 171–181.

[212] X.D. Chen, X.Y. Xu, S.K. Nguang, A.E. Bergles, Characterization of the effect of corrugation angles on hydrodynamic and heat transfer performance of four-start spiral tubes, J. Heat Transf. 123 (6) (2001) 1149–1158.

[213] P.K. Chaurasiya, S.K. Singh, P.K. Jain, U. Rajak, T.N. Verma, A.K. Azad, K. Choudhary, A.M. Alosaimi, A. Khan, Heat transfer and friction factor correlations for double pipe heat exchanger with inner and outer corrugation, Energy Sources Part A 45 (1) (2023) 18–45.

[214] V. Zimparov, Enhancement of heat transfer by a combination of three start spirally corrugated tubes with a twisted tape, Int. J. Heat Mass Transf. 44 (2001) 551–574.

[215] M.R. Manglik, J. Zhang, A. Muley, Low Reynolds number forced convection in three-dimensional wavy-plate-fin compact channels: fin density effects, Int. J. Heat Mass Transf. 48 (2005) 1439–1449.

[216] N.R. Rosaguti, D.F. Fletcher, B.S. Haynes, Laminar flow and heat transfer in a periodic serpentine channel, Chem. Eng. Technol. 28 (3) (2005) 353–361.

[217] N.R. Rosaguti, D.F. Fletcher, B.S. Haynes, Laminar flow and heat transfer in a periodic serpentine channel with semi-circular cross-section, Int. J. Heat Mass Transf. 49 (2006) 2912–2923.

[218] P.E. Geyer, D.F. Fletcher, B.S. Haynes, Laminar flow and heat transfer in a periodic trapezoidal channel with semi-circular cross-section, Int. J. Heat Mass Transf. 50 (2007) 3471–3480.

[219] A.M. Abed, M.A. Alghoul, K. Sopian, H.A. Mohammed, H.sh. Majdi, A.N. Al-Shamani, Design characteristics of corrugated trapezoidal plate heat exchangers using nanofluids, Chem. Eng. Process. 87 (2015) 88–103.

[220] Y. Sui, C.J. Teo, P.S. Lee, Y.T. Chew, S. C, Fluid flow and heat transfer in wavy microchannels, Int. J. Heat Mass Transf. 53 (2010) 2760–2772.

[221] Y. Sui, P.S. Lee, C.J. Teo, An experimental study of flow friction and heat transfer in wavy microchannels with rectangular cross section, Int. J. Therm. Sci. 50 (2011) 2473–2482.

[222] Y. Lei, Z. Chen, Numerical study on cooling heat transfer and pressure drop of supercritical CO_2 in wavy microchannels, Int. J. Refrig. 90 (2018) 46–57.

[223] M. Khoshvaght-Aliabadi, P. Ghodrati, H. Mortazavi, Y.T. Kang, Numerical analysis of heat transfer and flow characteristics of supercritical CO2-cooled wavy mini-channel heat sinks, Appl. Therm. Eng. 226 (2023), 120307.

[224] Y.G. Lv, Z.X. Wen, Q. Li, Y. Qiu, Numerical investigation on thermal hydraulic performance of hybrid wavy channels in a supercritical CO_2 precooler, Int. J. Heat Mass Transf. 181 (2021), 121891.

[225] Z.L. Chiam, P.S. Lee, P.K. Singh, N. Mou, Investigation of fluid flow and heat transfer in wavy micro-channels with alternating secondary branches, Int. J. Heat Mass Transf. 101 (2016) 1316–1330.

[226] D. Shi, K.T. Lin, M.A. Jog, R.M. Manglik, Characterization and scaling of forced convective swirl in sinusoidal wavy-plate-fin cores of compact heat exchangers, J. Heat Transf. 143 (2021), 021901.

[227] L. Lin, J. Zhao, G. Lu, X.D. Wang, W.M. Yan, Heat transfer enhancement in microchannel heat sink by wavy channel with changing wavelength/amplitude, Int. J. Therm. Sci. 118 (2017) 423–434.

[228] M. Khoshvaght-Aliabadi, S. Deldar, A. Salimi, M.M. Rashidi, Effects of cross-section geometry on performance of corrugated miniature heat sink: uniform, convergent, divergent, and hybrid cases, Int. Commun. Heat Mass Transf. 127 (2021), 105269.

[229] H.A. Mohammed, P. Gunnasegaran, N.H. Shuaib, Influence of channel shape on the thermal and hydraulic performance of microchannel heat sink, Int. Commun. Heat Mass Transf. 38 (2011) 474–480.

[230] K. Ghachem, W. Aich, L. Kolsi, Computational analysis of hybrid nanofluid enhanced heat transfer in cross flow micro heat exchanger with rectangular wavy channels, Case Stud. Therm. Eng. 24 (2021), 100822.

[231] V.S. Duryodhan, A. Singh, S.G. Singh, A. Agrawal, Convective heat transfer in diverging and converging microchannels, Int. J. Heat Mass Transf. 80 (2015) 424–438.

[232] C. Bai, H. Cao, G. Zhang, M. Tian, Diverging small channel for condensation heat transfer enhancement, Int. J. Heat Mass Transf. 133 (2019) 218–225.

[233] M. Hashemian, S. Jafarmadar, J. Nasiri, H.S. Dizaj, Enhancement of heat transfer rate with structural modification of double pipe heat exchanger by changing cylindrical form of tubes into conical form, Appl. Therm. Eng. 118 (2017) 408–417.

[234] C.J. Ho, P.C. Chang, W.M. Yan, P. Amani, Thermal and hydrodynamic characteristics of divergent rectangular minichannel heat sinks, Int. J. Heat Mass Transf. 122 (2018) 264–274.

[235] J. Hao, C. Ju, C. Li, L. Tian, Z. Ge, X. Du, Comparison and evaluation of supercritical CO2 cooling performance in horizontal tubes with variable cross-section by field synergy theory, Int. J. Energy Res. 46 (2022) 14133–14144.

[236] C. Li, J. Hao, X. Wang, Z. Ge, X. Du, Dual-effect evaluation of heat transfer deterioration of supercritical carbon dioxide in variable cross-section horizontal tubes under heating conditions, Int. J. Heat Mass Transf. 183 (2022), 122103.

[237] Z. Yi, Y. Xu, X. Chen, Cooling heat transfer of supercritical CO_2 in diverging and converging microtubes, Chem. Eng. Technol. 45 (2) (2022) 302–308.

[238] C.S. Iweka, O.G. Fadodun, Numerical modeling of heat transfer in Al_2O_3/H_2O nanofluid flowing through a Bessel-like converging pipe, Arch. Thermodyn. 42 (2) (2021) 121–153.

[239] O.G. Fadodun, A. Olatinwo, A.A. Amosun, S.F. Olukotun, A.A. Owojori, M.T. Ojo, Optimization of heat transfer performance of CuO/H_2O nanofluid in Bessel-like converging pipe using a two-phase mixture model, Heat Transf. 51 (2022) 7081–7108.

[240] A. Kaood, A. Aboulmagd, A. ElDegwy, Entropy generation analysis of turbulent flow in conical tubes with dimples: a numerical study, J. Therm. Anal. Calorim. (2023), https://doi.org/10.1007/s10973-023-12127-y.

[241] M. Hashemian, S. Jarmadar, H.S. Dizaji, A comprehensive numerical study on multi-criteria design analyses in a novel form (conical) of double pipe heat exchanger, Appl. Therm. Eng. 102 (2016) 1228–1237.

[242] L. Ma, W. Liu, Z.C. Liu, J.G. Yang, J. Yang, S.Y. Wang, K. Yang, A.W. Fan and X.M. Huang, "Heat transfer pipe". China Patent CN102564189A, 11 07, 2012.

[243] J. Yang, L. Ma, J. Liu, W. Liu, Thermal–hydraulic performance of a novel shell-and-tube oil cooler with multi-fields synergy analysis, Int. J. Heat Mass Transf. 77 (2014) 928–939.

[244] Z.M.A. Alsulaiei, H.M. Hasan, M.H. Fagr, Flow and heat transfer in obstacled twisted tubes, Case Stud. Therm. Eng. 7 (2021), 101286.

[245] A.K.A. Razzaq, K.S. Mushatet, A numerical study for a double twisted tube heat exchanger, Int. J. Heat Technol. 39 (5) (2021) 1583–1589.

[246] A.K.A. Razzaq, K.S. Mushatet, Evaluation the performance of the double tube heat exchanger by using combined twisted tube and nano fluid, Int. J. Mech. Eng. 7 (1) (2022) 6618–6628.

[247] P.M. Ligrani, M.M. Oliveira, T. Blaskovich, Comparison of heat transfer augmentation techniques, AIAA J. 41 (3) (2003) 337–362.

[248] F. Kock, H. Herwig, Local entropy production in turbulent shear flows: a high-Reynolds number model with wall functions, Int. J. Heat Mass Transf. 47 (2004) 2205–2215.

[249] S. Khanmohammadi, N. Mazaheri, Second law analysis and multi-criteria optimization of turbulent heat transfer in a tube with inserted single and double twisted tape, Int. J. Therm. Sci. 145 (2019), 105998.
[250] K. Manjunath, S.C. Kaushik, Second law thermodynamic study of heat exchangers: a review, Renew Sustain. Energy Rev. 40 (2014) 348–374.
[251] Z.Y. Guo, D.Y. Li, B.X. Wang, A novel concept for convective heat transfer enhancement, Int. J. Heat Mass Transf. 41 (14) (1998) 2221–2225.
[252] Z.Y. Guo, W.Q. Tao, R.K. Shah, The field synergy (coordination) principle and its applications in enhancing single phase convective heat transfer, Int. J. Heat Mass Transf. 48 (2005) 1797–1807.
[253] F.M. White, Viscous Fuid Flow, 2nd edition, McGraw-Hill Inc, New York, 1991.
[254] W. Cui, D. Mao, B. Lin, J. Yang, Field synergy analysis on the mechanism of heat transfer enhancement by using nanofluids, Case Stud. Therm. Eng. 16 (2019), 100554.
[255] W. Li, Z. Yu, Y. Wang, Y. Li, Heat transfer enhancement of twisted tape inserts in supercritical carbon dioxide flow conditions based on CFD and vortex kinematics, Therm. Sci. Eng. Progress 31 (2022), 101285.